Studies Towards the Development of a Ratiometric Fluorescent Zinc Sensor

By Tasnia Kamal

Supervisor: Prof. M Watkinson

School of Biological and Chemical Sciences

Queen Mary University of London

Submitted March 2016

Table of contents

Acknowledgements

I would like to thank Professor Mike Watkinson, for his dedicated time and patience, as well as his constant guidance throughout this project. I am also grateful to Dr Phil Duncanson, for his comprehensive insight into synthetic chemistry, and continuous support in the lab. Finally I would like to thank Mariya and Aneta for their encouragement and advice, as well as making my time in the lab especially enjoyable.

Abbreviations

λ_{em} – wavelength of emission

λ_{ex} – wavelength of excitation

AD – Alzheimer's disease

a.u. – arbitrary units

BIPY – 2,2'-bipyridine

BODIPY – boron-dipyrromethene

CCS – changeable π-conjugated systems

COSY – correlation spectroscopy

CuAAC – copper-catalysed azide-alkyne cycloaddition

Cyclam – (1, 4, 8, 11-tetraazacyclotetradecane)

Cyclen - (1,4,7,10-tetraazacyclododecane)

DCM – dichloromethane

DIPEA – *N,N*-diisopropylethylamine

DMAP – 4-dimethylaminopyridine

DMF – *N,N*-dimethylformamide

DMSO – dimethyl sulfoxide

DPA – dipicolylamine

EDG – electron-donating group

EDTA – ethylenediaminetetraacetic acid

EI – electron ionisation

EPR – electron paramagnetic resonance spectroscopy

ESI - electrospray ionisation

EtOAc – ethyl acetate

Et_2OAc – ethyl acetoacetate

EtOH – ethanol

EWG – electron-withdrawing group

FRET – Förster resonance energy transfer

h – hour(s)

HeLa – Henrietta Lacks, a continuously-cultured cell line widely used in scientific research

HOMO – highest occupied molecular orbital

HSQC – heteronuclear single quantum coherence

ICT – intramolecular charge transfer

IR – infrared spectroscopy

LC-MS – liquid chromatography mass spectrometry

LRMS – low resolution mass spectrometry

LUMO – lowest unoccupied molecular orbital

MeCN – acetonitrile

MeOH – methanol

min – minute(s)

NIR – near infrared region

NMR – nuclear magnetic resonance

PEG – poly(ethyleneglycol)

PEG_4 – tetra(ethyleneglycol)

PET – photoinduced electron transfer

ppm – parts per million

R_f – retention factor

RT – room temperature

TEA – triethylamine

THF – tetrahydrofuran

TLC – thin layer chromatography

TRPEN - *N,N,N'*-tris(pyridin-2-ylmethyl)ethylenediamine

TsCl – *p*-toluene sulfonyl chloride

Abstract

Zinc is the second most abundant *d*-block metal in the human body and has many biological roles. The transportation, storage and specific cellular roles of zinc are not yet fully understood. Hence, the effects of zinc in diseases such as (but not limited to) Alzheimer's disease and diabetes are hypothesised but not yet conclusively proven. Zinc detection is crucial, and with the difficulties of detecting zinc spectroscopically, the field of fluorescent zinc sensors arose. Current challenges include the development of ratiometric zinc sensors – sensors that can quantitatively detect biological zinc sensors. The aim of this project was to synthesise a novel sensor **4** for the quantitative analysis of biological zinc levels. Sensor **4** uses one fluorophore as an internal standard, which will constantly fluoresce and another which will have a graded response towards zinc concentration levels. This report gives a background on the previous work in the field of fluorescent zinc sensors, reviewing the most popular receptor, fluorophore and linker types used. Also, a detailed discussion on the synthetic work towards sensor **4** is presented, highlighting areas for improvement and a look at future work to be done.

1. Introduction

Zinc biology is much more diverse and complex in comparison to iron and copper – and yet zinc remains the least understood of these three essential trace elements. The human body contains about 2-3 g of zinc – this whole-body content is controlled by zinc homeostasis which regulates zinc absorption and excretion. [1] High concentrations of zinc are found in a number of organs including the brain, retina and pancreas. Within a cell, zinc is distributed between the nucleus, cytoplasm and membrane. [2] In contrast to iron, which is found in specific organelles with explicit physiological roles, intracellular zinc is ubiquitous. [3] This alone suggests that zinc has a plethora of roles on the cellular level. Not to mention that zinc is present in over 3000 proteins[4] in the human body.

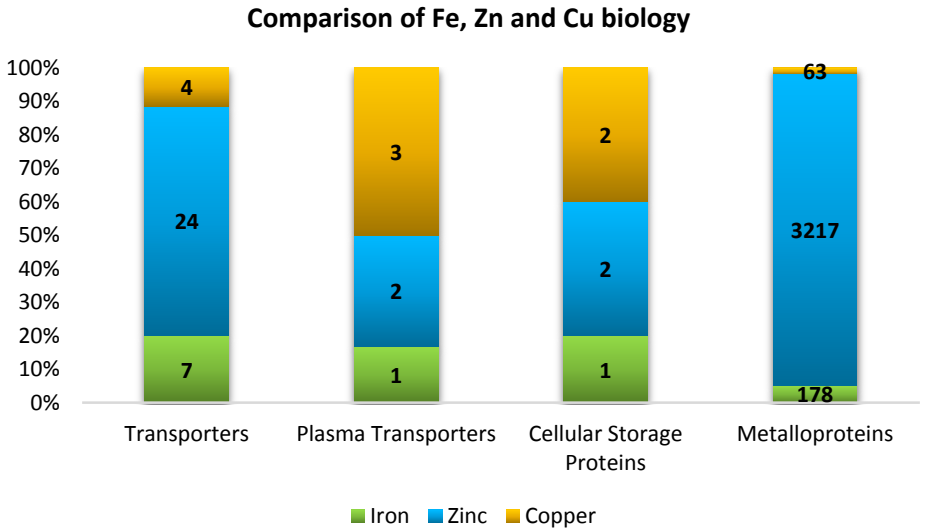

Graph 1.0 *A comparison of the number of storage proteins, metalloproteins and transporters found for three of the most abundant essential trace metals in the body; iron, zinc and copper.*

Many disease states including Type II Diabetes and AD now seem to be associated with compromised zinc homeostasis. However, it is still debated whether these fluctuating zinc levels are causal or symptomatic. To give one example, zinc-implicated AD is a widely debated topic. In 2014, work by Roberts and co-workers suggested that the decrease in zinc serum levels measured in patients with AD can be accounted for by the increase in age, not in the extent of the disease. However, in 2016, Kumar and co-workers argue that the matter is unclear and yet to be resolved. [5] Taking zinc-containing supplements has become a big trend – with the wide idea that more is better. However, zinc, iron and copper have competitive absorptions – this is why a zinc deficiency treated with zinc supplements can lead to copper deficiency. Hence, more is not always better – but without a clearer understanding, patients will continue to self-prescribe with these over-the-counter zinc supplements.

Thus, zinc exchange, transportation and use need to be studied in depth if we are to understand the true nature of zinc in biological systems. However the prevailing reason why zinc biology is so unclear is because zinc is so difficult to detect. Biologically, zinc exists as Zn^{2+} which has a d^{10} configuration, thus it is colourless, EPR inactive and "spectroscopically silent". To overcome this issue, fluorescent zinc sensors have been synthesised. Generally they work by binding zinc at a zinc-chelating centre, turning on a fluorescent centre (fluorophore). This fluorescence thus indicates the presence of zinc, as in **Figure 1.0**.

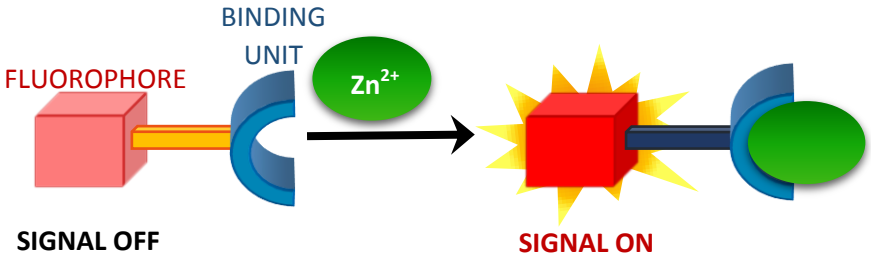

Figure 1.0 *The general concept of how fluorescent zinc sensors are used.*

The power of fluorescent zinc sensors is the ability to expose zinc in tissue samples as well as being observed temporally and spatially *in vivo*. The latter allows for the possibility to track zinc in live subjects, be that rats or even humans. The first task was to detect zinc levels qualitatively. These first generation zinc sensors, much like in **Figure 1.0**, had a "switch off/on" response to zinc. At the start, modified fluorescent molecules such as fluorescein and anthracene were used alone. These fluorescent molecules could bind to zinc, but to selectively bind zinc over other endogenous metal ions, zinc-chelating centres were attached to increase binding selectivities. In fact many of the sensors synthesised where analogues of previously known fluorescent calcium and magnesium sensors. For example 8-hydroxyquinoline, **1**, a quinoline derivative known for its "switch off/on" response to Mg(II), was also found to respond to Zn(II) in the same way (**Figure 1.1**). [6]

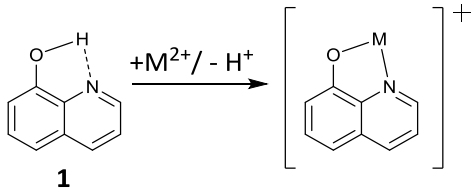

1

Figure 1.1 *"Switch off/on" response of 8-hydroxyquinoline to metal ions where M^{2+}= a metal with a +2 charge.*

Second generation sensors focused on detecting zinc spatially, either by modifying existing fluorescent zinc sensors or adding targeting moieties. Simple fluorescent molecules like quinoline do not have a wide scope of modification, limiting the range of cell types that can be targeted. As a result the general fluorophore-linker-receptor design was adopted as in **Figure 1.0**.[7] This structure separates the zinc-binding unit from the fluorescent centre, allowing for more modification and thus a wider library of zinc sensors. The "switch off/on" sensor **2** (**Figure 1.2**) by Watkinson and co-workers is a good example of this – where the fluorescent centre and the zinc-binding unit are linked through a triazole spacer using a very synthetically simple procedure. [8] The same research group then synthesised the second generation sensor **3** which has a targeting moiety, allowing **3** to target the extracellular membrane (**Figure 1.2**). [9]

One of the current targets in the field of zinc detection has been quantitative zinc measurements. This has given rise to ratiometric zinc sensors. These third generation sensors have a graded response to endogenous zinc concentrations. As mentioned, this research group synthesised the first and second generation zinc sensors **2** and **3**. Thus the aim of this report is to work towards the third generation zinc sensor, **4** (**Figure 1.2**). Sensor **4** uses two fluorophores, one as an internal standard and the other with a graded response to zinc concentrations.

This report aims to explain the main fluorescent mechanisms utilised by ratiometric fluorescent zinc sensors. To justify the rationale behind designing sensor **4** in particular, a short review of the most commonly used receptors, fluorophores and linkers is given. The synthesis towards the novel sensor **4** will be discussed, with a consideration for optimisation and prospective work.

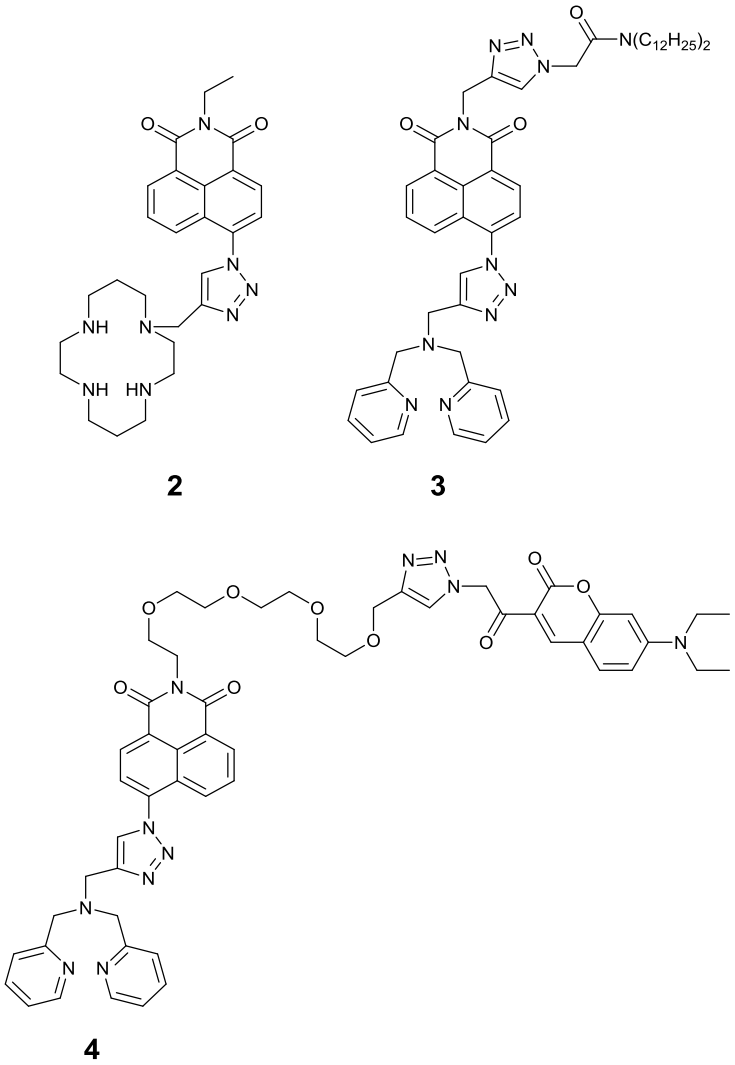

Figure 1.2 *Sensors **2** and **3** from work by Watkinson and co-workers,* [8,9] *and the target sensor for this report, **4**.*

1.1. Mechanisms of fluorescent sensors

1.1.1. The origin of fluorescence

Fluorescence in essence is the absorption of a photon, which provides an electron with energy to be promoted from the HOMO to an excited state (LUMO). The decay of the electron back to the ground state (HOMO) gives off the emission of a photon of lower energy (higher wavelength) than the photon absorbed. The discrepancy in photon energies absorbed and emitted are accounted for by non-radiative decay processes such as heat loss.

Electron excitation can occur from the absorption of one photon or two photons, as shown in (**Figure 1.3**). Both excitation methods are of equal energy, but as the two-photon excitation requires two photons, each photon is lower in energy compared to a one-photon excitation. A lower energy of excitation needed means that cells are; less likely to be damaged, less likely to autofluoresce, and can be observed at increased depths of a sample. Hence, two-photon excitations are usually preferred. Some biological entities do absorb and then emit light, and this is the origin of autofluorescence.

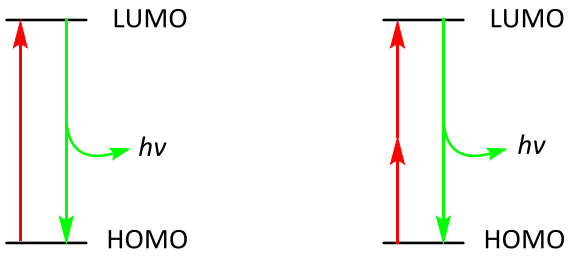

Figure 1.3 *One-photon excitation mechanism (left) and two-photon excitation mechanism (right).*

The quantum yield is a measure of fluorescence and it is one way of measuring the efficacy of a fluorescent compound. It is a ratio of the photons emitted against the photons absorbed (as given in **Equation 1.1**) and so the maximum value would be unity. A value of 1 is idealised and so in solution values are much lower, although values of 0.1 are still considered highly fluorescent.

$$\varphi_F = \frac{photons\ emitted}{photons\ absorbed}$$

Equation 1.1 *Quantum yield (φ_F).*

Fluorescence can occur through a number of different energy transfer mechanisms. This report aims to cover the three most commonly applied mechanisms for ratiometric fluorescent sensors; FRET, ICT and PET.

1.1.2. Förster resonance energy transfer (FRET) transmissions

FRET mechanisms occur in sensors which have two fluorophores linked at a distance of 10-100 Å. [10] In these sensors, there are two states, free and bound. In the free state, the sensor is not bound to a metal ion (in this case zinc). Fluorophore 1 (F1) fluoresces upon excitation but fluorophore 2 (F2) does not fluoresce. In the bound state the sensor binds zinc. Upon excitation in the bound state, instead of F1 emitting the energy as a photon of light, the energy is transferred to F2, which then releases the energy as photon of light (as shown in **Figure 1.4**). In this way the fluorescent emission spectra would show that, as the concentration of zinc increases, the emission of light from F1 would decrease and the emission of light from F2 would increase.

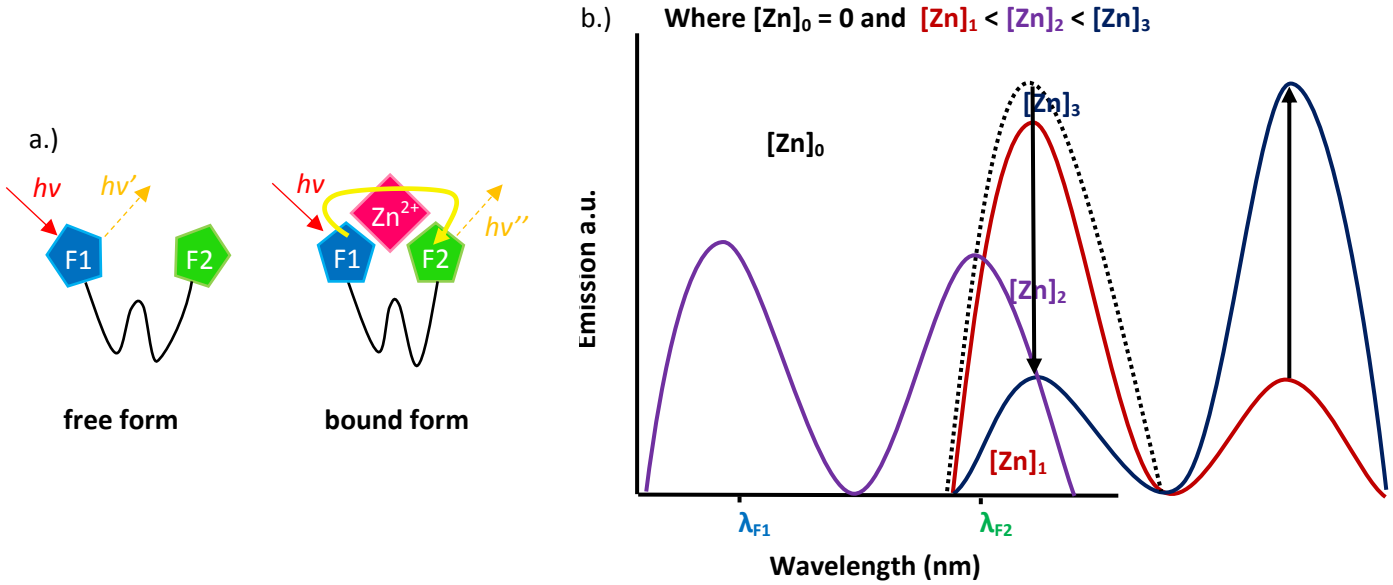

Figure 1.4 *FRET mechanism: a.) a cartoon depiction of the FRET mechanism using the free (left) and bound (right) form of the sensor, where hv is the energy of a photon of light; b.) The general emission spectra of a FRET-type sensor at different concentration of zinc, where [Zn] is the concentration of zinc, λ_{F1} is the emission wavelength of fluorophore 1 and λ_{F2} is the emission wavelength of fluorophore 2.*

1.1.3. Intramolecular charge transfer (ICT) transmissions

ICT transmissions occur in sensors which have a fluorophore with an EDG and an EWG, joined by conjugation. In the absence of zinc, the fluorophore will still have a fluorescence emission. This is because, when excited, the charge is transferred from the EDG to the EWG – this can happen with or without zinc. In the presence of zinc, this fluorescence emission shifts towards the blue region or the red region – these are called a blue shift and red shift respectfully. Whether a blue or red shift occurs is dependent on where the zinc ion binds. If the zinc ion binds to the EDG, the EDG will be less able to donate electrons to the EWG, thus causing a blue shift. If the zinc ion binds to the EWG, this increases the withdrawing capability of the EWG, thus causing a red shift. This is illustrated in **Figure 1.5** by showing the change in energy levels caused by zinc binding and the emission spectra of a typical blue and red shift ICT-type sensor. Due to the difference in wavelengths of their emissions on binding zinc, these ICT-type sensors can be used ratiometrically. [11,12]

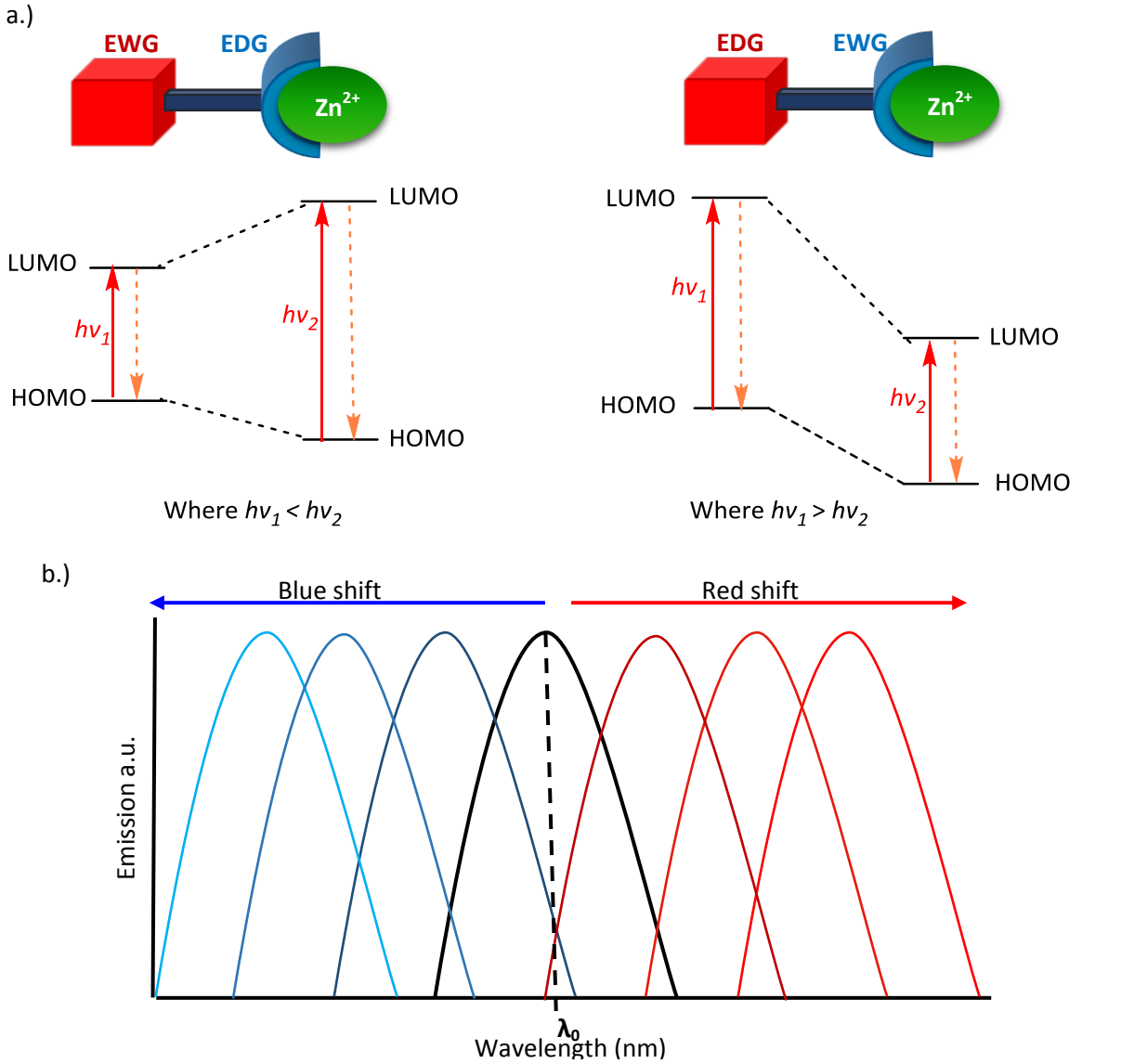

Figure 1.5 *The ICT mechanism. a.) on the left, the energy levels of an EDG upon zinc binding showing an increase in excitation energy required, hence a shorter wavelength, entailing a blue shift. On the right, the energy levels of an EWG upon zinc binding showing a decrease in energy required for electron excitation. This in turn means a longer wavelength, hence a red shift. b.) Another illustration of an ICT-type sensor, showing the change in wavelength of the sensor with a red shift or a blue shift in the emission spectra – where λ_0 denotes the starting wavelength of the sensor*

1.1.4. Photoinduced electron transfer (PET) transmissions

Turn on fluorescent sensors with a fluorophore-linker-receptor structure usually use a PET mechanism. The receptor has a lone pair of electrons, and the donation of an electron to the HOMO of the fluorophore is thermodynamically feasible, as shown in **Figure 1.6**. This full HOMO would require more energy to excite the electron to an excited state, thus quenching fluorescence. When a cation such as Zn^{2+} binds to the receptor lone pair, the energy level of the receptor lone pair lowers. Thus the bound receptor is no longer thermodynamically able to donate an electron to the fluorophore. Hence inhibiting PET transmission and recovering the fluorescence. [13]

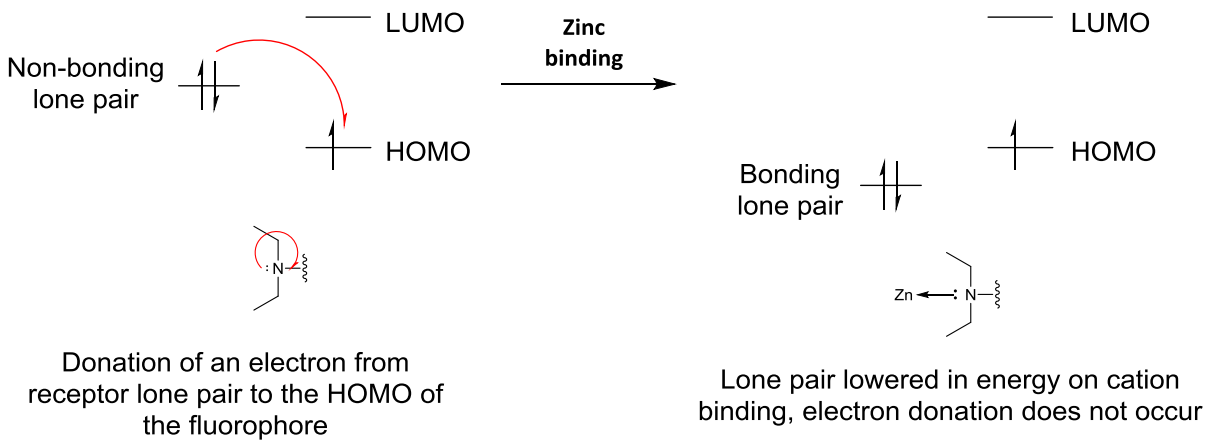

Figure 1.6 *PET mechanism of fluorescence using zinc as the cation example.*

PET-type sensors can display shifts in wavelength, but normally these are too small to make them ratiometric. By introducing another fluorophore as an internal standard, ratiometric measurements can be taken. This is the case with sensor **4**.

1.1.5. How the sensor is ratiometric

For sensor **4** discussed in this report, the naphthalimide fluorophore is switched on once Zn^{2+} binds. This switches the sensor "on" and the triazole moiety gives the naphthalimide a modulated response to levels of zinc. Thus, the fluorescent emission spectra of **4** would have a fluorescent emission peak (for naphthalimide) that appears only once a Zn^{2+} ion binds and which increases in intensity as zinc levels are increased. The coumarin fluorophore has a fluorescent emission peak always present and the intensity of the peak is constant – thus acting as an internal standard as shown in **Figure 1.7**. [14]

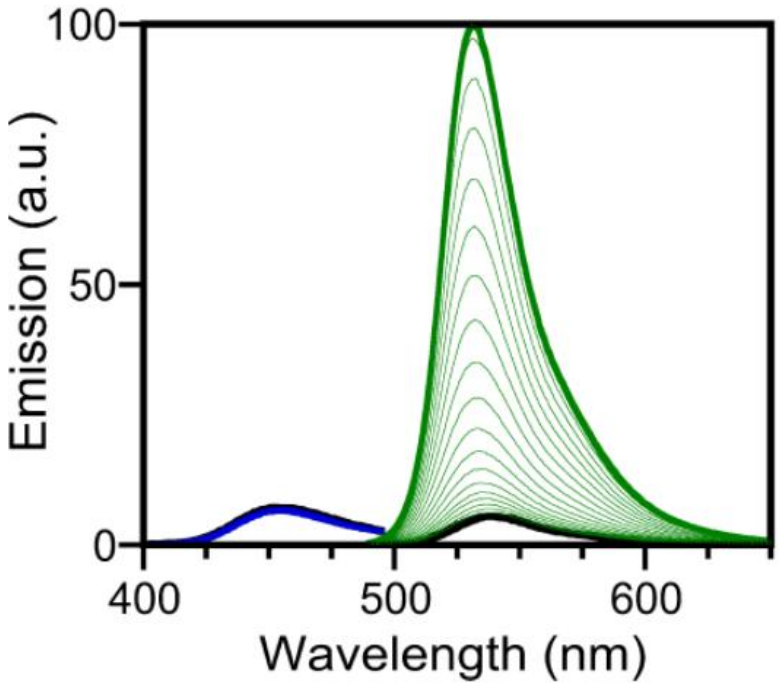

Figure 1.7 *The fluorescent emission spectra of a two-fluorophore zinc sensor. In blue, the emission wavelength of the reference fluorophore, constantly on. In green, the emission wavelength of the turn-on fluorophore, switching on and increasing in intensity as the Zn^{2+} concentration increases.*[14]

1.2. Receptor types

1.2.1. Schiff base receptors

The C=N bond of Schiff bases shows a large increase in fluorescence with chelation of Zn^{2+} to the nitrogen of the C=N moiety. In 2007, Wang and co-workers synthesised a coumarin derivative (**5**) which showed a red shift in λ_{em}, suggesting that it works via an ICT mechanism. Also, **5** had $\varphi_F = 0.3$, that is a 200-fold enhancement upon zinc chelation from $\varphi_F = 0.0015$. Moreover, **5** proved ratiometric, having shown increased fluorescent intensity from zinc concentrations of 0 to 100 µM. The team did acknowledge that their measurements were done in CH_3CN due to lack of solubility of **5** in aqueous solution – a drawback in terms of *in vivo* use. [15]

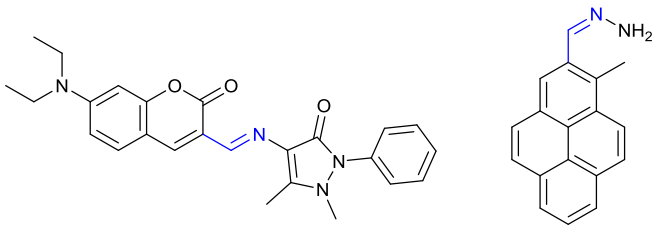

5 **6**

Figure 1.8 *Examples of Schiff bases incorporated into sensors for zinc detection. Receptor sections are highlighted in blue.*

In 2010 Yoon and co-workers synthesised the hydrazine-pyrene sensor **6** which had no change in the λ_{ex} upon binding zinc, thus indicating the use of a PET mechanism in action. Upon chelation of zinc, the electrons on the nitrogen of the C=N moiety were no longer available thus quenching the PET mechanism. Notably, **6** is very selective for zinc and was applied for detection of zinc levels in pancreatic cells. Thus confirming its viability *in vivo*. [16] Receptors employing Schiff bases are usually poorly soluble in aqueous solutions – **6** being an exception. Even without the issue of solubility, there is a risk of hydrolysis of the C=N bond, making Schiff bases generally unsuitable for biological use.

1.2.2. Iminodiacetic acid receptors

These receptors generally have very good affinity for Zn^{2+} ions in the nanomolar range such as **7** and **8** synthesised by Gee and co-workers,[17] **9** by Gunnlaugsson and co-workers,[18] and **10** by Katerinopolous and co-workers.[19] In fact **10** could detect zinc concentrations as low as 4 nM. This means that they are highly sensitive to zinc concentration levels. The main shortfall stems from the fact that these receptors were previously used as Ca^{2+} sensors. The affinity for Ca^{2+} is usually very weak to negligible as in the case of the examples given here. However, it could be argued that even a low risk of competitive Ca^{2+} binding *in vivo* can interfere with accurate measurements of zinc levels.

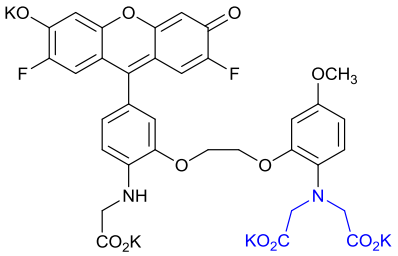

7

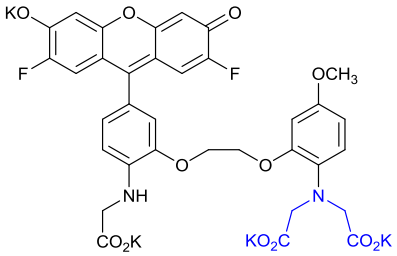

8

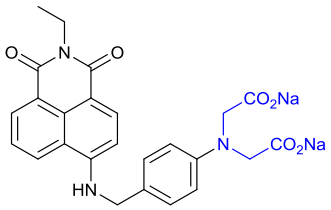

9

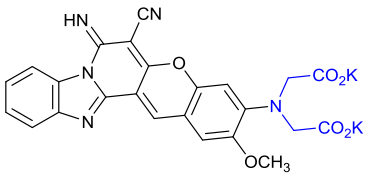

10

Figure 1.9 *Notable iminodiacetic acid-based receptors. Sensors **7** and **8** use a fluorescein fluorophore, **9** uses a naphthalimide fluorophore and **10** uses a chromeno[3',2':3,4]pyrido[1,2a][1,3]benzimidazole fluorophore. Receptor sections are highlighted in blue.*

1.2.3. Acyclic and cyclic polyamine receptors

Aliphatic amines are the simplest examples of fluorescent transition metal sensors that use a PET mechanism. They have modest selectivity for Zn^{2+} over other transition metals. The use of polyamines does increase binding affinity to transition metal ions but not necessarily increase selectivity for Zn^{2+}.

To compare polyamine receptor, **11**-**13** were proposed which all use anthracene receptors. Sensor **11** uses two diamine receptors[20] and **12** uses a tetraamine receptor. [21] Sensor **13** employs a tetraamine receptor bound to two terminal anthracene fluorophores. Sensor **13** is one of the first ratiometric zinc sensors successful in aqueous solution. One drawback of polyamines is the competitive binding of protons and metal ions to the nitrogen atom. [22]

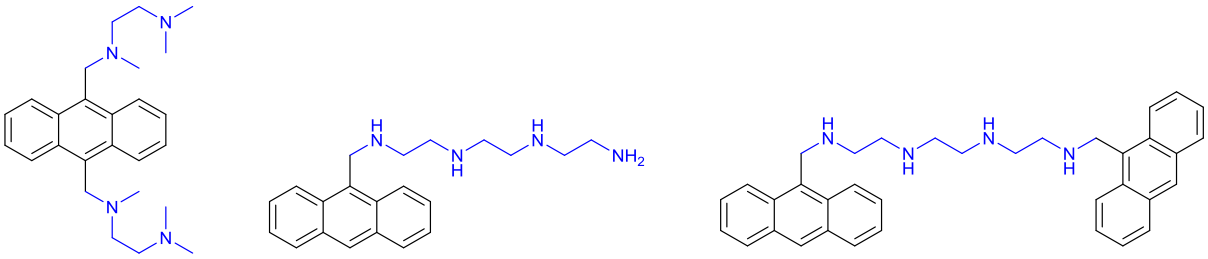

11 **12** **13**

Figure 1.10 *Acyclic polyamine sensors using anthracene with receptor sections highlighted in blue.*

Macrocyclic polyamines generally form stable Zn^{2+} complexes in aqueous solutions at neutral pH. Following from this, the use of cyclens and cyclams have been successful in zinc sensing such as **2** and **14** respectfully. [22,9]

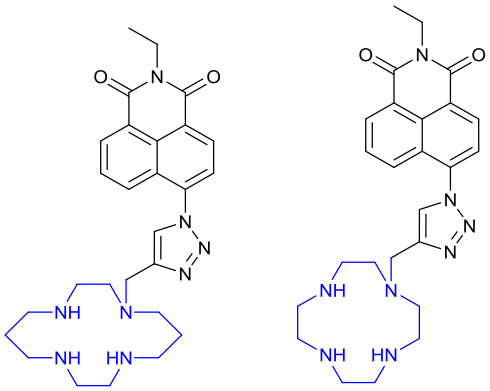

2 **14**

Figure 1.11 *Cyclic polyamine examples using a cyclen receptor (left) and cyclam receptor (right) by Watkinson and co-workers.*

1.2.4. Bipyridine (BIPY) receptors

BIPY receptors are simple to prepare and functionalise, they are stable at physiological pH and can bind to an array of *d*- and *f*-block metals. Sensor **15** has λ_{ex} = 370 nm and λ_{em} = 370 nm when free (in CH_3CN). Upon 1.5 equivalents of zinc, λ_{em} increases to 528 nm due to the binding of Zn^{2+} to BIPY, causing a visible colour change to green via a PET mechanism. With the addition of another zinc equivalence, λ_{em} increases further to 587 nm. This second addition causes zinc to bind at a second binding site – the spirolactam carbonyl on the rhodamine, causing the rhodamine-moiety to fluoresce (shown in pink in **Figure 1.12**). The zinc-spirolactam binding introduces a FRET mechanism, causing a second colour change from green to orange. [23]

Another notable BIPY based sensor is **16**, synthesised by Mandal and co-workers. This sensor interestingly uses a three-photon excitation. Three-photon excitations allow for even lower energies of excitation to be used compared to two-photon excitations. [24] Also, **16** was used in HeLa cells (at 1200 nm, 40 nm per photon) confirming their biocompatibility.

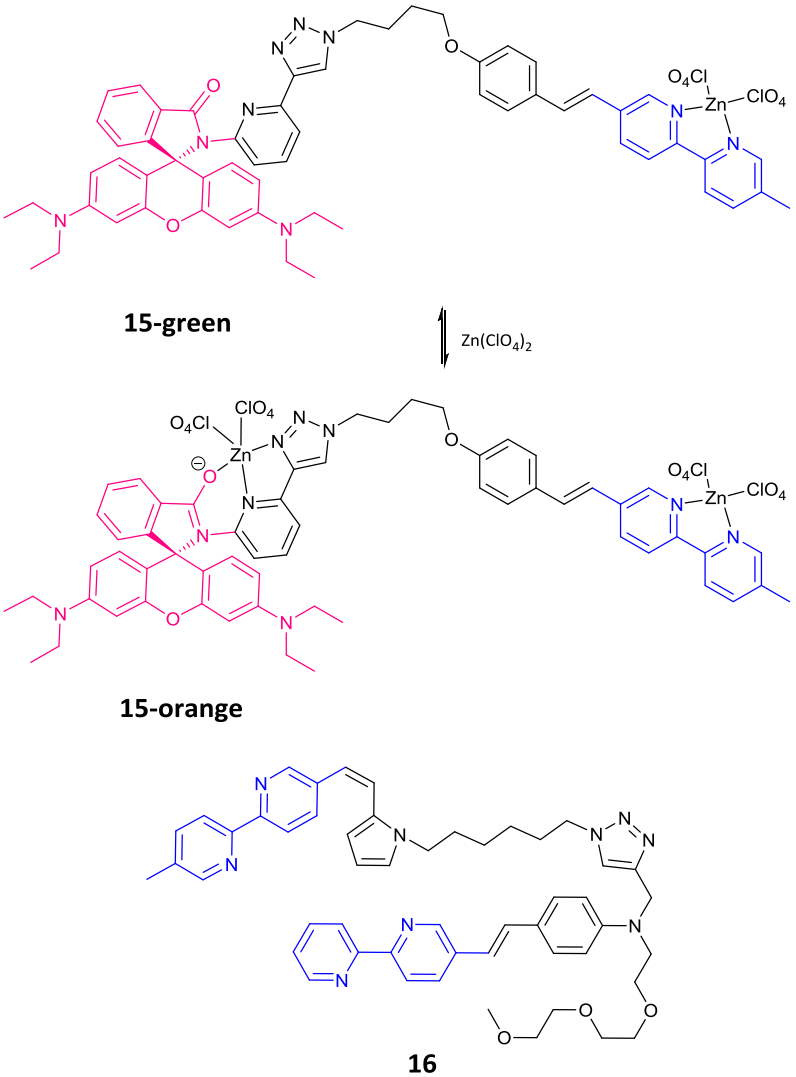

Figure 1.12 *Sensors **15** and **16**, showing the BIPY receptor in blue. In the case of **15**, the PET-FRET mechanism of **15** is shown where the second rhodamine-based binding site is highlighted in pink. $Zn(ClO_4)_2$ is used in this example as it is the usual zinc source when testing zinc sensors.*

1.2.5. Quinoline receptors

Compound **17** was the first sensor selective enough for Zn^{2+} even at high concentrations of Ca^{2+} and Mg^{2+} ions.[25] It is also membrane-permeable but has poor water solubility. Compound **18** (**Figure 1.13**) was reported as a water soluble and ratiometric fluorescent zinc sensor.[26]

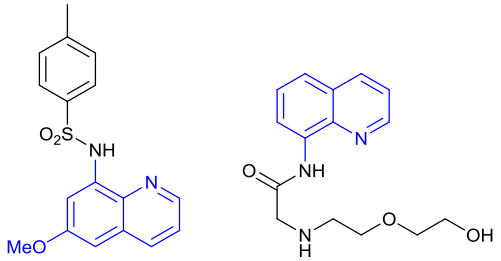

17 **18**

Figure 1.13 *Quinoline based receptors exemplifying the different solubilities possible.*

Quinoline on its own is not a good enough receptor, it needs ligands to help coordinate Zn^{2+}. [27] Jiang and co-workers incorporated DPA at position 2 and a carboxylic acid at position 8 of 8-hydroxy-2-methylquinoline to give compound **19**.[28] Sensor **19** is a water soluble, hexadentate sensor that has a high binding affinity and high selectivity for Zn^{2+}. The zinc coordination was confirmed by studying the crystal structure and through NMR spectra.

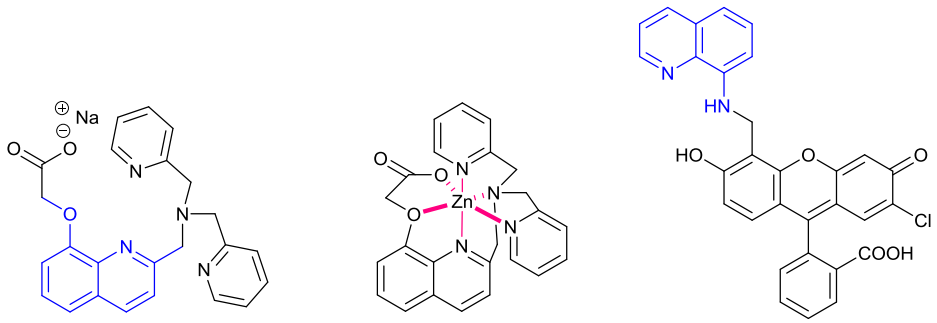

19 **Zinc-bound 19** **20**

Figure 1.14 *Sensors **19** and **20** with the quinoline receptor in blue, and the zinc-bound **19,** where the hexadentate coordination of zinc is highlighted in pink.*

Quinoline derivatives act as both receptor and fluorophore. However, they usually require high energy UV excitation which can damage the tissue in biological environments. [28] Lippard and co-workers synthesised **20** (**Figure 1.14**), which overcomes these shortfalls by using quinoline as a receptor and fluorescein as a fluorophore.[29] Sensor **20** proved to be cell-permeable and sensitive to zinc concentrations at the micromolar level – more sensitive than most other DPA receptor based sensors which are covered in the section below.

1.2.6. Di-2-picolylamine (DPA) receptors

DPA is the most prevalent of the receptors due to its high selectivity for Zn^{2+} ions and general good membrane permeability. [27] DPA based receptors are also very biocompatible, have fast chelation to Zn^{2+} ions and are commercially available. [27] In the past DPA has been directly linked to a fluorophore at the secondary amine, and compound **21** synthesised by Xu and co-workers, uses an amide derivative of DPA.[30] This sensor is an example of "receptor transformation", as shown in **Figure 1.15**. Upon binding to a heavy metal ion such as Cd^{2+}, the fluorescence shows a blue shift from λ_{em} = 483 nm to λ_{em} = 446 nm, making the solution blue. However, Zn^{2+} preferentially binds to sensor **21**, meaning that even if Cd^{2+} is bound, a Zn^{2+} ion can displace the heavy metal ion. This is because both metal ions bind through a different tautomer, with zinc binding through the imidic tautomer.

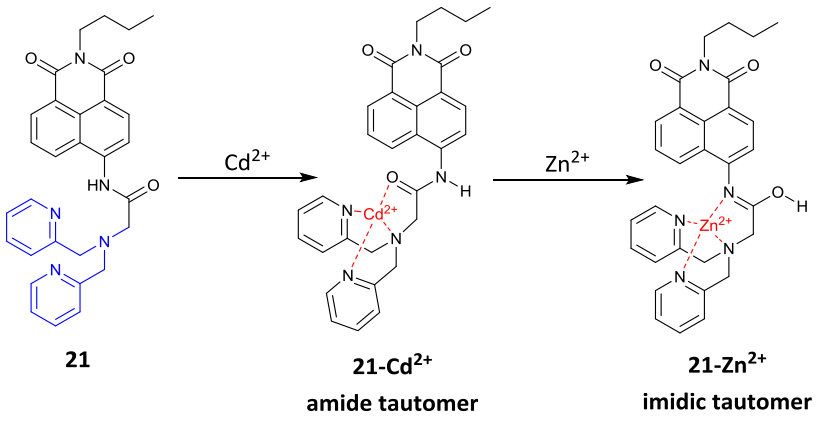

Figure 1.15 *The different binding modes of **21** with Cd^{2+} and Zn^{2+}.*

1.2.7. N,N,N'-tris(pyridin-2-ylmethyl)ethylenediamine (TRPEN) receptors

In 2006, Xu and co-workers, synthesised **22**, which utilises a DPA-derived TRPEN receptor to yield a ratiometric zinc sensor (φ_F = 0.14).[31] The secondary amine of the TRPEN receptor is deprotonated when zinc binds (pK_a = 6.5 when bound). Thus in 2007, Xu's team also synthesised **23** which has an extra site for deprotonation, increasing the cation binding affinity. [32] Moreover, **23** could also distinguish between Cd^{2+} and Zn^{2+} through an ICT mechanism. With Cd^{2+} chelation **23** had a blue shift from λ_{em} = 531 nm to λ_{em} = 487 nm, whereas Zn^{2+} chelation caused a red shift from λ_{em} = 531 nm to λ_{em} = 558 nm (φ_F = 0.60 and 0.23 for Cd^{2+} and Zn^{2+} respectively).

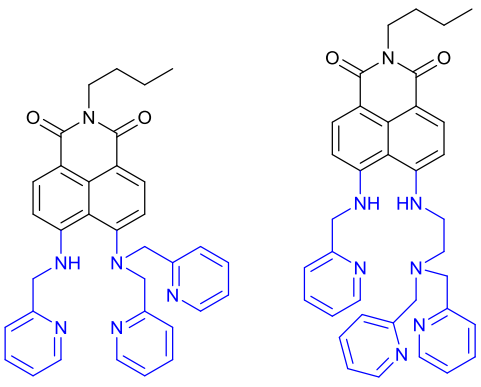

Figure 1.16 *Sensors utilising the TRPEN receptor, highlighted in blue.*

1.2.8. Triazole receptors

Triazole groups have also been shown to act as monodentate ligands for Zn^{2+} ions when used in conjunction with another receptor. Using a triazole to link a main receptor to a fluorophore thus provides the main receptor with another ligand to chelate Zn^{2+}.[28] Furthermore, they are biocompatible and easy to prepare through CuAAC reactions. Sensor **24** uses DPA as the main receptor and triazole as the contributing receptor. [33]

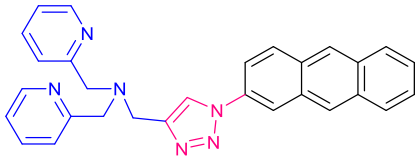

24

Figure 1.17 *A DPA-triazole-anthracene sensor where the DPA moiety is highlighted in blue and the triazole moiety is highlighted in pink.*

1.2.9. Conclusion on receptor types

The main criteria that need to be fulfilled by any receptor are:

- High binding affinity for zinc
- High binding selectivity for zinc over other endogenous transition or alkali metals
- Good sensitivity to zinc ion levels, in the nM to µM range
- Stability to physiological conditions: pH stability around pH 7 and good aqueous solubility.

In any case, it seems clear that due to the countless criteria that need to be fulfilled, receptor diversity is key. Examples of such sensors are **21** (**Figure 1.15**) which uses DPA as the main receptor and a Schiff base as the contributing receptor and **24** (**Figure 1.17**) which again uses DPA as the main receptor and a triazole group as the contributing receptor.

Moreover, the triazole linkage is very accessible, arising from a convenient CuAAC reaction which has been successfully employed in previous work within this research group. These CuAAC reactions generate compounds by linking modular units together via a facile, high yielding and selective reaction – thus "clicking" them together. The full advantages of using the CuAAC reaction will be discussed within this report. This modular approach is explained further later on in this report.

For this reason, a DPA-triazole based zinc sensor was chosen for synthesis in this project. As discussed above, the tridentate DPA along with the monodentate triazole group together would chelate Zn^{2+} in a four coordination geometry

1.3. Fluorophore types

Fluorescent sensors allow the spatial and temporal visualisation of desired targets *in vivo* with very simple instrumental set up. As mentioned previously, autofluorescence can become problematic when applying fluorescent sensors to a system and taking measurements. Autofluorescence causes background noise, thus a high signal to noise ratio means that there is little noise compared to the signal measured. To minimise autofluorescence and achieve a high signal to noise ratio, fluorophores with low excitation energies (high λ_{ex}) are preferred. Hence, fluorophores with λ_{ex} values closer to the infrared region are preferentially desired – these are called Near Infrared (NIR) fluorophores[34] – these are fluorescent compounds that have emission wavelengths in the 650 – 900 nm range. Not all the fluorophores mentioned in this report are of the NIR type but NIR fluorophores would be more biologically viable. There are quite a few fluorophore types and the most popular fluorophores are discussed in this section to give an idea of the advantages and disadvantages of each.

It should be noted that many fluorophores fall into the CCS family, including fluorescein, coumarin, rhodamine, cyanine and BODIPY, where extending the π-system increases fluorescence through substitution on the aromatic ring.[35] The correlation between increasing conjugation and increased fluorescence measured through φ_F was investigated by Yamaguchi and co-workers in 2008. [36] Four of the compounds investigated were naphthalene (**25**), anthracene (**26**), pyrene (**27**) and perylene (**28**) shown in **Figure 1.18a**. The team measured φ_F experimentally for **25**-**28** and compared these values against the measured λ_{ex} and λ_{em} of each compound. The tabulated and graphically represented results in **Figure 1.18b-c** show that there is a correlation between increasing conjugated systems and increased absolute φ_F.

a.)

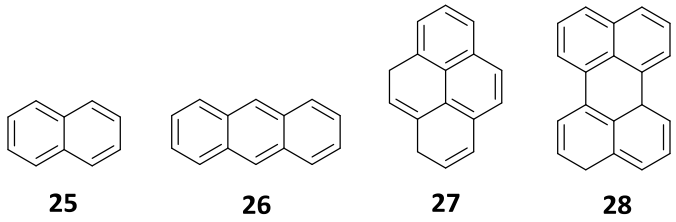

b.)

Compound	φ_F	λ_{ex} (nm)	λ_{em} (nm)
25	0.02	286	323
26	0.13	379	383
27	0.26	338	373
28	0.90	438	448

c.)

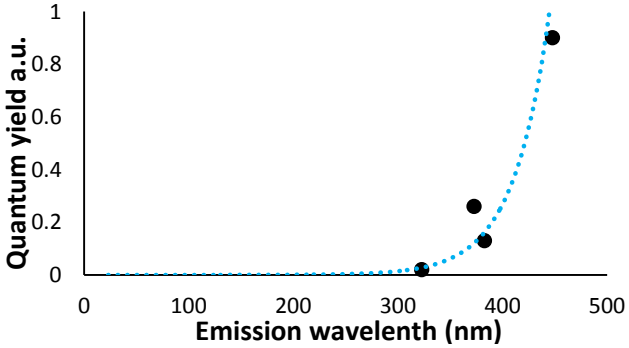

Figure 1.18 *a.) The structures of compounds studied by Yamaguchi and co-workers in order of least conjugated to most conjugated π systems (left to right). b.) The tabulated results found by the group for compounds* ***25-28****. Measurements were taken in chloroform for all compounds except for* ***27*** *which was done in cyclohexane. This may account for the results of* ***27*** *not matching the general trend of increasing conjugation leading to increasing λ_{em}. c.) A graph showing the exponential relationship between the quantum yield and λ_{em} for increasingly conjugated systems.*

1.3.1. Fluorescein fluorophores

Fluorescein (**29**) is one of the first fluorescent compounds to be utilised and the source of its fluorescence is the pyronin moiety as shown in **Figure 1.19**.[34]

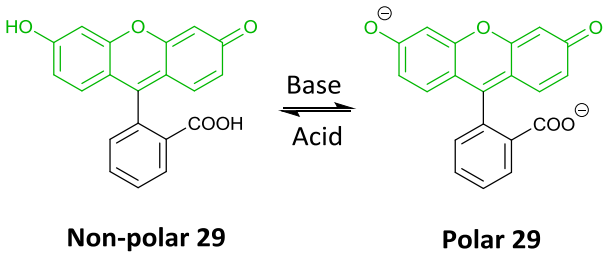

Figure 1.19 *The structure of polar and non-polar fluorescein (pK_a = 6.4), with the pyronin unit highlighted in green.*

Lippard and co-workers used a fluorescein-based fluorophore linked to two DPA receptors, **30** (φ_F = 0.87), as a starting point to create a library of fluorescent zinc sensors. [37] The team even introduced peptides to introduce rigidity between two fluorophores in the case of **31** and as biological targeting units in **32** (φ_F = 0.79).[14,38] Theoretically these peptide chains can be hydrolysed by proteolytic enzymes, yet Lippard and co-workers reported that **31** could quantitatively detect zinc levels in prostatic cells and **32** was said to target the plasma membrane well.

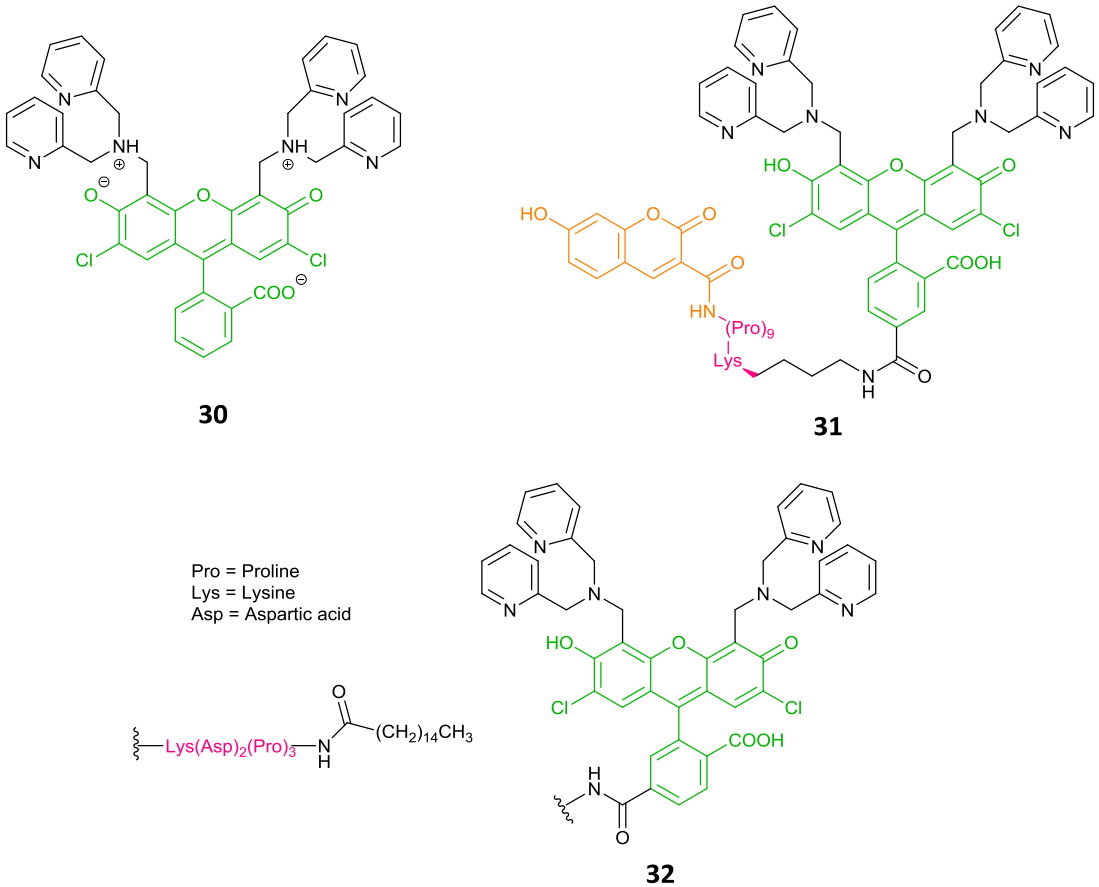

Figure 1.20 *Fluorescein-DPA receptors synthesised by Lippard and co-workers. Fluorescein units are highlighted in green, peptide units in pink, and in the case of **31**, the second fluorophore (coumarin) is in orange.*

1.3.2. Rhodamine fluorophores

As with fluorescein, the pyronin unit is the origin of rhodamine fluorescence (**33**). First described in 1887 by Maurice Ceresole,[39] in recent years this fluorophore has gained popularity again as a fluorophore of choice. This popularity can be attributed to advances in increasing the emission wavelength of rhodamine based fluorophores towards the NIR region. One of the few notable advances made was of **34**, a cyanine-rhodamine fluorophore with strong NIR fluorescence by Lin and co-workers.[40] Sensor **34** displayed solubility in ethanol with a very good φ_F of 0.56 and a λ_{em} of 721 nm (NIR).

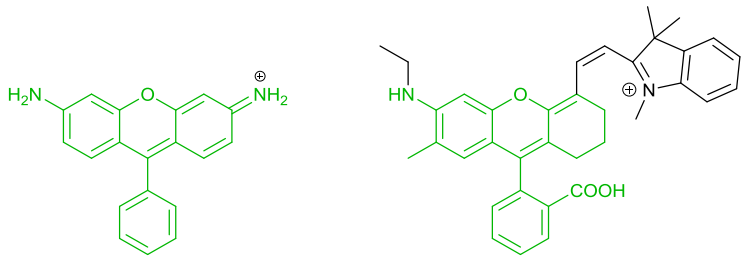

33 **34**

Figure 1.21 *The rhodamine core (left) and a NIR rhodamine-based fluorophore (right).*

Rhodamine based fluorophores are relatively hydrophilic due to the cationic nature, causing accumulation in mitochondria – thus limiting their use. Conversely, NIR rhodamine based fluorophores tend to be more hydrophobic than regular rhodamine based fluorophores, compromising their cell permeability. In fact, sulfonate incorporated rhodamines show nearly no cell permeability. [41] Finding a balance between cell permeability and cell accumulation is challenging but key.

1.3.3. Coumarin fluorophores

Coumarin is a relatively photostable fluorophore with a long emission wavelength and facile synthesis and functionalisation.[42] Coumarins on their own have a low fluorescent quantum yield and so strategic substitution is required. Tasior and co-workers showed that substitution of coumarin at the 7- position with a diethylamino group along with an ethoxycarbonyl group at the 3- position (**35**) increased the λ_{em} from 380 nm to 529 nm (φ_F = 0.002 to φ_F = 0.81).[43] In fact the 7-diethylamino group alone increased the emission wavelength to 440 nm (φ_F = 0.73). Thus coumarin based fluorophores are best designed with an electron-donating group at the 7- position and an electron-withdrawing group at the 3- position to maximise resonance stabilisation as shown in **Figure 1.22**.

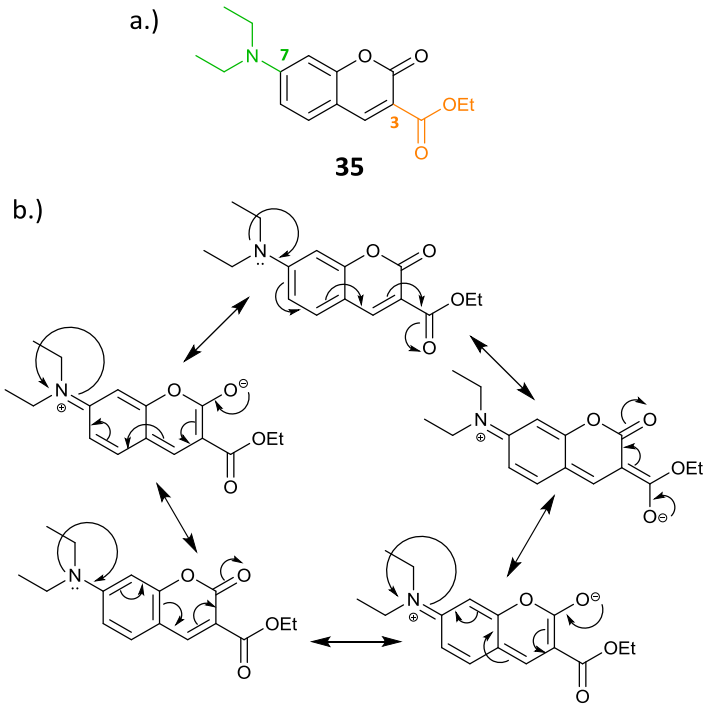

Figure 1.22 *a.) Coumarin substituted at the 7- (green) and 3-position (orange). b.) Resonance stabilisation of* ***35****.*

As mentioned previously, coumarins are part of the CCS family of fluorophores. Shi and Ma found that CCS fluorophores are well suited for qualitative "switch off/on" sensors.[35] The more desired ratiometric sensors however, can be achieved by incorporating a second reference fluorophore in the sensor.

1.3.4. 4-amino-1,8-naphthalimide fluorophores

Some naphthalimide based sensors have been mentioned already (**21-23**) which used DPA and DPA-derived receptors. In 2013, Zhao and co-workers synthesised a naphthalimide based sensor with a "switch off/on" response highly selective to Zn^{2+} over many metal ions including Na^{+}, Cu^{2+}, Fe^{2+} and Mg^{2+}. The sensor **36** displayed a λ_{em} at 556 nm with a λ_{ex} of 410 nm, with an increasing intensity of emission with the addition of up to 20 increasing equivalents of Zn^{2+}. The free sensor was weakly fluorescent with a φ_F of 0.016, and upon zinc chelation, **36** had up to a 13-fold increase in fluorescence (φ_F = 0.208). Interestingly, **36** also showed different fluorescent emission colours in the cell nucleus compared to the cytoplasm. This is attributed to differing binding capabilities of **36** to DNA and RNA, broadening the biological potential of **36**. [44]

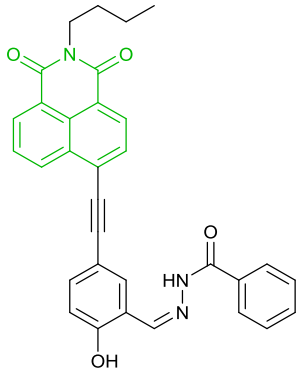

36

Figure 1.23 *A naphthalimide based sensor, with the naphthalimide fluorophore highlighted in green.*

1.3.5. Conclusion on fluorophore types

There are quite a few fluorophores to choose from, and as mentioned, a two fluorophore system is being used in this project. Bag and co-workers[45] showed that triazoles linked to a fluorophore have the ability to modulate the fluorescent emission response of the fluorophore – giving rise to a ratiometric quality. Thus naphthalimides with a triazole linked to it shows promise as a potential fluorophore and the fact that a DPA-triazole receptor is being chosen in this report further compliments the use of a naphthalimide-triazole based sensor.

On top of this, the coumarin fluorophore is particularly interesting as they are part of the CCS family of fluorophores and the work by Shia and Ma showed that using a reference fluorophore in a sensor can give a sensor the desirable ratiometric quality.[35] In this way, a coumarin fluorophore will also be incorporated in the sensor as a reference fluorophore to give this sensor a ratiometric ability.

The modulated effect that triazole has on the naphthalimide fluorophore will allow for changes in fluorescence emissions over different concentrations of zinc and the coumarin fluorophore will be constantly fluorescing ("on") to act as the reference fluorophore. This coumarin moiety will be attached to the naphthalimide moiety by a linker to ensure the two fluorescent centres do not quench each other. This gives the design of the sensor as DPA-triazole-naphthalimide-linker-coumarin. The chosen linker design will be discussed in the following section.

1.4. Linker types

The role of the linker is two-fold. It acts as a spacer between the two fluorophores so as to minimise the chances that the two fluorophores interact with each other and give skewed measurements.

As shown previously is compounds **31** and **32**, Lippard and co-workers incorporated peptide linkers into fluorescent sensors. The polypeptide chain is rigid – thus in the case of a two-fluorophore sensor, it can ensure that the respective fluorophores are not spatially close enough to self-quench in a FRET-like manner. These peptide chains can also help with biological targeting. However, the use of peptides are precarious *in vivo* due to the risk of peptide bond hydrolysis by proteases. For this reason a peptide linkage was avoided in this project.

Also, as the sensor rationalised thus far has extensive conjugation throughout it will be very hydrophobic which is not ideal for biological use due to non-specific binding but more importantly aqueous solubility.[46] A hydrophilic linker would introduce a balance between the high conjugation and the hydrophilic environment. Tahtaoui and co-workers[47] found that using a polyethylene glycol (PEG) linker overcame these issues of hydrophobicity (**37** in **Figure 1.24**). Furthermore, Kumar and co-workers reported that using a PEG linker improved solubility of a coumarin based sensor in a range of solvents.[48] A tetraethylene glycol (PEG_4) linker (**38**) will be employed between the naphthalimide and coumarin fluorophores. Assuming the linker does not fold under biological conditions, a space of roughly 14.0 Å would be introduced between the two fluorophores, based on the value of 3.5 Å for one PEG monomer. [49]

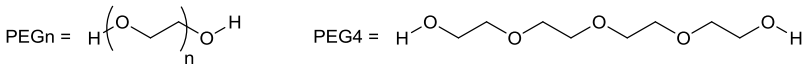

37 **38**

Figure 1.24 *PEG linkers.*

1.5. The copper-catalysed azide-alkyne cycloaddition (CuAAC)

As mentioned, Bag and co-workers found that fluorophores can present modulated responses when linked to a triazole unit.[45] Following on from this, Ramchander and co-workers investigated the use of naphthalimide fluorophores with triazole units linked to them.[50] Their rationale was that a modular approach to sensor synthesis is attractive due to ease of synthesis and manipulation.

The term "click" chemistry was first coined by Sharpless in 2001 describing high yielding reactions, with high atom economy and a large thermodynamic driving force. Furthermore, these reactions are simple to perform and carried out in benign solvents with products that are easily isolatable (preferably though non-chromatographic methods). The "clicking" of smaller units together makes the synthesis of larger molecules more accessible and allows a large library of analogues to be synthesised. [51] The Huisgen 1,3-dipolar cycloaddition of azides to alkynes (**Figure 1.25**) fulfils many of the criteria of a click reaction. However, a mixture of the 1,4- and 1,5-disubstituted triazoles is obtained, not to mention the high temperatures required. For this reason the Huisgen 1,3-dipolar cycloaddition is not strictly considered a click reaction.

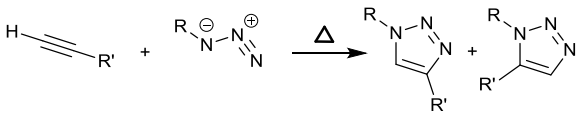

Figure 1.25 *The Huisgen 1,3-dipolar cycloaddition, forming two regioisomers, the 1,4-disubstituted triazole (left) and the 1,5-disubstituted triazole (right).*

The introduction of the CuAAC reaction (**Figure 1.26**) differs from the Huisgen 1,3-dipolar cycloaddition only in the addition of a copper catalyst and the mild temperatures used. These reactions can even occur at room temperature and lead to the stereoselective production of the 1,4-disubstituted triazole. [52] The CuAAC reaction has, in theory, 100% atom economy due to the production of only on product from the complete incorporation of starting azide and alkyne. Hence this copper-catalysed version of the Huisgen 1,3-dipolar cycloaddition is indeed the most popular type of "click" reaction used in chemical synthesis.

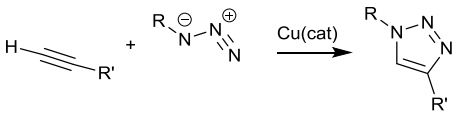

Figure 1.26 *The CuAAC reaction, selectively forming the 1,4-disubstituted triazole.*

Just last year, Bertrand and co-workers isolated a bis(copper) intermediate from the CuAAC reaction, supporting the full CuAAC mechanism as shown in **Figure 1.27**. The CuAAC mechanism can also go via a mono(copper) intermediate, but the team used kinetic studies to show that the reaction involving two equivalents of copper catalyst is kinetically favoured. [53]

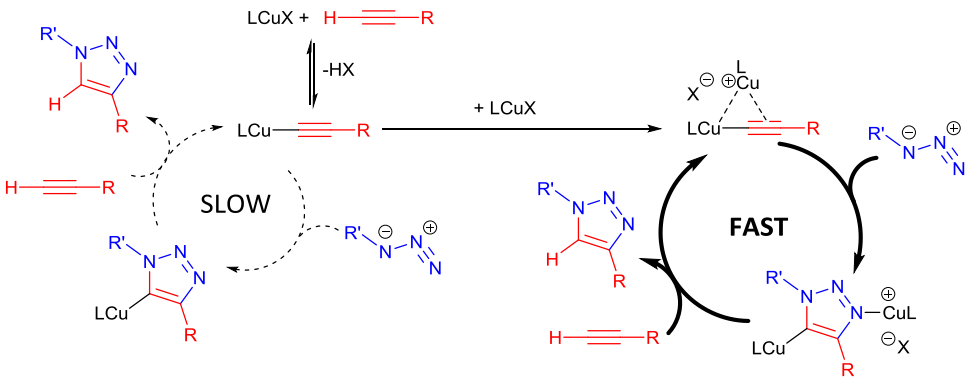

Figure 1.27 *The CuAAC reaction, showing the mono-copper pathway (left) and the bis-copper pathway (right), where L = $NCCH_3$ and X = PF_6. Both mechanisms were found to be possible, but the bis-copper pathway was found to be kinetically favoured.*

1.6. The final sensor to be synthesised

The sensor **4** to be synthesised in this project was DPA-triazole-naphthalimide-PEG_4-coumarin, shown in **Figure 1.28**. To summarise, the DPA acts as the main receptor region, coordinating Zn^{2+} with the three nitrogen atoms in DPA. The advantages of the triazole moiety are threefold. Firstly they allow for the facile synthesis of the sensor in a modular fashion using "click" chemistry. Secondly, the act as a contributing receptor to chelate Zn^{2+} ions which increases binding affinity. And lastly, they have the ability to introduce a modulated fluorescent emission response into the fluorophore at different Zn^{2+} concentrations. The naphthalimide fluorophore linked to the triazole should give a modulated response to zinc ion levels and the coumarin fluorophore is used as a reference fluorophore. The two fluorophores being used are linked by a PEG_4 linker that increases solubility in biological environments and decreases chances of self-quenching between the two fluorophores.

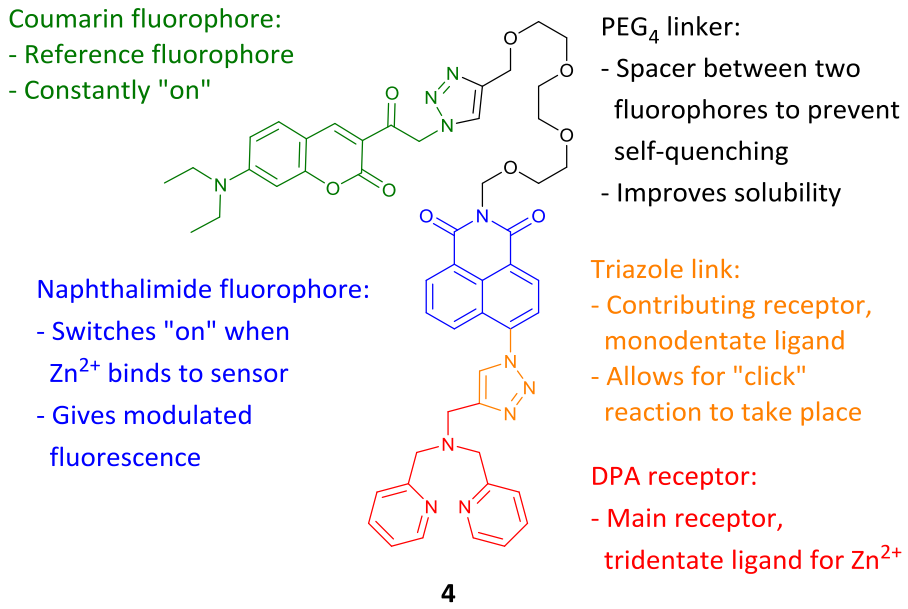

Figure 1.28 *Final sensor to be synthesised.*

2. Discussion of synthetic work

2.1. Synthesis of CuAAC precursors

As the CuAAC synthesis follows a modular approach, the synthesis of modular units needed to be completed first. The retrosynthetic breakdown of the modular units needed to synthesise **4** is shown in **Figure 2.0**.

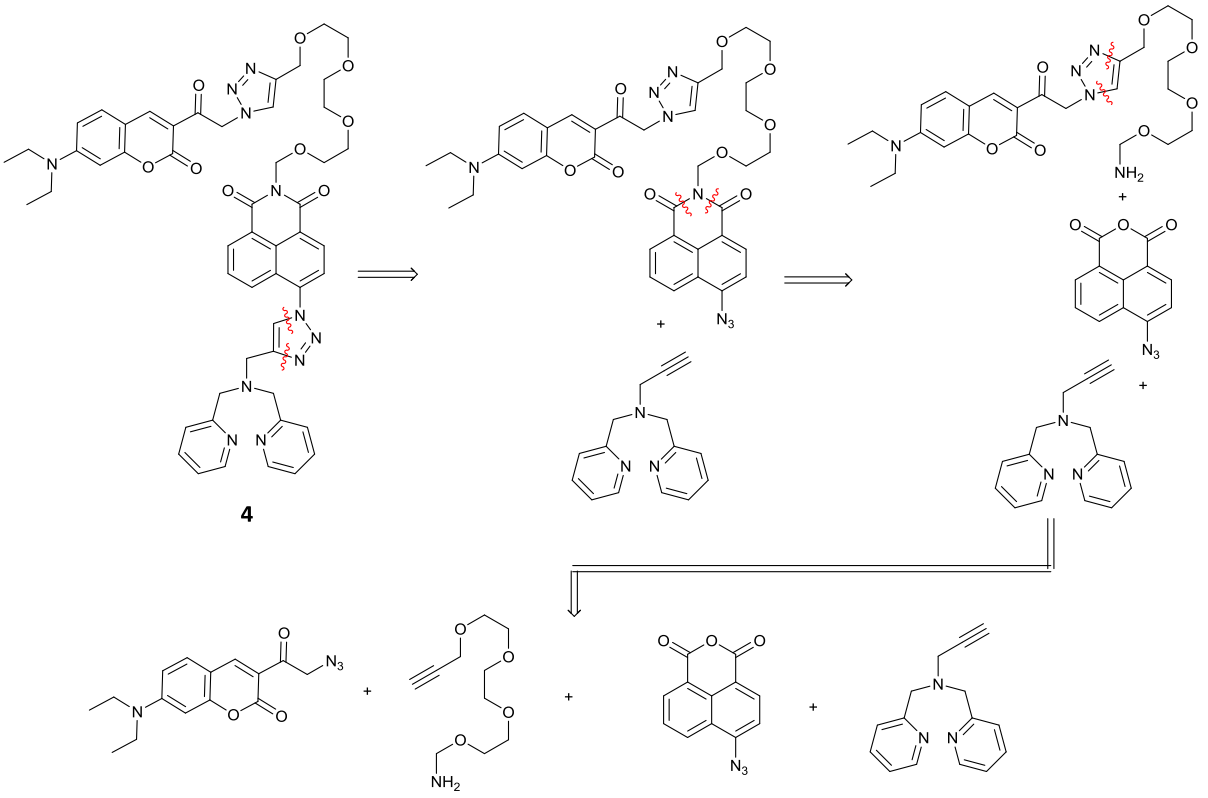

Figure 2.0 *The retrosynthetic analysis of sensor* ***4*** *into 4 modular units to be synthesised.*

*2.1.1. Synthesis of azido coumarin (**39**)*

The first unit to be synthesised was the coumarin fluorophore **39**, using the synthetic approach shown in **Figure 2.1**.

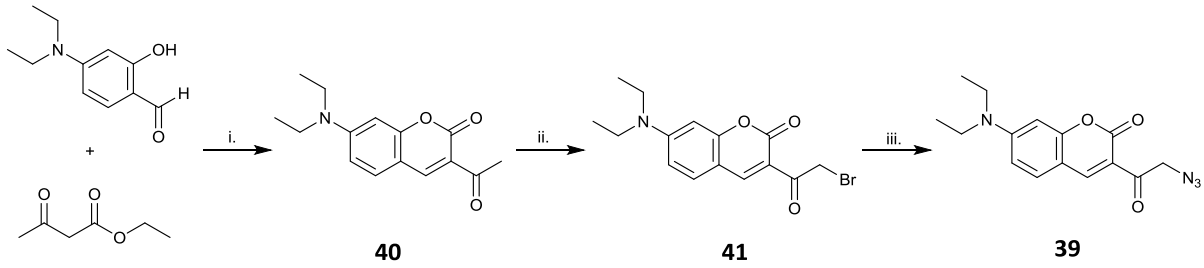

***Figure 2.1** Synthetic route towards **39**. i.) Piperidine, RT, 30 min. ii.) $CuBr_2$, EtOH, reflux under N_2, 90 °C, overnight. iii.) NaN_3, dry THF, 40 °C, overnight.*

The base-catalysed condensation of commercially available reagents, 4-(diethylamino) salicylaldehyde and ethyl acetoacetate was carried out to give **40** in good yield (80%) with minimal purification. [54] Production of **40** was confirmed by ^{1}H NMR, which also confirmed the reaction went cleanly and no further purification step was needed. The aromatic starting material has only three aromatic protons and thus three aromatic signals would be seen in the ^{1}H NMR. A successful condensation of the two starting reagents requires the formation of a new C-C bond to give another aromatic ring. Thus **40** would have four aromatic hydrogens, showing four aromatic signals in the ^{1}H NMR as shown in **Figure 2.2.**

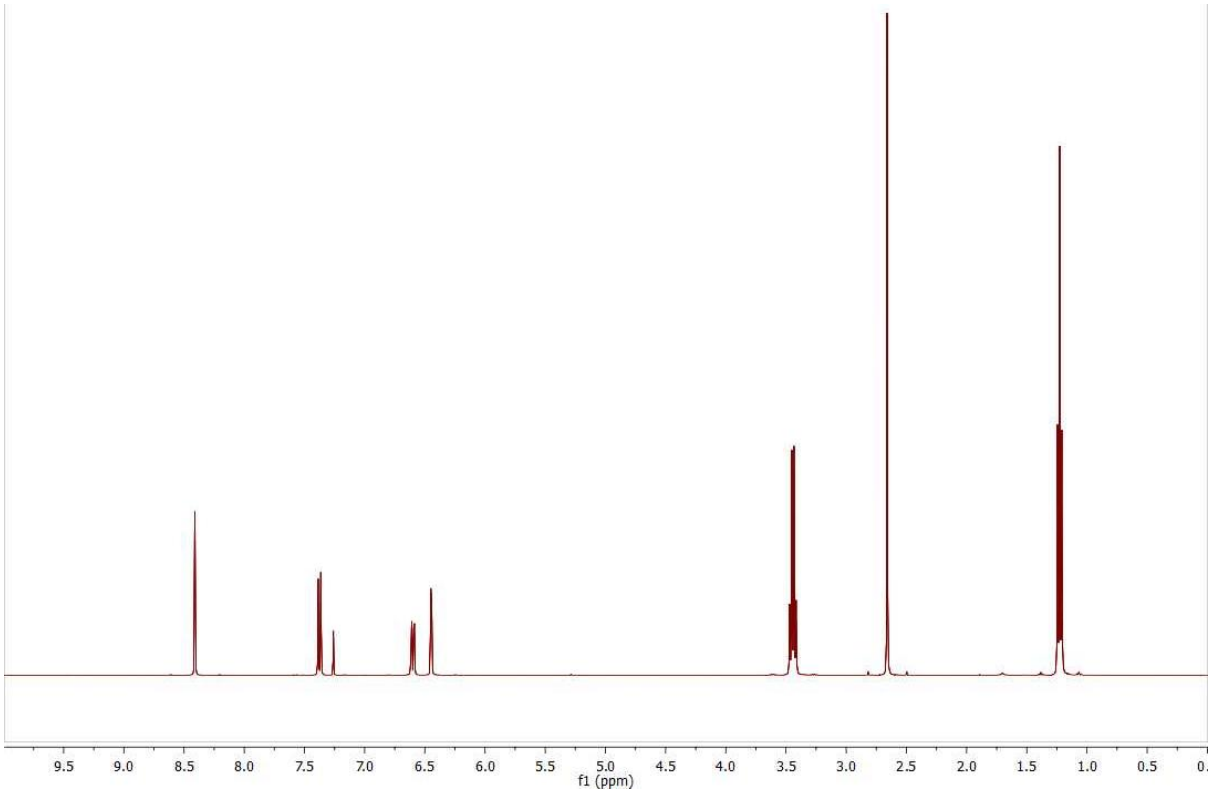

***Figure 2.2** ^{1}H NMR spectra of **40** showing four peaks in the aromatic region ($CHCl_3$ peak at 7.26 ppm).*

Thus compound **40** was carried forward to synthesise **41**. Previous work in our research group included efforts in effective bromination steps and found that the procedure by Lin and co-workers worked well, with no by-products.[55] Thus **40** was brominated using $CuBr_2$ as the bromine source. The literature procedure by Lin and co-workers uses **40**:$CuBr_2$ in a 1:2 ratio. This is because the mechanism involves a bis(copper) intermediate (**Figure 2.3**). [56] The reaction was carried out three times and the results are tabulated in **Table 1.0**.

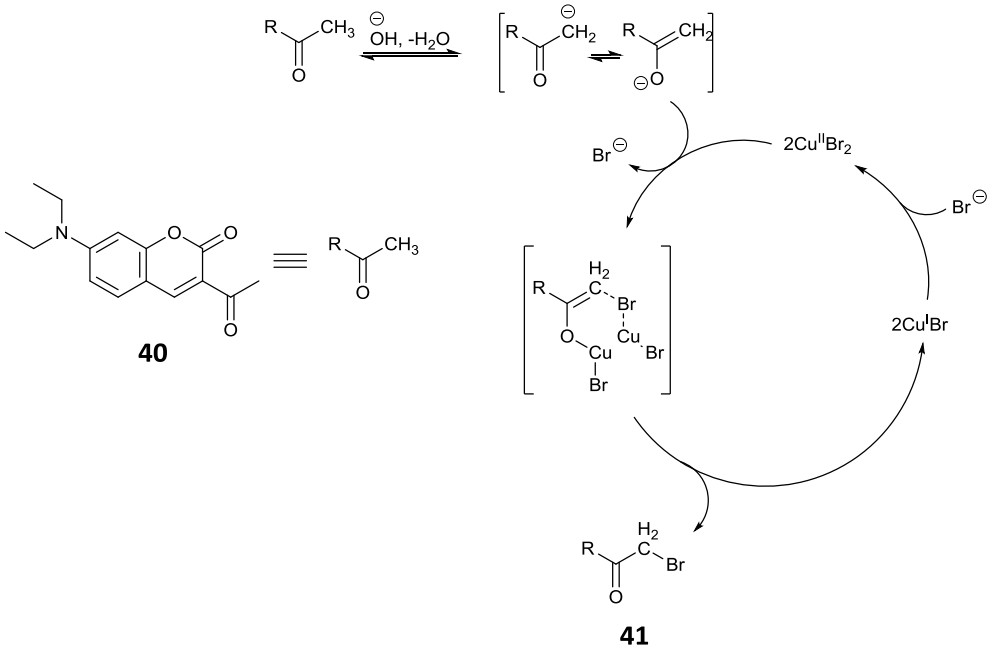

Figure 2.3 *The catalytic pathway for the selective bromination of ketone **40** to α-bromoketone **41**, adapted from the bis-copper pathway reported by MacMillan and co-workers.[56]*

Table 1.0 *Reactions conditions used for the synthesis of **41**. All reactions were carried out in ethanol and refluxed at 90 °C. The percentage conversion was calculated from ^{1}H NMR integration values. (N/A = not applicable).*

Entry	40 (mmol)	$CuBr_2$ (mmol)	Time (h)	Conversion (%)	Purification technique	Yield of 41 (%)
1	1.90	4.10	17	78	repeated columns	34
2	3.15	8.10	19	100	N/A	43
3	5.75	12.0	20	86	recrystallisation	47

The reactions all had high percentage conversions, and even though a 1:2 ratio of **40**:$CuBr_2$ is needed, it was found that a slight excess of $CuBr_2$ allowed the reaction to go further towards completion. There is a minor structural change going from **40** to **41**, hence their respective R_f values were very close to each other. This made chromatographic separation quite difficult and methods such as dry packing were used in an effort to improve chromatographic purification of **41**. [57] However, the optimal purification technique was found to be recrystallization from DCM to yield **41** at 47%.

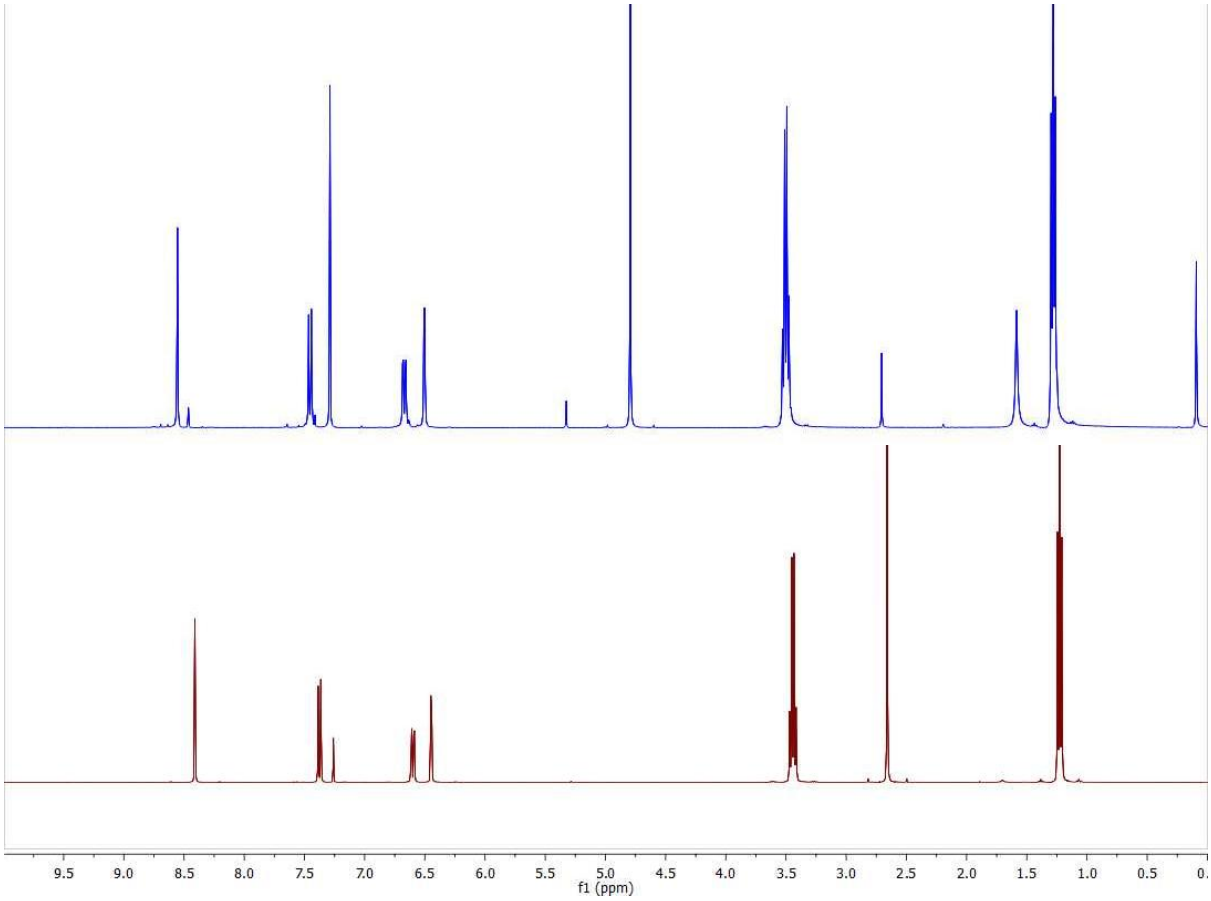

Figure 2.4 *Overlapping ^{1}H NMR spectra of starting material **40** (red) and product **41** (blue).*

Compound **41** was confirmed by ^{1}H NMR (**Figure 2.4**), showing the appearance of the CH_2Br peak at 4.77 ppm. There is a residual peak at 2.67 ppm which indicates minimal amounts of **40** present, and also a peak at about 1.5 ppm which could be residual moisture. It should be noted that the solubility of **41** is not very high in $CDCl_3$ (the solvent used for all NMR spectra). Therefore, as **41** is partially insoluble in $CDCl_3$, the relative amount of impurities in solution increase – resulting in increased peak intensity of the impurities in the ^{1}H NMR spectra. NMR spectra in DMSO were unsuccessful too.

Carrying on the synthetic route, **41** was used to synthesise the final coumarin unit, **39**. This was done using a previously used method in our research group. The reaction used NaN_3 in THF and after leaving the reaction stirring overnight, a crude ^1H NMR was taken. The only change in spectra would be a shift in ppm for the CH_2Br transforming to CH_2N_3. The crude ^1H NMR showed only one peak at 4.66 ppm, but as the chemical shift for CH_2Br is about 4.77 ppm, it could not be conclusively said that the azido coumarin **39** was formed. For this reason an IR was taken, and the presence of the N_3 vibration at 2100 cm^{-1} confirmed the successful production of **39**.[58] This was purified by triturating with hexane, giving **39** in 52% yield.

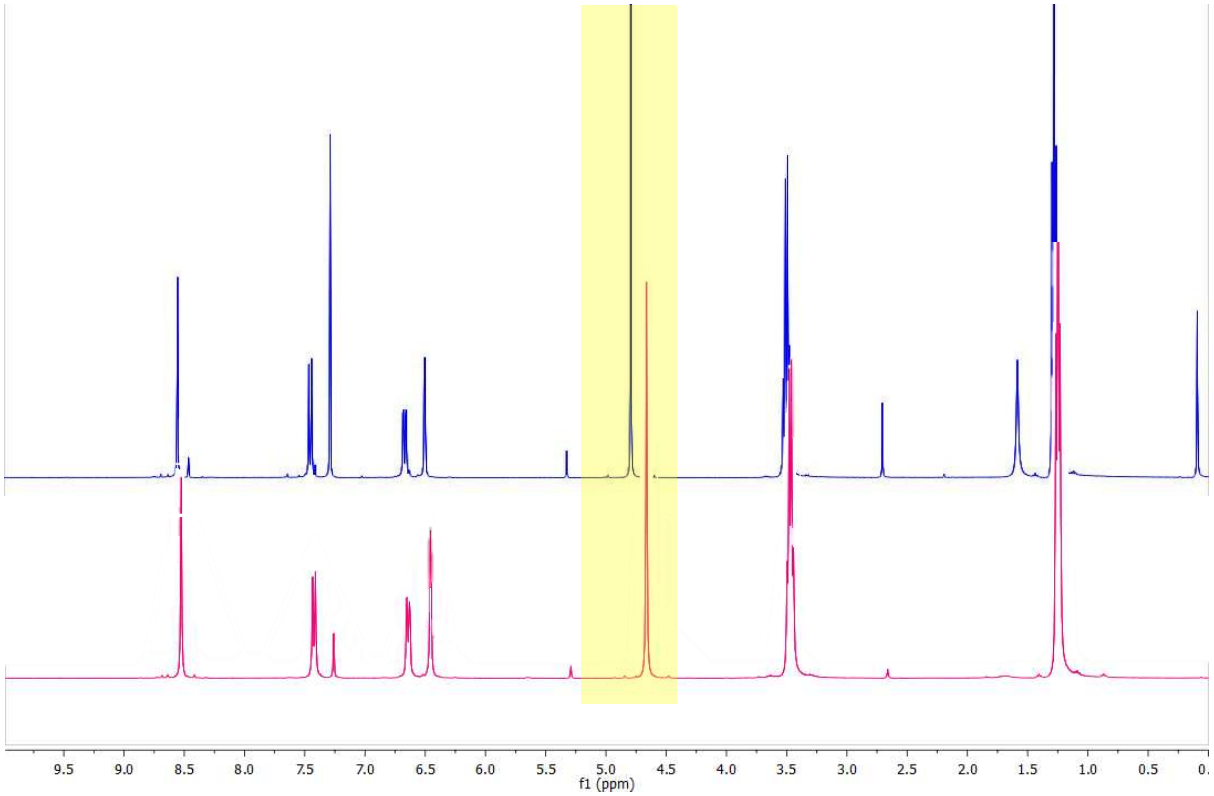

Figure 2.5 *Overlapping ^1H NMR spectra of **41** (blue) and **39** (pink) showing little change in chemical shift at 4.7 ppm (region highlighted in yellow).*

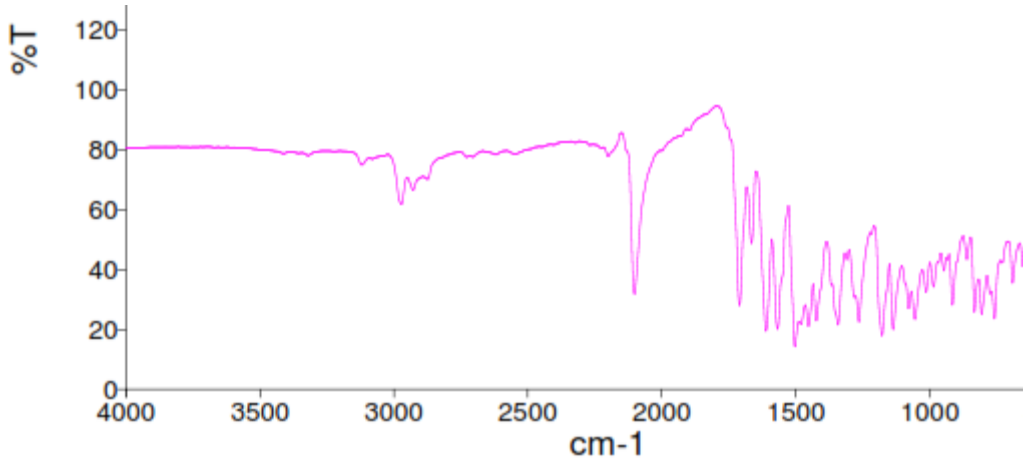

Figure 2.6 *IR of **39** showing the characteristic azide band at 2100 cm^{-1}.*

*2.1.2. Synthesis of PEG_4 amine (**42**)*

Initially, **42** was to be prepared via the Gabriel synthesis,[59] which is a routine method of transforming halides to primary amines. The initial synthetic route towards **42** is shown in **Figure 2.7**.

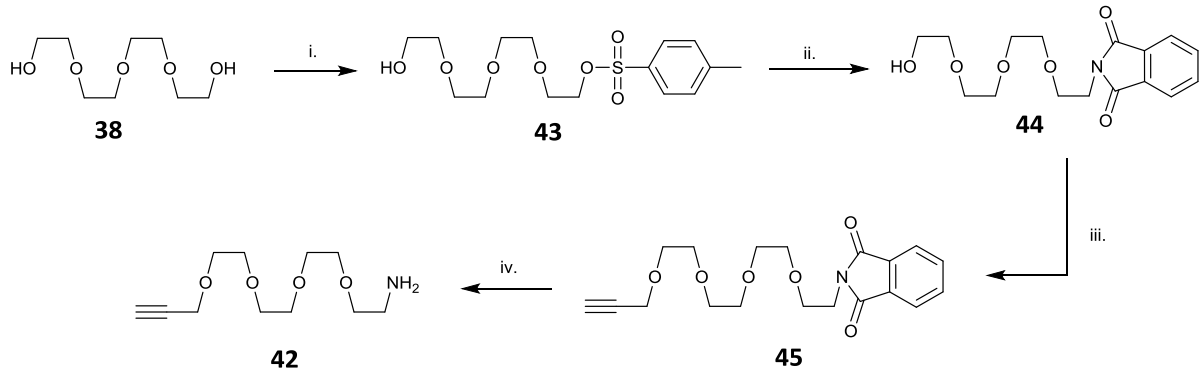

***Figure 2.7** Initial synthetic route towards **42**. i.) TsCl, NaOH, THF, RT, overnight. ii.) Potassium phthalimide, DMF, reflux at 120 °C, overnight. iii.) Propargyl bromide, NaH, dry DMF, RT, overnight. iv.) Hydrazine, $HCl_{(aq)}$, overnight.*

Compound **43** is formed from the readily available reagents **38**, *p*-toluene sulfonyl chloride and sodium hydroxide, and the reaction was performed in THF. To avoid disubstitution, **38** was used in excess, and subsequently no disubstituted products were detected. Purification by silica gel chromatography gave **43** in 84% yield. However, when the reaction was repeated, 2 aqueous extractions, were able to remove the excess **38**, giving **43** in 76% yield. Although the second attempt gave a lower yield, this does suggest that **43** does not necessarily need to be purified by column. The main product to remove is the excess **38** which could be achieved by an aqueous solvent extraction. Production of **43** was confirmed by ^{13}C NMR showing 8 peaks in the 60-75 ppm range for the 8 OCH_2 groups in compound **43**.

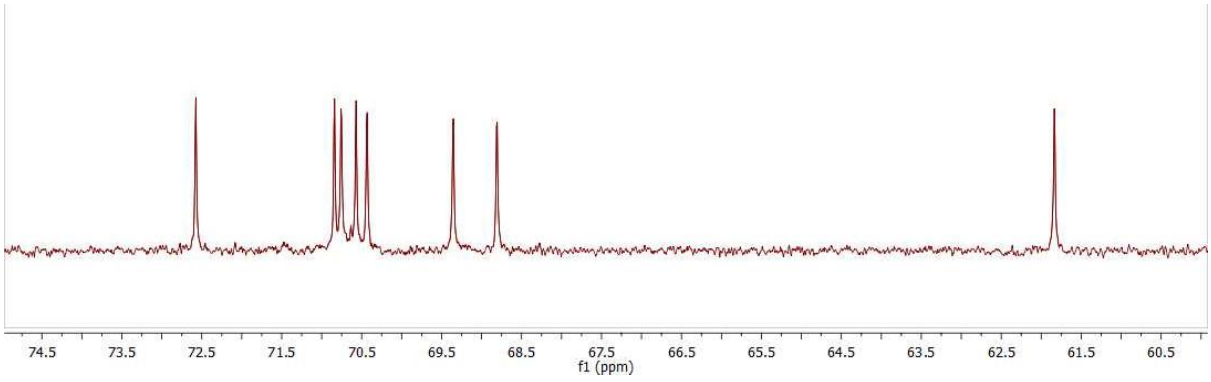

***Figure 2.8** Zoomed in section of ^{13}C NMR of **43** showing 8 peaks in the 75-60 ppm range.*

The next step was the synthesis of **44** from **43** using potassium phthalimide in DMF. The reaction was carried out four times and the reaction conditions with yields are shown in **Table 1.1**.

Table 1.1 *Reaction conditions used for the synthesis of **44**. All entries were refluxed in DMF at 120 °C.*

Entry	43 (mmol)	Potassium phthalimide (mmol)	Time (h)	Purification technique	Yield of 44 (%)
1	5.94	7.13	18	column	38
2	5.94	7.13	22	repeated columns	54 (crude)
3	12.0	14.5	54	trituration	22
4	19.1	21.6	66	N/A	28

To follow the reaction, aliquots of the reaction mixture were removed, worked up and ^{1}H NMR spectra taken. This was done until the peak at 4.15 ppm for CH_2OS in **43** stopped decreasing – indicating the extent of conversion had been reached. In the case of entry 4, the absence of a peak at 4.15 ppm indicated full conversion and so no further purification was required.

From **Table 1.1**, it can be seen that purification proved tricky. In entry 2, repeated columns were tried, but **43** and **44** co-eluted, and so only a crude yield of **44** is given. It should be noted that the columns in entries 1 and 2 did not use the dry packing method. Thus to optimise purification, dry packing could be used. Alternatively, purification by triturating **44** from diethyl ether is possible but not as high yielding. Production of **44** was confirmed by the presence of 7 peaks in the 60-75 ppm range in the ^{13}C NMR spectra corresponding to the 7 OCH_2 in **44**.

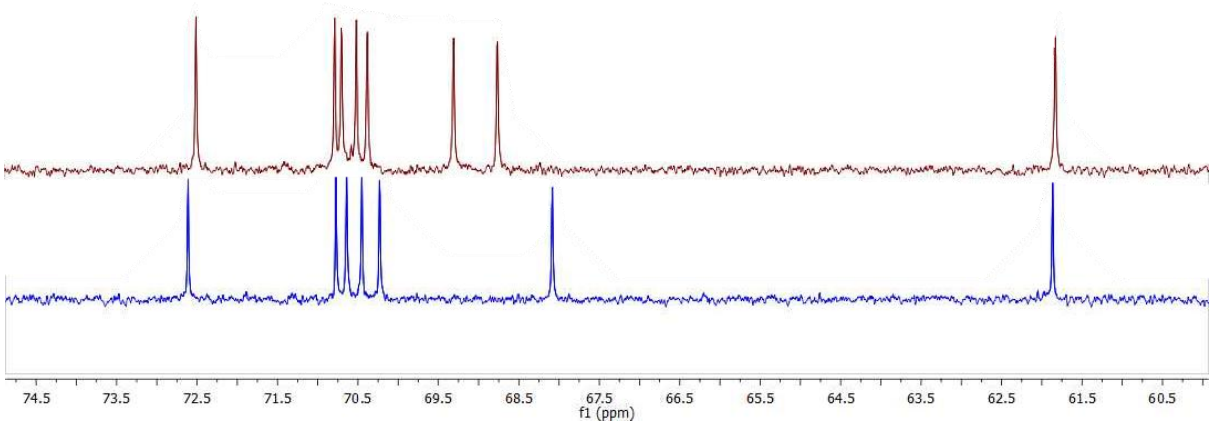

Figure 2.9 *Overlapping sections of ^{13}C NMR spectra of **43** (red) showing 8 peaks and **44** (blue) showing 7 peaks.*

The synthesis of **45** from **44** was attempted twice using a 60% dispersion of NaH in mineral oil and an 80% solution of propargyl bromide in toluene. In the first attempt, the reaction was carried out in dry DMF but did not yield anything. A crude ^{1}H NMR taken after the reaction was left to stir overnight, showed some peaks in the baseline. However, the alkyne peak that should appear around 2.1 ppm was not seen. Thus it is likely that the reaction did not occur, and only the starting **44** was seen.

The second attempt at synthesising **45** was performed in THF instead of DMF as THF has a lower boiling point and so it can be removed with relative ease. Upon removal of THF, a ^{1}H NMR of the crude showed a very small signal at 2.1 ppm. However, there was not enough to isolate and definitively characterise as compound **45**.

For this reason an alternative approach for the preparation of **42** was proposed (**Figure 2.10**), where the propargylation is attempted first, followed by amine formation via the Gabriel synthesis.

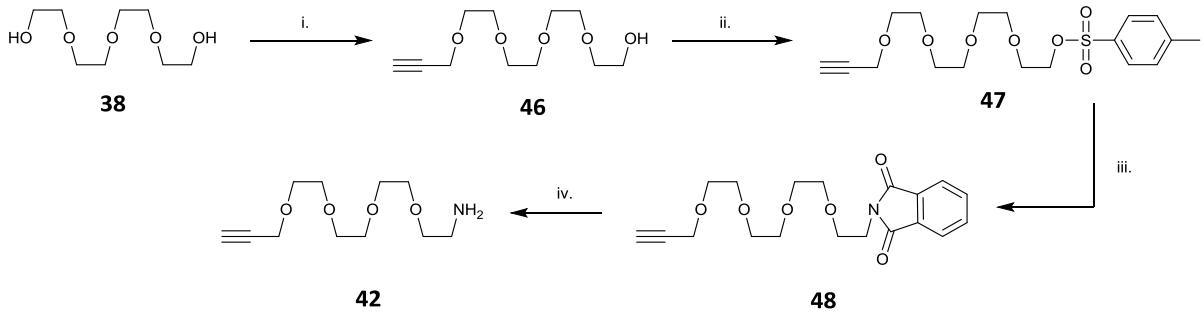

Figure 2.10 *The proposed alternative synthetic route towards **42**. i.) Propargyl bromide, NaH, dry THF, RT, 66 h. ii.) TCl, TEA, DCM, DMAP (catalyst), RT, stir under N_2 overnight. iii.) Potassium phthalimide, DMF, reflux at 120 °C, overnight. iv.) Hydrazine, $HCl_{(aq)}$, overnight.*

The first step in this alternative synthesis was the propargylation of **38** to **46**, using the same NaH and propargyl bromide source as used previously in the synthesis of **45**.[60] Compound **38** was used in excess to minimise dialkylation, the unreacted **38** that remained was easily removed by aqueous extractions. Consequently, no dialkylated product was produced, and **46** required very simple synthetic set up without the need for further chromatographic purification.

Compound **46** was produced in a 14% yield, and characterisation was confirmed by ^{13}C NMR (**Figure 2.11**) showing 9 peaks in the 57-71 ppm range for each of the 9 OCH_2 groups and 2 peaks in the 74-80 ppm range for the two alkyne carbons. It is postulated that the reason for the low yield and maybe even the reason why the synthesis of **45** was unsuccessful was due to the NaH source. The dispersion was quite old and so the quality of the dispersion can be questioned. Ideally, the synthesis of **45** and **46** would be repeated using a newly bought dispersion of NaH, or even the dry pellets of NaH which are commercially available.

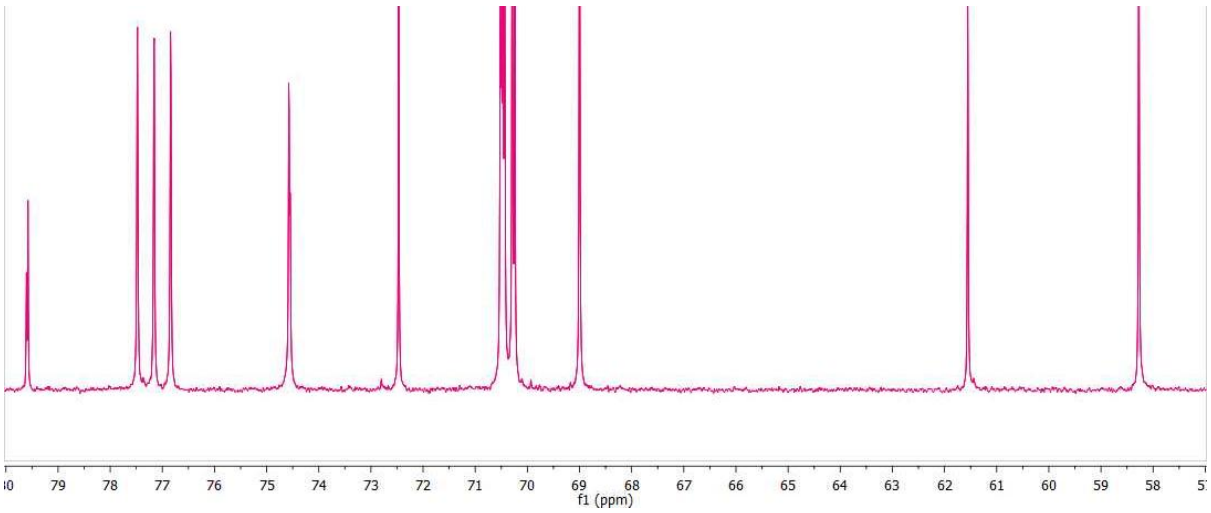

Figure 2.11 *^{13}C NMR of **46** showing 9 peaks between 57-71 ppm and 2 peaks between 74-80 ppm.*

Compound **46** was carried forward to synthesise **47** using a literature procedure. [61] This approach used *p*-toluene sulfonyl chloride as well as TEA, DCM and a DMAP catalyst. The crude was purified by silica gel chromatography to give **47** in a reasonable 67% yield. Compound **47** was characterised by the presence of the tosyl peaks in the aromatic region. The ^{1}H NMR of **47** did show minimal peaks for TEA which could not be removed even with further aqueous extractions (**Figure 2.12**).

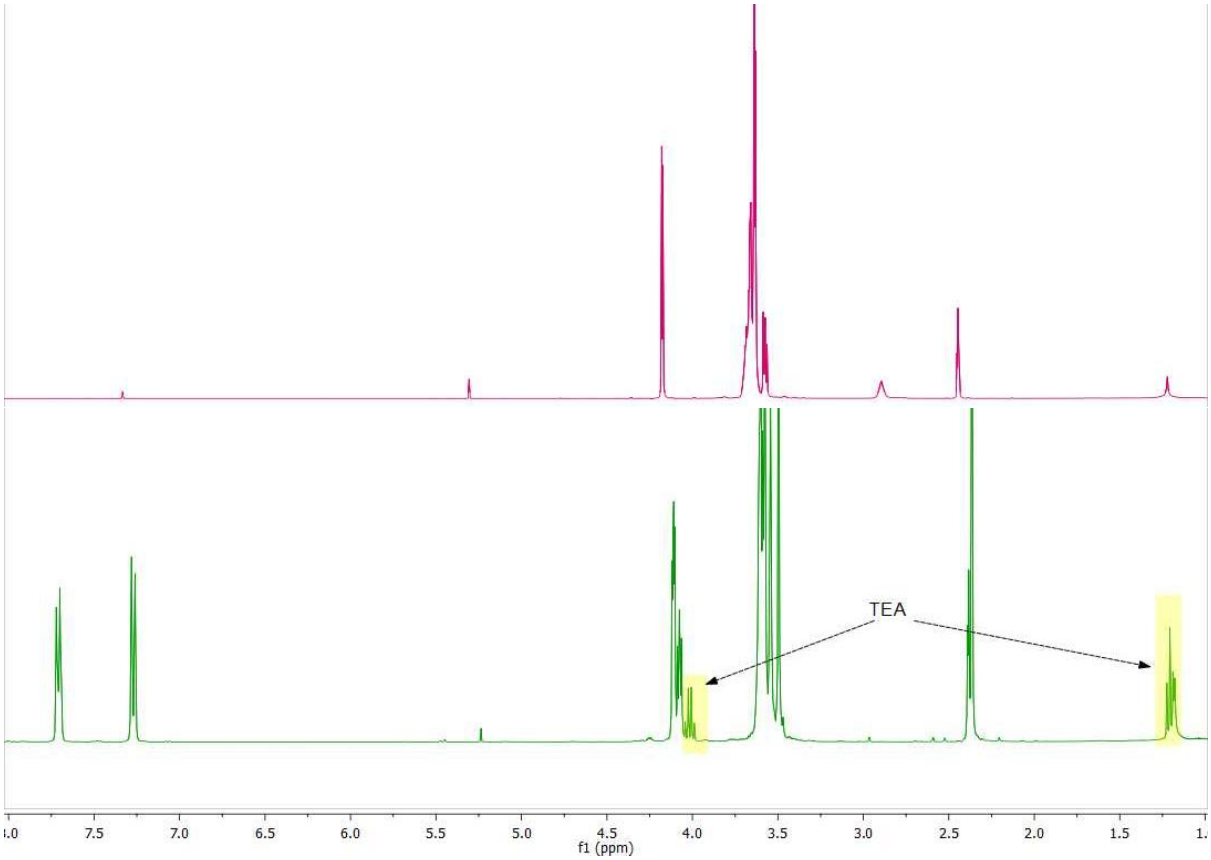

Figure 2.12 *Overlapping ^{1}H NMR spectra of **46** (pink) and **47** (green). Spectra of **47** shows presence of tosyl in aromatic region and also minimal TEA (highlighted in yellow).*

Due to the time constraints of this project, the further synthesis from **47** to **42** was not possible. However, the transformation of the tosyl group to the phthalimide group has already been shown and the Gabriel synthesis is a routine procedure and so the reduction of the phthalimide to yield **42** should be straightforward.

*2.1.3. Synthesis of alkynyl DPA (**49**)*

As the naphthalimide unit is commercially available, this unit did not need to be synthesised. Therefore the next unit to be synthesised was the zinc chelating unit **49**. Two reported methods were trialled, both using 2-(chloromethyl) pyridine hydrochloride and propargyl amine (in a 2:1 ratio) (**Figure 2.13**) which are commercial available.

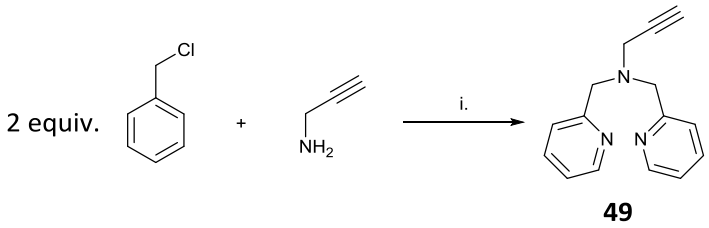

***Figure 2.13** Synthesis of zinc-chelating centre **49**. i.) CH_3CN, K_2CO_3, 80 °C, reflux for 66h.*

The first attempt was following a literature procedure by Lippard and co-workers. [62] This method used a 3:1 solution of MeOH/water. After one night refluxing at 65 °C a crude ^{1}H NMR was taken, suggesting the addition of one pyridyl moiety rather than two (**Figure 2.14**) – hence only the monopyridyl compound was produced.

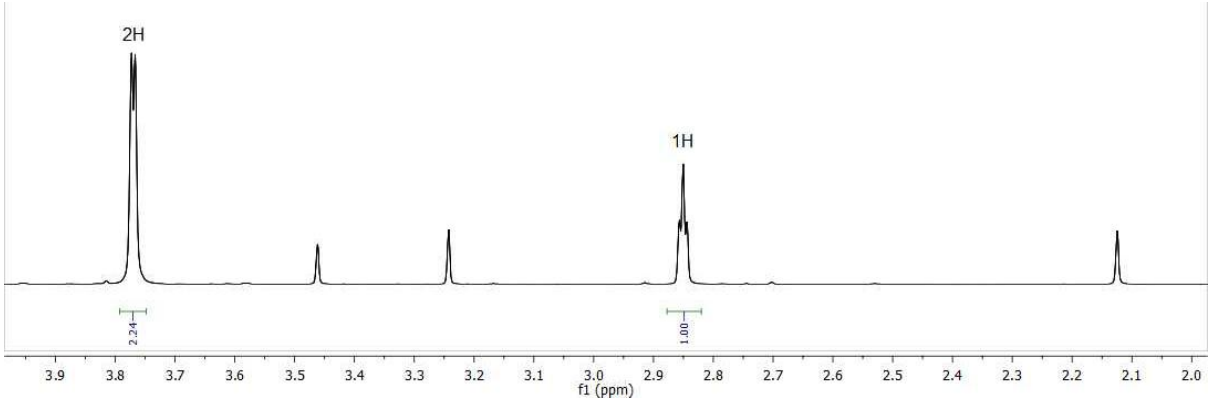

***Figure 2.14** A section of the crude ^{1}H NMR spectra of the monopyridyl amine produced, showing a 2:1 ratio between the peak for the CH_2 near the pyridyl moiety and the CH on the alkyne.*

At first, 2 equivalents of 2-(chloromethyl) pyridine hydrochloride were added, but as mentioned, only the monopyridyl compound was seen after one night of refluxing. Thus one more equivalent of 2-(chloromethyl) pyridine hydrochloride was added. However, after another night refluxing, the reaction was worked up by aqueous extraction and no product was seen. It is thought that the extra equivalent added may have produced a quaternary ammonium ion, and as this is soluble in water, it was lost in the aqueous workup and thus not seen in the spectra.

In the second attempt, the two reagents were refluxed in CH_3CN instead, with the addition of potassium carbonate (following a procedure by Castro and co-workers).[63] This method proved successful, giving **49** in 37% yield. The presence of the dipyridyl addition was confirmed by ^1H NMR, showing a 4 to 1 ratio between the integration values of the pyridyl CH_2 and the alkyne CH (**Figure 2.15**).

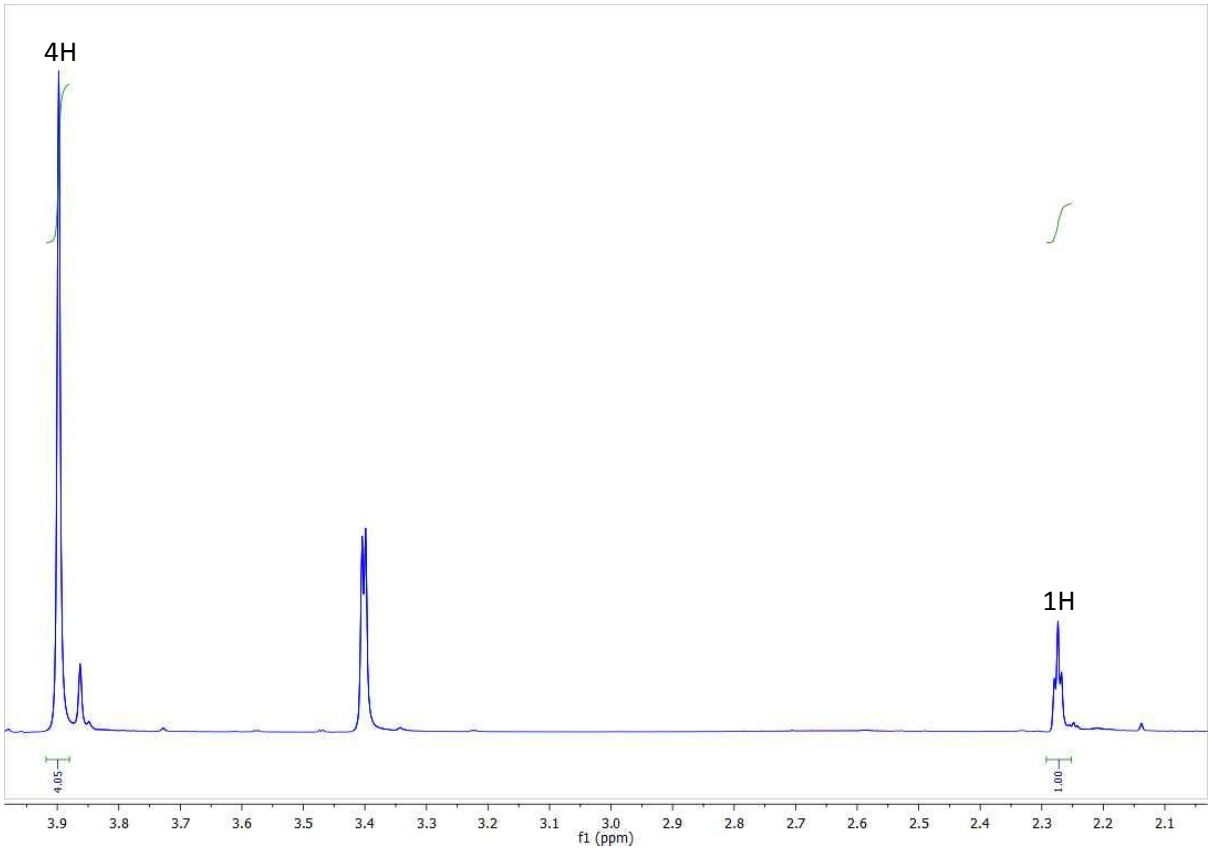

Figure 2.15 *A section of the crude ^1H NMR spectra of the dipyridyl amine **49** produced, showing a 4:1 ratio between the peak for the CH_2 near the pyridyl moiety and the CH on the alkyne.*

2.2. Synthesis of CuAAC "click" compound (**50**)

As **42** was not synthesised in time, the CuAAC "click" reaction was carried out between **39** and **47** to show that the CuAAC reaction can be used to join all the modular units together. This procedure was simple to perform, however the crude product had to be purified by column chromatography twice. The first column was performed using a DCM/MeOH (95:5) eluent to remove any of the unreacted **39** and **47**, and also the DIPEA used. However, some of the alkyne co-eluted with **50** and so another column was needed to remove the unreacted **47** using an EtOAC/MeOH (92:8) mixture, giving **50** in a 20% yield.

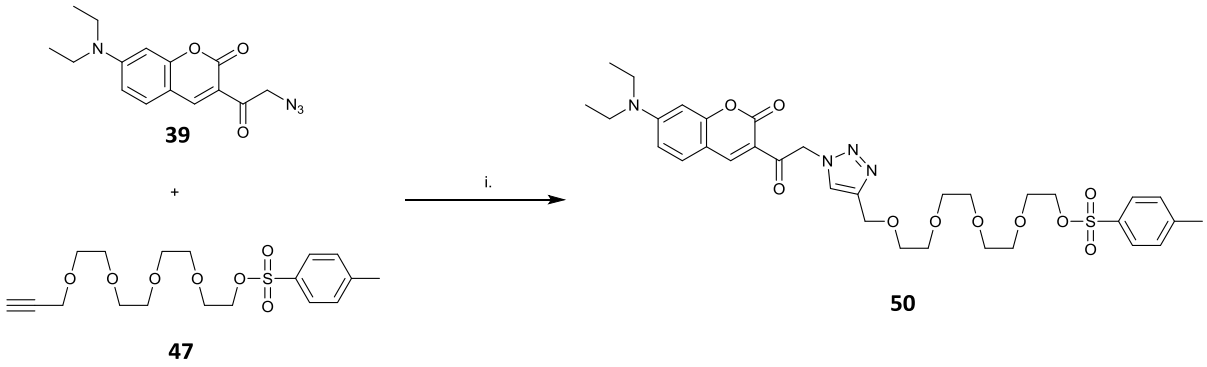

Figure 2.16 *CuAAC reaction between **39** and **47**. i.) DIPEA, dry DCM, tetrakis(acetonitrile)copper(I) hexafluorophosphate (catalyst), RT, reflux under N_2 for 72 h.*

The "click" between **39** and **47** forms two new C-N bond, only one of which has a proton environment. The presence of this triazole CH peak at 7.65 ppm in the ^{1}H NMR of **50** is confirmation of a successful "click" reaction (**Figure 2.17**)**.** This was established as the triazole CH by using COSY (^{1}H-^{1}H coupling) spectra, which showed the peak at 7.65 ppm did not couple with any other peaks in the ^{1}H NMR spectra. The full ^{1}H and ^{13}C NMR spectra of **50** were characterised using COSY and HSQC (^{1}H-^{13}C coupling) spectra.

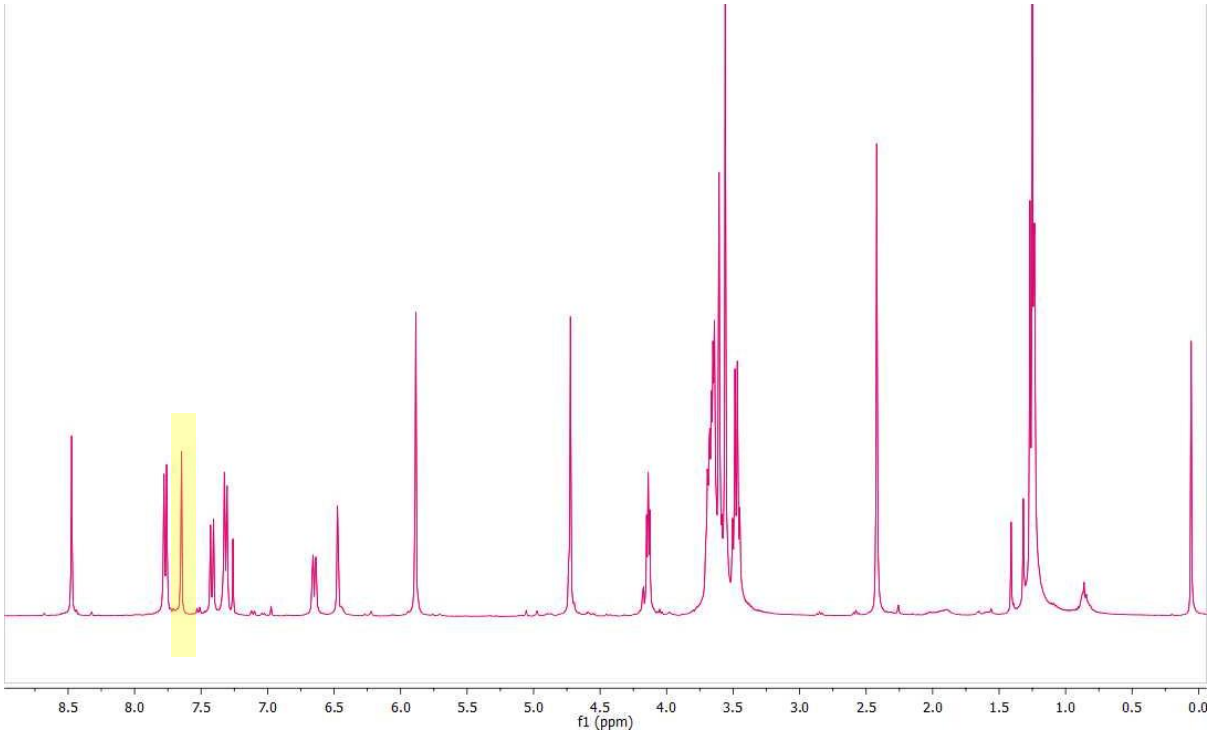

Figure 2.17 *^{1}H NMR of **50** with the triazole CH singlet at 7.65 ppm highlighted in yellow.*

3. Conclusion

To conclude, 7 steps in a 12 step synthesis towards **4** were completed, all reactions starting from relatively cheap, commercially available reagents. Also, the naphthalimide fluorophore is commercially available as the 4-bromo-naphthalic anhydride which is ready to react with the amine **42**. The remaining steps in the synthesis from **50** to **4** are shown below in **Figure 3.0**.

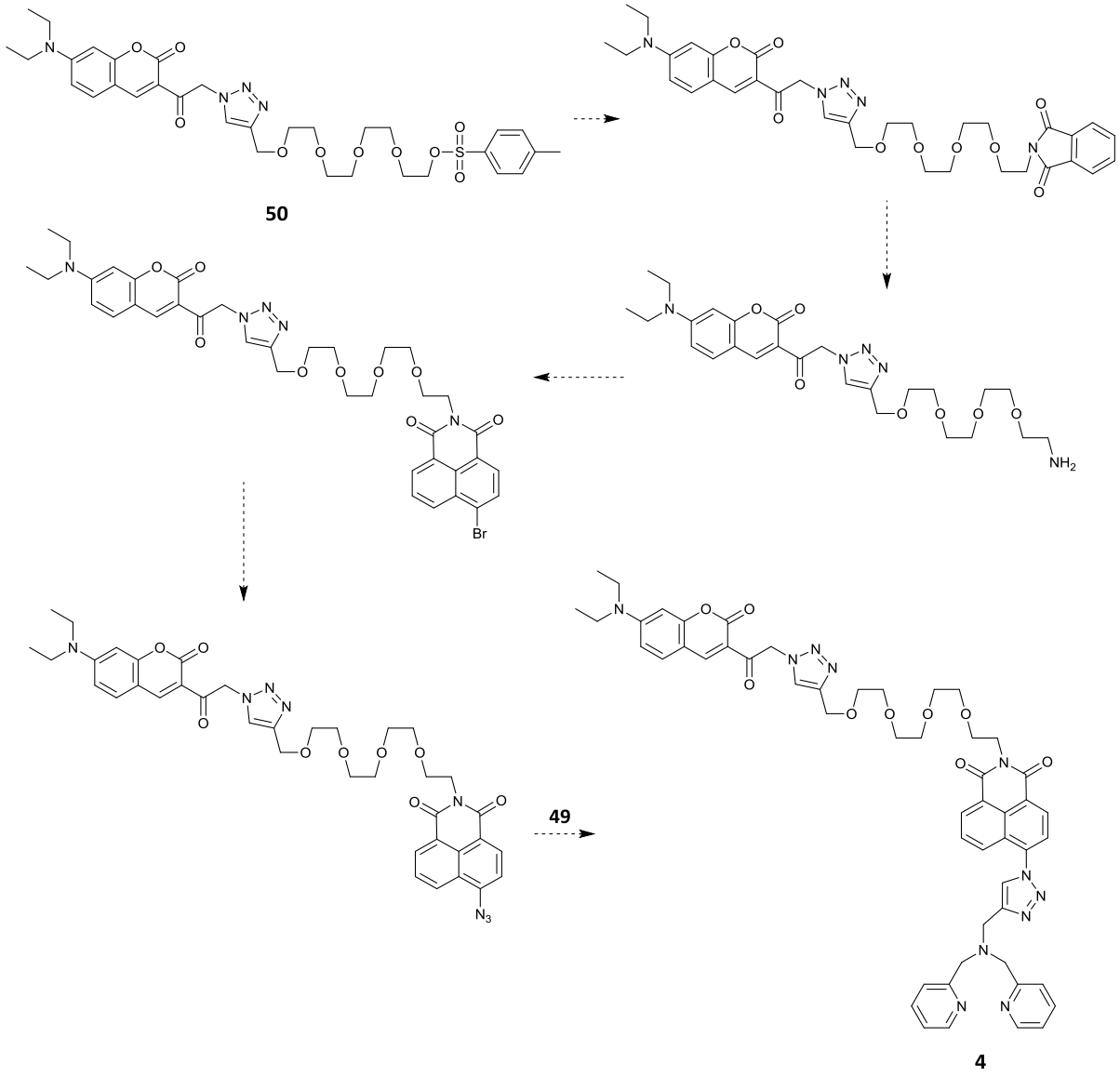

Figure 3.0 *Remaining synthetic route towards* ***4****.*

The synthesis of **45** proved problematic and thus delayed progress towards the synthesis of the deprotected amine linker **42** and thus of the complete synthesis of **4**. With further time it would be beneficial to try the synthesis of **45** again using a new NaH source as well as **46** in the alternative synthesis as well. However, one of the benefits of using a modular approach towards the synthesis of the final sensor **4** is that any such problems are relatively simple to fix. This is because any issues with modular units can be dealt with independently without having to start completely from the beginning as you would do with traditional linear syntheses.

The successful CuAAC reaction between **39** and **47** to give **50** was achieved. The substitution of a tosyl group with a phthalimide group was demonstrated in the synthesis of compound **44**. Due to time constraints, the reduction of the phthalimide group to the amine was not possible but this is a routine deprotection step in the Gabriel synthesis shown many times in the literature. Alternatively the tosyl group can be substituted to an azide – this way the deprotection to an amine can go via the Staudinger mechanism.[64] This ability to easily change the synthetic route of modular units is an advantage of using the CuAAC "click" reactions.

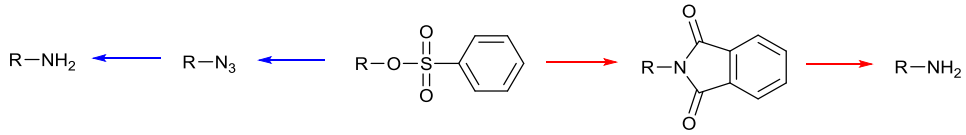

Figure 3.1 *The two possible routes from a tosyl group to an amine: the formation of an azide and then reduction to an amine via the Staudinger reaction (left, in blue), the formation of a phthalimide group and then reduction to an amine via the Gabriel synthesis (right, in red).*

It would be ideal in the future to test out sensor **4** firstly at different concentrations of zinc in aqueous solution, and then *in vivo* as well. Also, the PEG_4 linker is present in sensor **4** to improve aqueous solubility and create sufficient space between the two fluorophores so as to reduce the risk of self-quenching. As mentioned previously, peptide linkers have very good rigidity but their use biologically can be questioned. The risk of using a PEG_4 linker is the possibility of the linker folding in on itself to minimise its free energy. In this case, the risk of self-quenching increases. Therefore it would be also necessary to perform some molecular modelling of **4**, to better assess the risk of linker folding and hence self-quenching.

4. Experimental

General Procedures

All starting materials were obtained commercially and used without further purification. Solvents used were reagent grade and any dry solvents were obtained from the MBraun MB SPS-800 purification system. Reaction flasks were dried at 135 °C, and any air- and moisture-sensitive reactions were performed under nitrogen. Solutions of aqueous ammonia were diluted from reagent grade solutions of 35%. Solutions of dilute HCl were diluted from reagent grade solutions of 35%. Propargyl bromide was used as an 80% solution in toluene. Sodium hydride was used as a 60% dispersion in mineral oil. Thin layer chromatography was performed using silica gel 60 F254 plastic-backed plates (Merck) and analysed under UV light. Flash column chromatography was carried out using silica gel of 60 Å pore size. Columns were prepared using either the dry packing method (for **40**, **47** and **50**) or the slurry method (all other products). Melting points were recorded using open capillary tubes on a Gallenkamp melting point apparatus. Infrared spectra were recorded on a Perkin Elmer Spectrum 65 spectrometer. ^{1}H and ^{13}C NMR spectra were recorded at 300 K on a Bruker AVIII 400 Spectrometer, and all samples were referenced to $CDCl_3$ (^{1}H NMR residual solvent peak of $CHCl_3$: 7.26, ^{13}C NMR deuterated solvent peak of $CDCl_3$: 77.16). ^{1}H NMR data are reported in the order: chemical shift (in ppm, δ), number of protons, multiplicity (s, singlet; d, doublet; t, triplet; m, multiplet), coupling constant (if applicable) in Hertz (Hz), and assignment (protons are italicised in some cases to indicate assignments more clearly). ^{13}C NMR data are reported as chemical shift (in ppm, δ). Low resolution mass spectrometry used Electrospray ionisation (ESI) as the ionisation source, obtained on an Agilent LC-MS. Experimental procedures of each compound synthesised are preceded by their experimentally found data and then their respective NMR spectra.

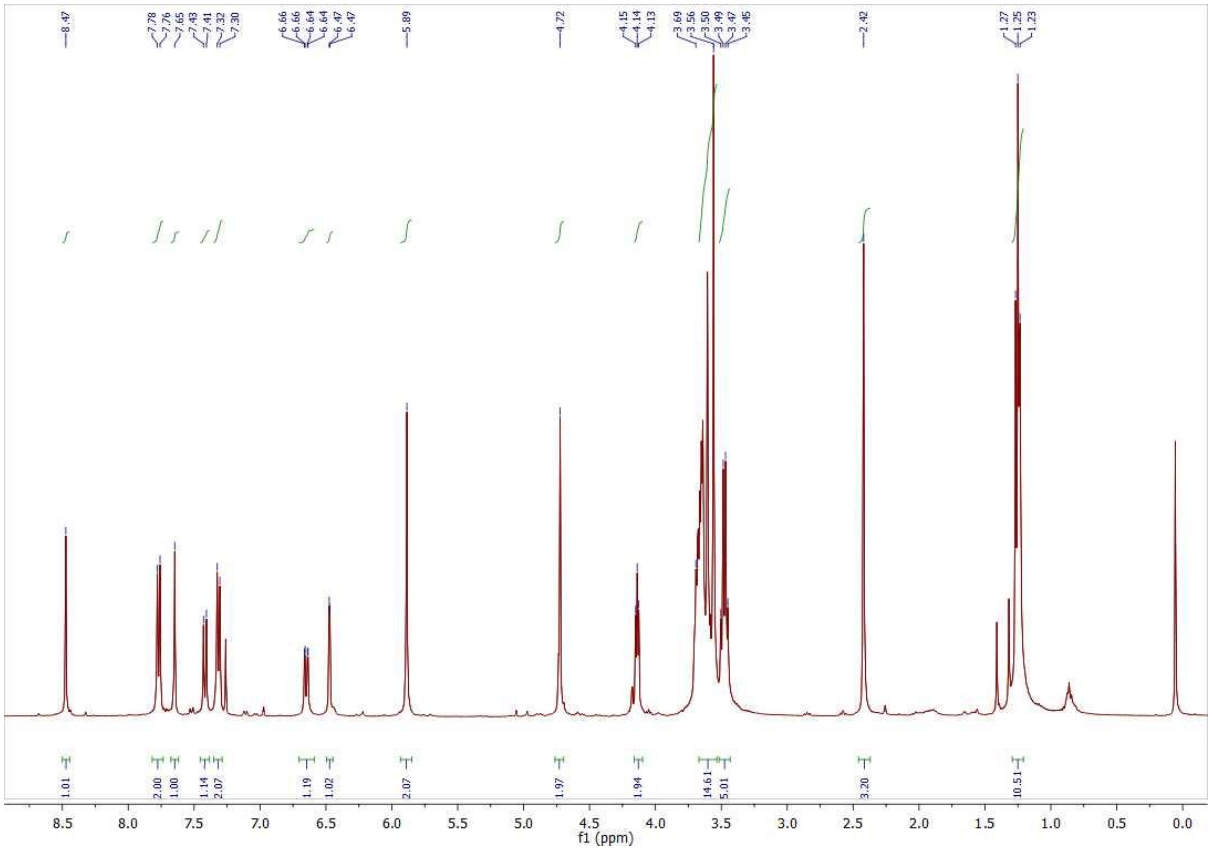
8.47
7.78
7.76
7.65
7.43
7.41
7.32
7.30
6.66
6.66
6.64
6.64
6.47
6.47
5.89
4.72
4.15
4.14
4.13
3.69
3.56
3.50
3.49
3.47
3.45
2.42
1.27
1.25
1.23
1.01
2.00
1.00
1.14
2.07
1.19
1.02
2.07
1.97
1.94
14.61
5.01
3.20
10.51
f1 (ppm)

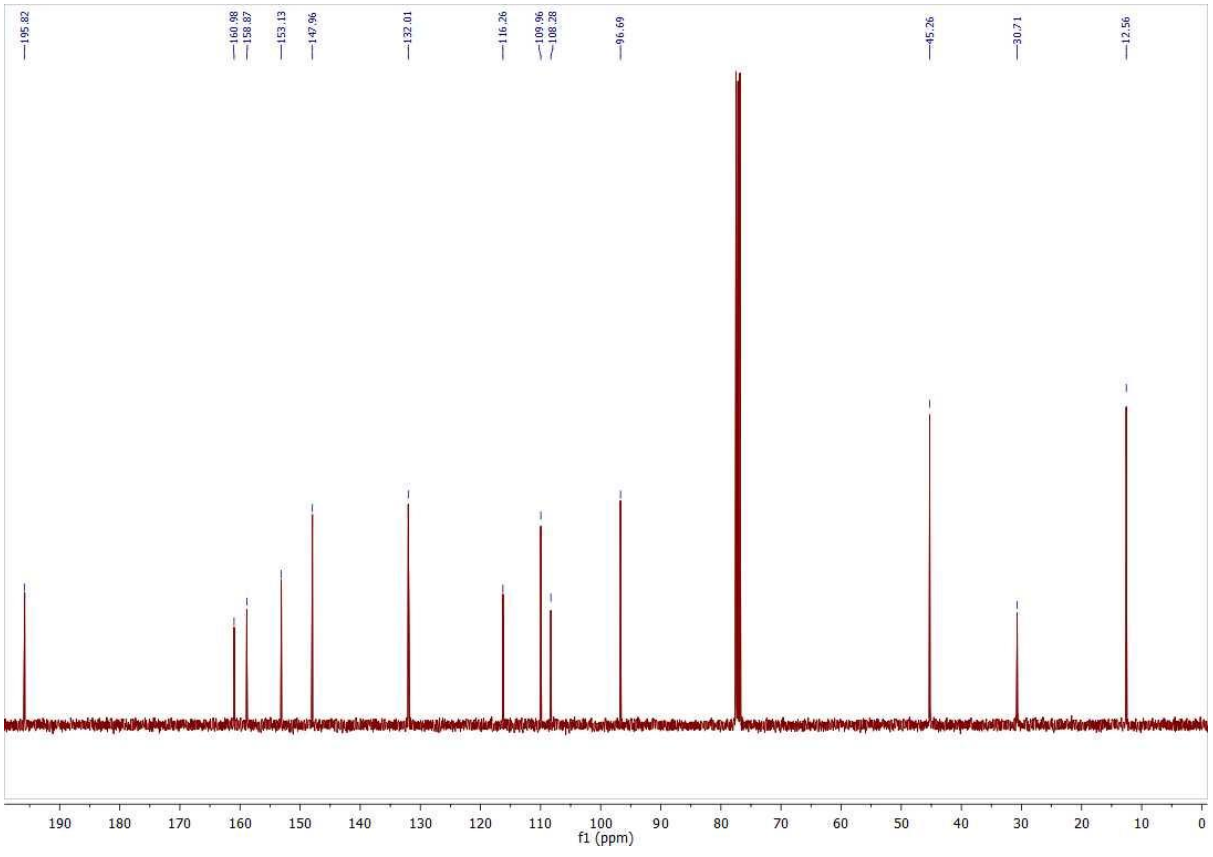
195.82
160.98
158.87
153.13
147.96
132.01
116.26
109.96
108.28
96.69
45.26
30.71
12.56
f1 (ppm)

3-Acetyl-7-(diethylamino)-2H-chromen-2-one (40). To a stirred volume of piperidine (13 mL, 131.6 mmol) was added 4-(diethylamino) salicylaldehyde (3.60 g, 18.6 mmol) and ethyl acetoacetate (2.42 g, 18.6 mmol). The reaction was allowed to stir at room temperature for 30 min and the resulting solid was filtered under suction, washing with cold ethanol to collect **40** as a bright yellow solid (3.87 g, 80%). (Following the procedure by Secci and co-workers[54])

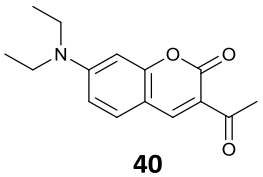

40

40 (3.87 g, 80%). Mp 154°C. Lit. 154 °C.[58] υ_{max}/cm^{-1} 2960 (sp^3 CH), 1730 (ester C=O), 1660 (ketone C=O), 1350 (C-N), 1290 (ester C-O). δ_H (400 MHz; $CDCl_3$): 1.23 (6H, t, *J* 7.2, C*H*$_3$CH$_2$), 2.66 (3H, s, C*H*$_3$CO), 3.44 (4H, q, *J* 7.2, CH$_3$C*H*$_2$), 6.45 (1H, d, *J* 2.4, Ar-H), 6.60 (1H, dd, *J* 9.0, *J* 2.5, Ar-H), 7.38 (1H, d, *J* 9.0, Ar-H), 8.41 (1H, s, Ar-H). δ_C (100 MHz; $CDCl_3$): 12.6 (2 x C), 30.7, 45.3 (2 x C), 96.7, 108.3, 110.0, 116.3, 132.0, 148.0, 153.1, 158.9, 161.0, 195.8. LRMS (ESI) m/z 260.4 $[M+Na]^+$ (45%).

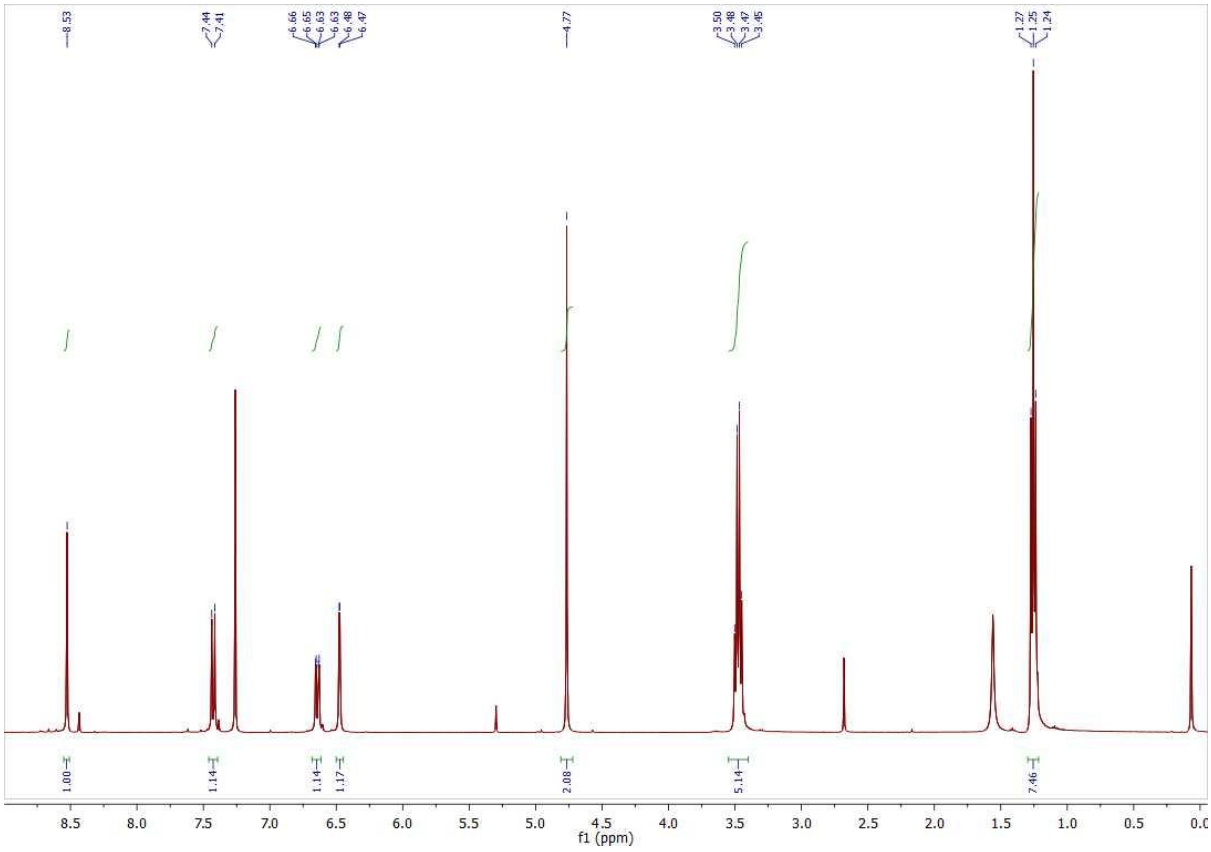

3-(2-Bromoacetyl)-7-(diethylamino)-2H-chromen-2-one (41). A solution of copper(II) bromide (2.67 g, 12.0 mmol) in ethanol (75 mL) was added to a solution of **40** (1.49 g, 5.75 mmol) in ethanol (108 mL). The reaction vessel was flushed with N_2 and then left to reflux at 90 °C overnight. The ethanol was removed under reduced pressure (60 °C) and the residue cooled in an ice bath. The resulting precipitate was collected under suction, washing with cold ethanol. The crude solids were dissolved in DCM (25 mL) and extracted with a saturated solution of EDTA in aqueous ammonia (3 x 25 mL, 17% ammonia solution). The organic layers were collected, dried with $MgSO_4$, filtered and the DCM removed under reduced pressure (30 °C). The crude was recrystallised from hot DCM and collected under suction to give **6** as dark yellow crystals (0.91 g, 47%). (Following the procedure by Lin and co-workers[55])

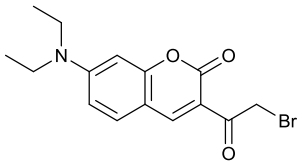

41

41 (0.91 g, 47%). Mp 196-200°C (from DCM). Lit. 211-213°C.[65] υ_{max}/cm^{-1} 2960 (sp^3 CH), 1710 (ester C=O), 1690 (ketone C=O), 1350 (C-N), 1280 (ester C-O), 620 (C-Br). δ_H (400 MHz; $CDCl_3$): 1.26 (6H, t, *J* 7.1, C*H*$_3$CH$_2$), 3.48 (4H, q, *J* 7.1, CH$_3$C*H*$_2$), 4.77 (2H, s, C*H*$_2$Br), 6.48 (1H, d, *J* 2.3, Ar-H), 6.64 (1H, dd, *J* 2.3 and 9.0, Ar-H), 7.43 (1H, d, *J* 9.0, Ar-H), 8.53 (1H, s, Ar-H). LRMS (ESI) m/z 338.3 $[M]^+$ (Br^{79}) (46%), 340.1 $[M]^+$ (Br^{81}).

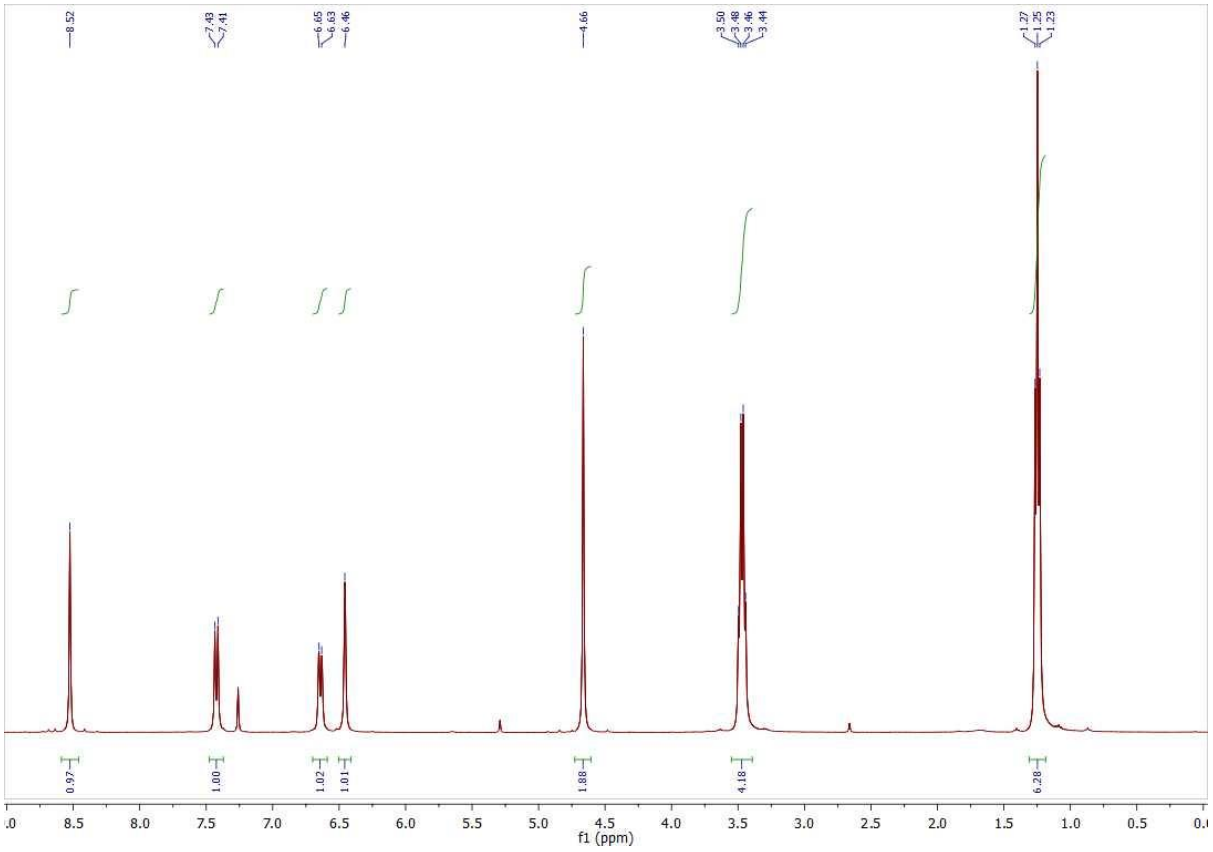
8.52
7.43
7.41
6.65
6.63
6.46
4.66
3.50
3.48
3.46
3.44
1.27
1.25
1.23
0.97
1.00
1.02
1.01
1.88
4.18
6.28
f1 (ppm)

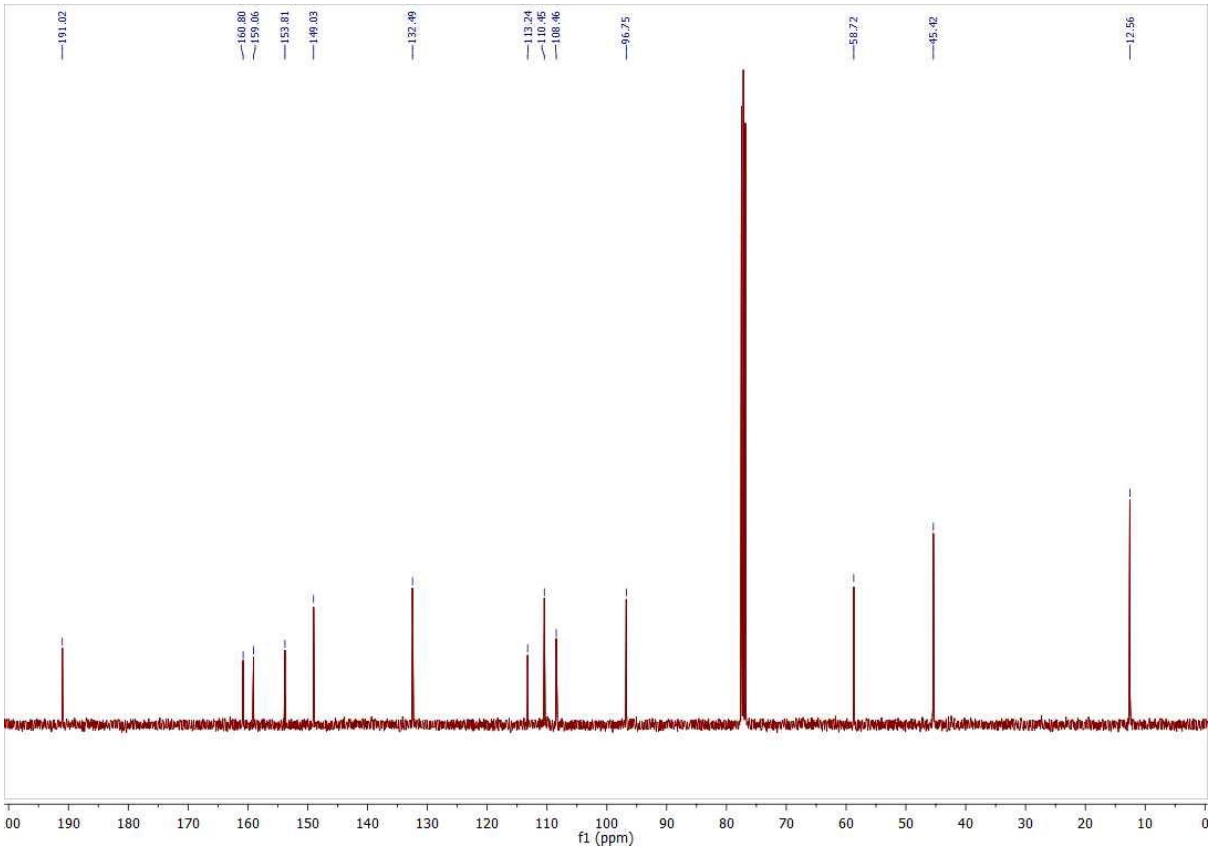
191.02
160.80
159.06
153.81
149.03
132.49
113.24
110.45
108.46
96.75
58.72
45.42
12.56
f1 (ppm)

3-(2-Azidoacetyl)-7-(diethylamino)-2H-chromen-2-one (39). 41 (0.50 g, 1.48 mmol) was added to dry THF (20 mL) and the reaction vessel flushed with N_2. NaN_3 (0.55 g, 8.48 mmol) was added to this and the mixture allowed to stir at 40 °C overnight. The reaction was quenched with water (25 mL) and extracted with DCM (3 x 25mL). The organic phases were collected, dried with $MgSO_4$, filtered and the DCM removed under reduced pressure (30 °C). The crude solid was redissolved in minimal DCM and triturated with hexane (50 mL). The precipitate was collected under suction and allowed to dry overnight to give **39** as a brown solid (0.23 g, 52%).

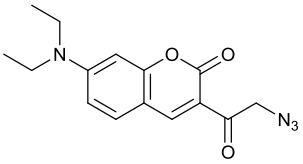

39

39 (0.23 g, 52%). Mp 165-167^{o}C (from hexane). Lit. 172-175 °C.[66] υ_{max}/cm^{-1} 2970 (sp^3 CH), 2100 (N_3), 1710 (ester C=O), 1660 (ketone C=O), 1360 (C-N), 1260 (ester C-O). δ_H (400 MHz; $CDCl_3$): 1.25 (6H, t, *J* 7.0, C*H*$_3$CH$_2$), 3.47 (4H, q, *J* 7.0, CH$_3$C*H*$_2$), 4.66 (2H, s, C*H*$_2$N$_3$), 6.46 (1H, s, Ar-H), 6.64 (1H, d, *J* 8.9, Ar-H), 7.42 (1H, d, *J* 8.9, Ar-H), 8.52 (1H, s, Ar-H). δ_C (100 MHz; $CDCl_3$): 12.6, 45.4, 58.7, 96.8, 108.5, 110.5, 113.2, 132.5, 149.0, 153.8, 159.0, 160.8, 191.0. LRMS (ESI) m/z 244.5 $[C_{15}H_{16}O_3]^+$ (17%), 301.3 $[M+H]^+$ (83%).

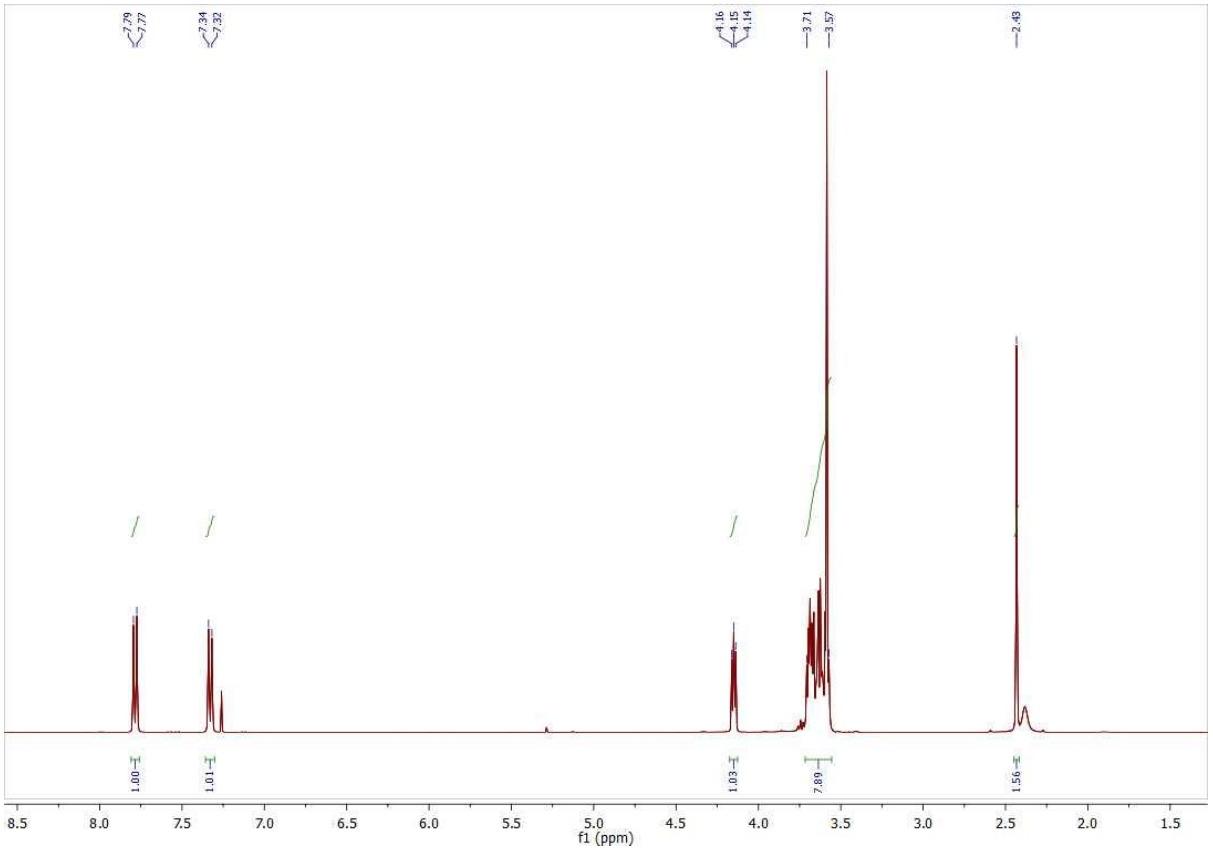
7.79
7.77
7.34
7.32
4.16
4.15
4.14
3.71
3.57
2.43
1.00
1.01
1.03
7.89
1.56
8.5 8.0 7.5 7.0 6.5 6.0 5.5 5.0 4.5 4.0 3.5 3.0 2.5 2.0 1.5
f1 (ppm)

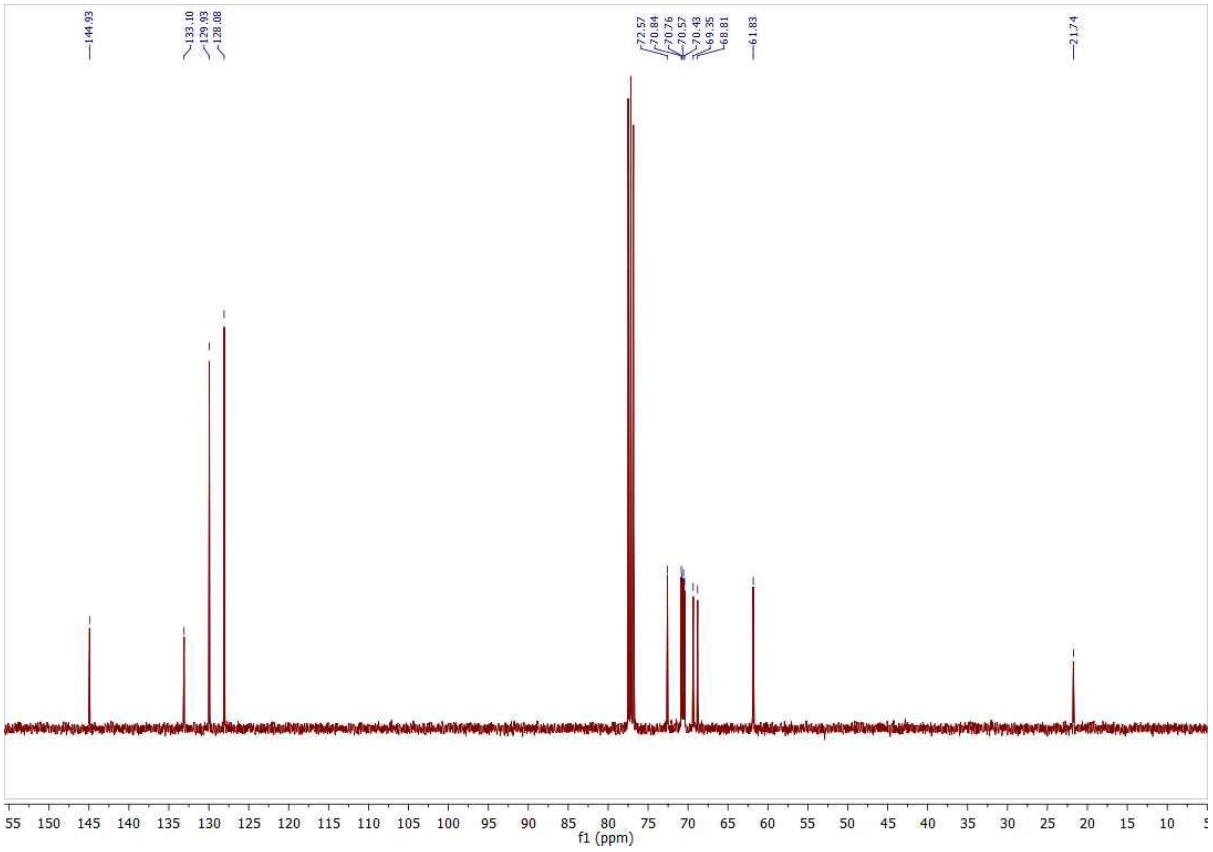
144.93
133.10
129.93
128.00
72.57
70.84
70.76
70.57
70.43
69.35
68.81
61.83
21.74
55 150 145 140 135 130 125 120 115 110 105 100 95 90 85 80 75 70 65 60 55 50 45 40 35 30 25 20 15 10
f1 (ppm)

2-(2-(2-(2-Hydroxyethoxy)ethoxy)ethoxy)ethyl 4-methylbenzenesulfonate (43). To a solution of NaOH (1.65 g, 41.3 mmol) in water (10.0 mL), a solution of **38** (51 mL, 295 mmol) in THF (10 mL) was added and allowed to stir at 0 °C. To this, a solution of *p*-toluenesulfonyl chloride (4.83 g, 25.3 mmol) in THF (33 mL) was added dropwise over an hour. The reaction was kept at 0 °C for a further hour and then allowed to warm to room temperature and left overnight. The THF was removed under reduced pressure (50 °C) and the remaining aqueous phase diluted with water (50 mL) and extracted with DCM (25 mL x 4). The organic phases were collected, combined, dried with $MgSO_4$, filtered and the DCM removed under reduced pressure (30 °C) to leave a crude pale yellow oil. Silica gel chromatography, eluting with a DCM/MeOH (95:5) mixture gave **43** as a colourless oil (7.38 g, 84%). (Following the procedure by Zhang and co-workers[67])

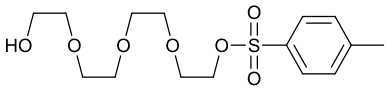

43

43 (7.38 g, 84%). υ_{max}/cm^{-1} 3400br (OH), 2870 (sp^3 CH), 1350 (S=O), 1100 (aliphatic ether CO), 920 (S-O), 820 (*p*-disubstituted Ar). δ_H (400 MHz; $CDCl_3$): 2.43 (3H, s, CH_3), 3.57-3.71 (14H, m, OCH_2), 4.15 (2H, t, *J* 4.8, CH_2OS), 7.33 (2H, d, *J* 8.2, Ar-H), 7.78 (2H, d, *J* 8.2, Ar-H). δ_C (100 MHz; $CDCl_3$): 21.7, 61.8, 68.8, 69.4, 70.4, 70.6, 70.8 (2 x C), 72.6, 128.1 (2 x C), 129.9 (2 x C), 133.1, 144.9. LRMS (ESI) m/z 371.3 $[M+Na]^+$ (86%).

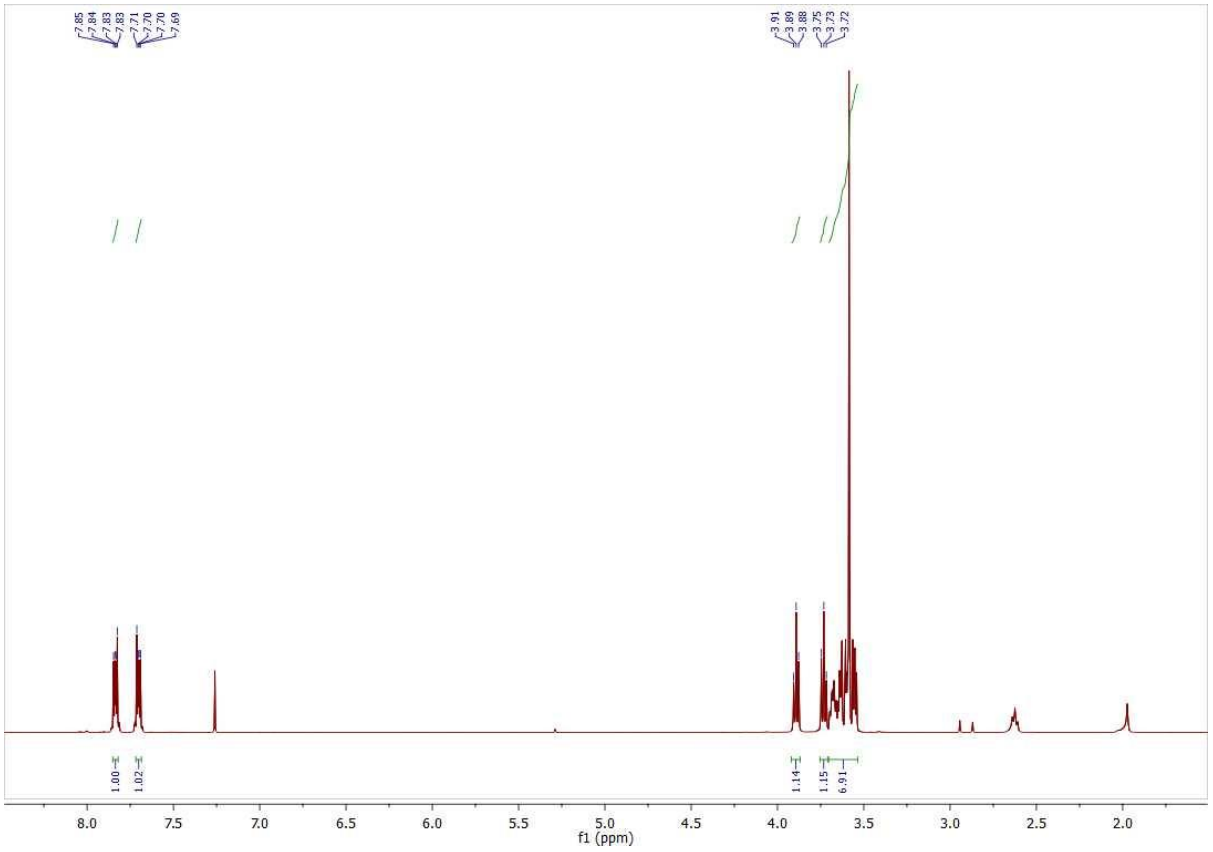
7.85
7.84
7.83
7.83
7.71
7.70
7.70
7.69
3.91
3.89
3.88
3.75
3.73
3.72
1.00
1.02
1.14
1.15
6.91
8.0
7.5
7.0
6.5
6.0
5.5
5.0
4.5
4.0
3.5
3.0
2.5
2.0
f1 (ppm)

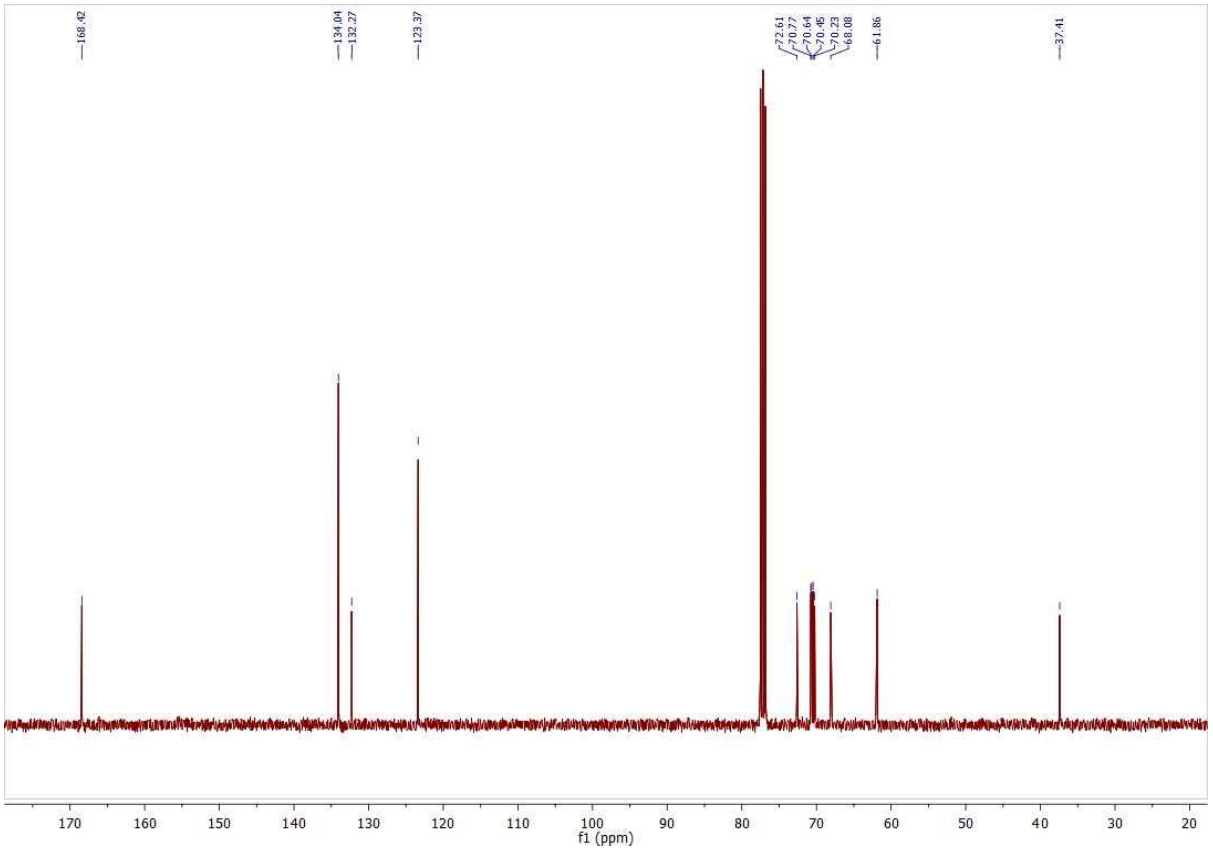
168.42
134.04
132.27
123.37
72.61
70.77
70.64
70.45
70.23
66.08
61.86
37.41
170
160
150
140
130
120
110
100
90
80
70
60
50
40
30
20
f1 (ppm)

2-(2-(2-(2-(2-Hydroxyethoxy)ethoxy)ethoxy)ethyl)isoindoline-1,3-dione (44). Potassium phthalimide (1.32 g, 7.13 mmol) was added to a solution of **43** (2.07 g, 5.94 mmol) in DMF (14 mL). The mixture was allowed to reflux at 120 °C overnight. The DMF was removed under reduced pressure (40 °C). The crude oil was dissolved in DCM (25 mL) and extracted with water (25 mL x 3). The organic phases were combined, dried with $MgSO_4$, filtered and the DCM removed under reduced pressure (30 °C). Silica gel chromatography, eluting with a DCM/MeOH (95:5) mixture gave **44** as a colourless oil (0.73 g, 38%).

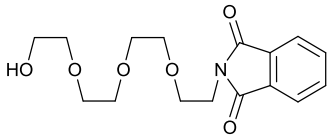

44

44 (0.73 g, 38%). υ_{max}/cm^{-1} 3460 (OH), 2870 (sp^3 CH), 1710 (conj. amide CO), 1100 (aliphatic ether CO), 730 (*o*-disubstituted Ar). δ_H (400 MHz; $CDCl_3$): 3.54-3.70 (14H, m, OCH_2), 3.72-3.91 (2H, m, NCH_2), 7.69-7.85 (4H, m, Ar-H). δ_C (100 MHz; $CDCl_3$): 37.4, 61.9, 68.1, 70.2, 70.5, 70.6, 70.8, 72.6, 123.4 (2 x C), 132.3 (2 x C), 134.0 (2 x C), 168.4 (2 x C). LRMS (ESI) m/z 324.4 $[M+H]^+$ (7%), 346.2 $[M+Na]^+$ (68%).

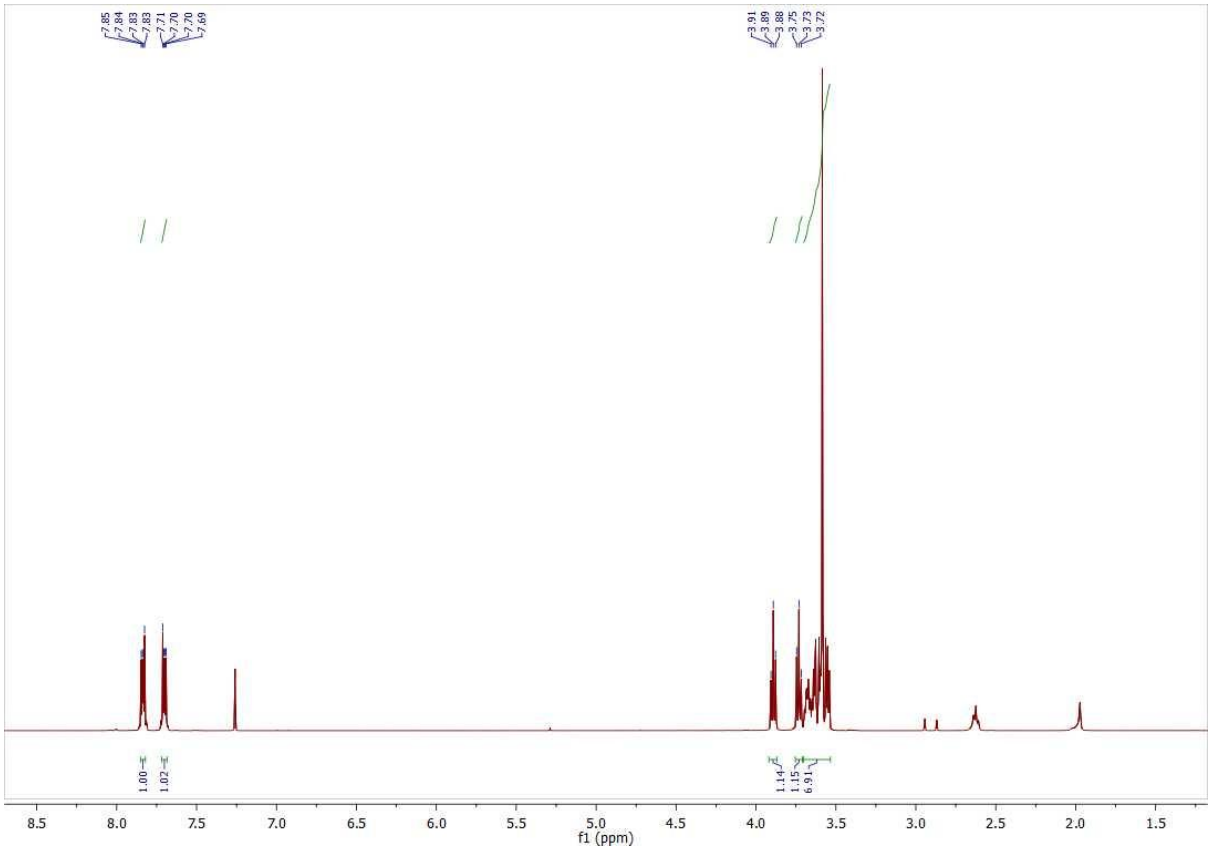
7.85
7.84
7.83
7.83
7.71
7.70
7.70
7.69
3.91
3.89
3.88
3.75
3.73
3.72
1.00
1.02
1.14
1.15
6.91
8.5
8.0
7.5
7.0
6.5
6.0
5.5
5.0
4.5
4.0
3.5
3.0
2.5
2.0
1.5
f1 (ppm)

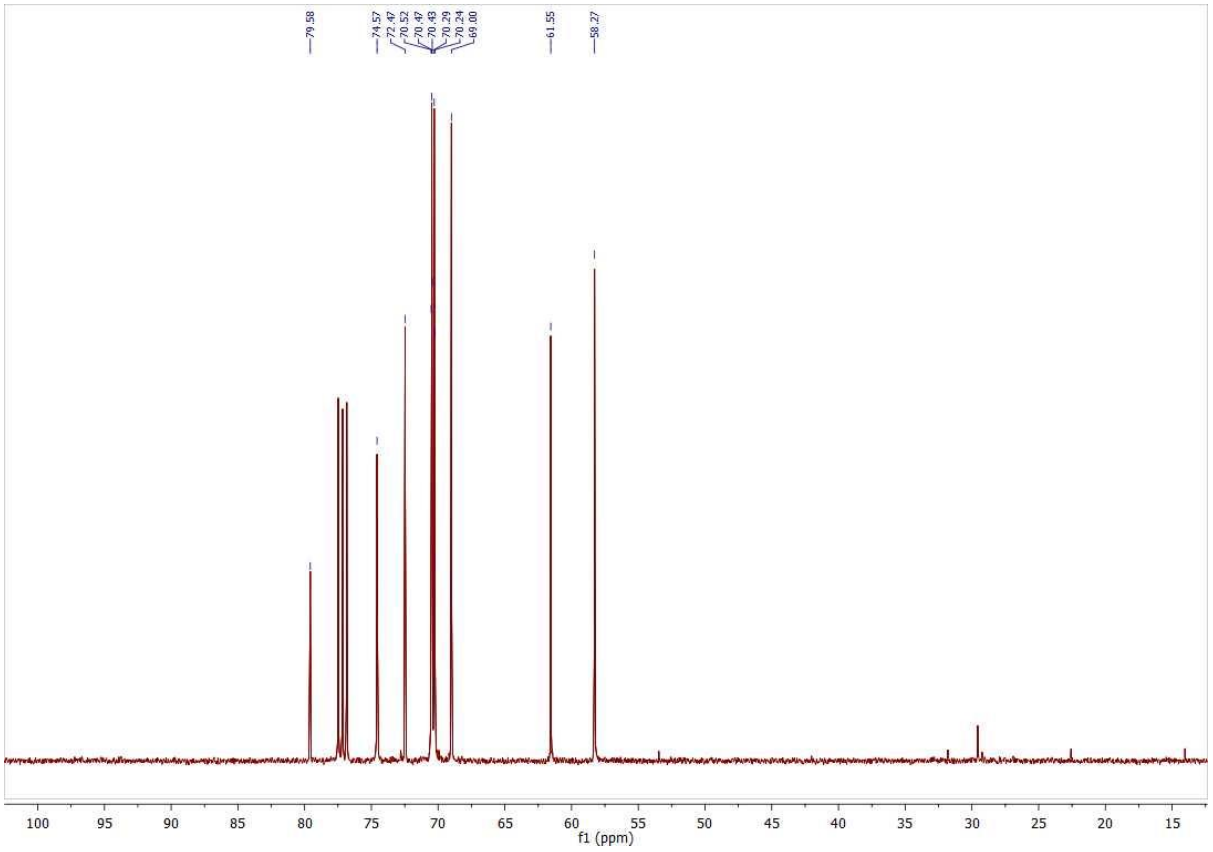
79.58
74.57
72.47
70.52
70.47
70.43
70.29
70.24
69.00
61.55
58.27
100
95
90
85
80
75
70
65
60
55
50
45
40
35
30
25
20
15
f1 (ppm)

3,6,9,12-Tetraoxapentadec-14-yn-1-ol (46). To a stirred solution of sodium hydride (3.33 g, 83.3 mmol, 60% dispersion) in dry THF (40 mL), **38** (40 mL, 208 mmol) was added in small portions under N_2. A solution of propargyl bromide (7.5 mL, 50.0 mmol, 80% solution) in dry THF (60 mL) was added dropwise to the mixture over 30 min. The reaction mixture was left to stir at room temperature overnight. The THF was removed under reduced pressure (40 °C) and the residual crude quenched with water (20 mL) then stirred for 10 min. This was then dissolved in DCM (40 mL) and extracted with brine (3 x 10 mL). The organic phases were collected, dried with Na_2SO_4, filtered and the DCM removed under reduced pressure (30 °C). Redissolve the residue in DCM (25 mL) and extract a second time with water (3 x 25 mL). The organic phases were collected, dried with $MgSO_4$, filtered and the DCM removed under reduced pressure to achieve **46** as a colourless oil (1.51 g, 14%). (Following the procedure by Pintér and co-workers[60])

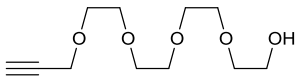

46

46 (1.51 g, 14%). δ_H (400 MHz; $CDCl_3$): 2.39 (1H, t, *J* 2.4, C≡CH), 3.50-3.63 (16H, m, OCH_2), 4.12 (2H, d, *J* 2.4, CHCC*H*$_2$). δ_C (100 MHz; $CDCl_3$): 58.3, 61.6, 69.0, 70.2, 70.3, 70.4, 70.5 (2 x C), 72.5, 74.6, 79.6.

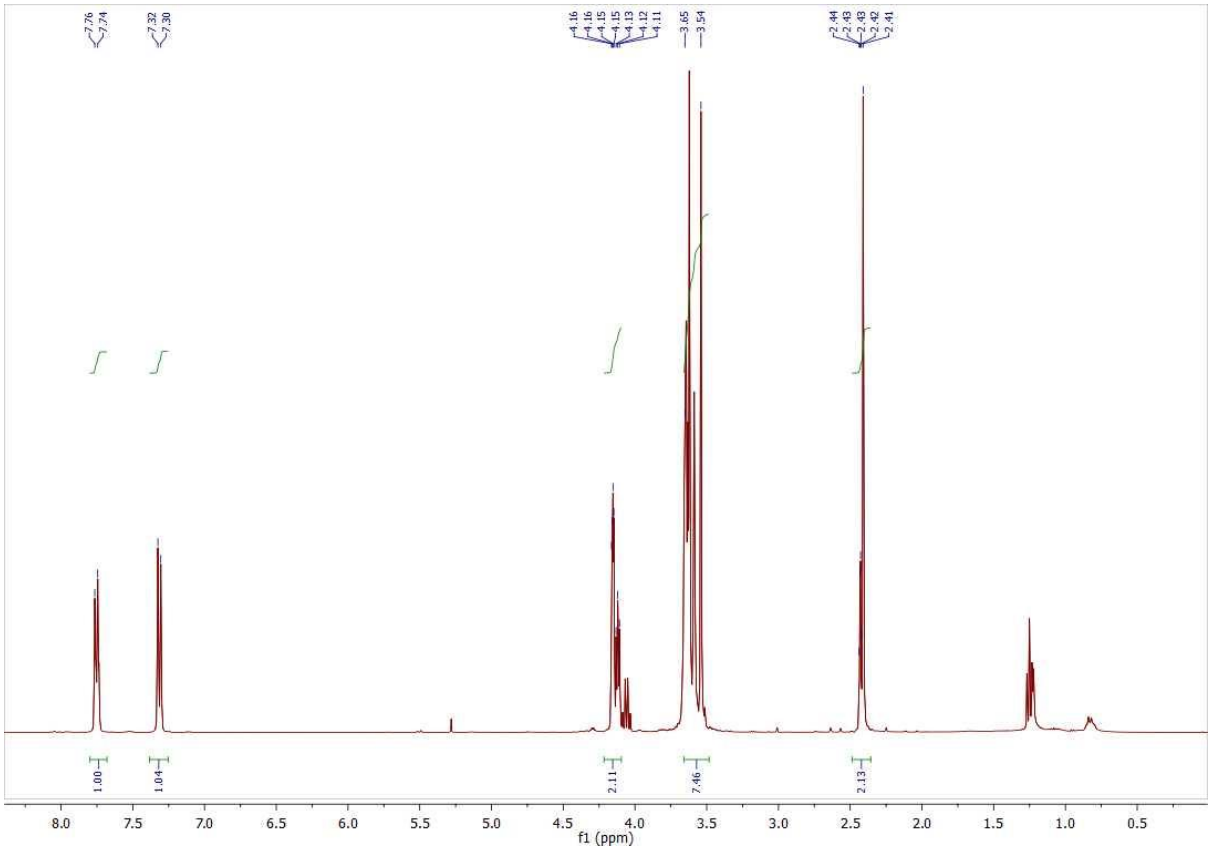
7.76
7.74
7.32
7.30
4.16
4.16
4.15
4.15
4.13
4.12
4.11
3.65
3.54
2.44
2.43
2.43
2.42
2.41
1.00
1.04
2.11
7.46
2.13
f1 (ppm)

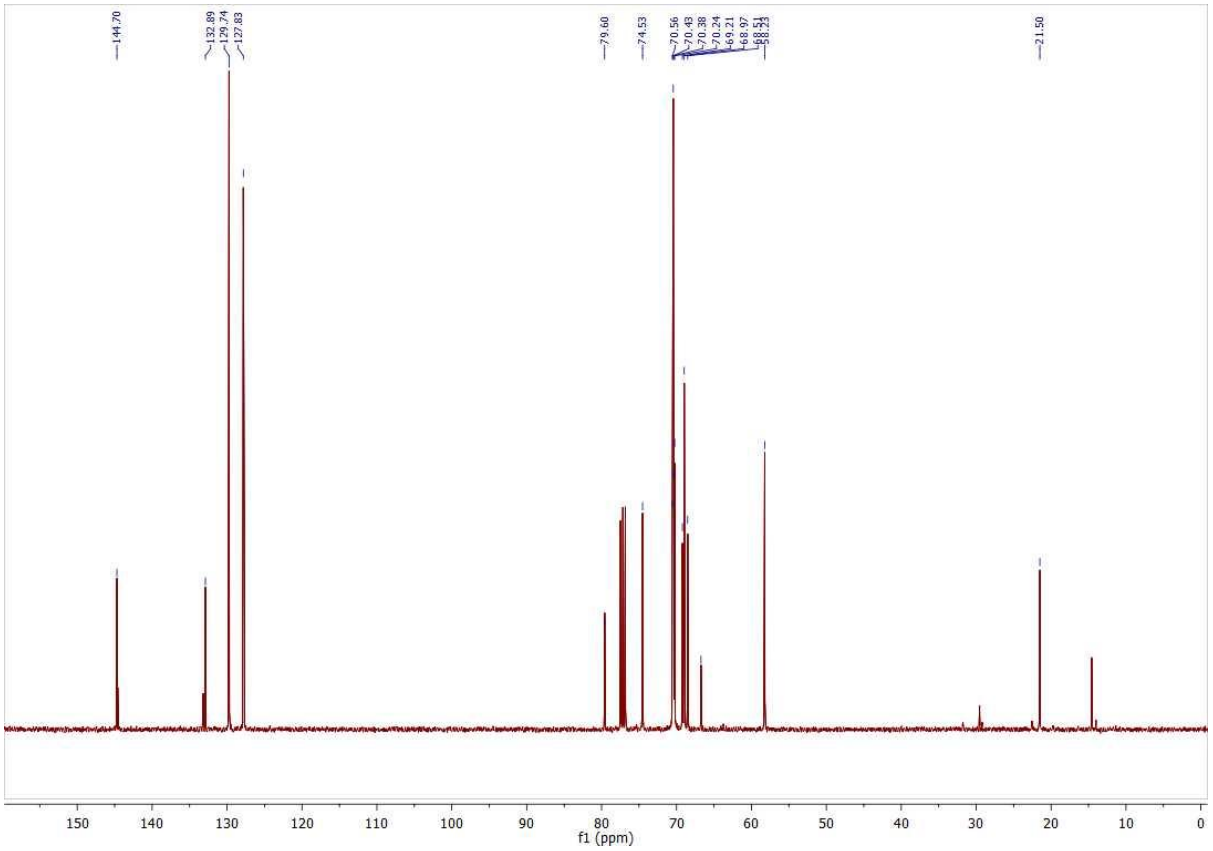
144.70
132.89
129.74
127.83
79.60
74.53
70.56
70.43
70.38
70.24
69.21
68.97
68.51
58.23
21.50
f1 (ppm)

3,6,9,12-Tetraoxapentadec-14-yn-1-yl 4-methylbenzenesulfonate (47). To a stirred solution of **6** (1.51 g, 4.06 mmol) in dry DCM (28 mL) was added; *p*-toluenesulfonyl chloride (0.70 g, 3.39 mmol), TEA (1.04 g, 10.3 mmol), and DMAP (0.1 g, 0.820 mmol). The reaction mixture was flushed with N_2 and left to stir at room temperature overnight. The crude was then extracted first with water (3 x 25 mL) and the collected organic phases extracted a second time with dilute HCl solution (3 x 25 mL, 15% solution). The organic phases were dried with $MgSO_4$, filtered and the DCM removed under reduced pressure (30 °C). Silica gel chromatography, eluting with a DCM/MeOH (95:5) mixture gave **47** as a pale yellow oil (0.88 g, 69%). (Following the procedure by Entract and co-workers[61])

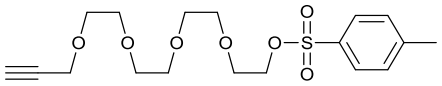

47

47 (0.88 g, 69%). υ_{max}/cm^{-1} 3280 (alkyne CH stretch), 2870 (sp^3 CH), 1350 (S=O), 1100 (aliphatic ether CO), 920 (S-O), 820 (*p*-disubstituted Ar). δ_H (400 MHz; $CDCl_3$): 2.41-2.43 (4H, m, CH_3, HC≡C), 3.54-3.65 (14H, m, OCH_2), 4.10-4.16 (4H, m, CH_2OS, C*H*$_2$C≡CH), 7.31 (2H, d, *J* 8.2, Ar-H), 7.75 (2H, d, *J* 8.2, Ar-H). δ_C (100 MHz; $CDCl_3$): 21.5, 58.2, 66.7, 68.5, 69.0, 69.2, 70.2, 70.4 (2 x C), 70.6, 74.5, 79.6, 127.8 (2 x C), 129.7, 132.9 (2 x C), 144.7. LRMS (ESI) m/z 409.2 $[M+Na]^+$.

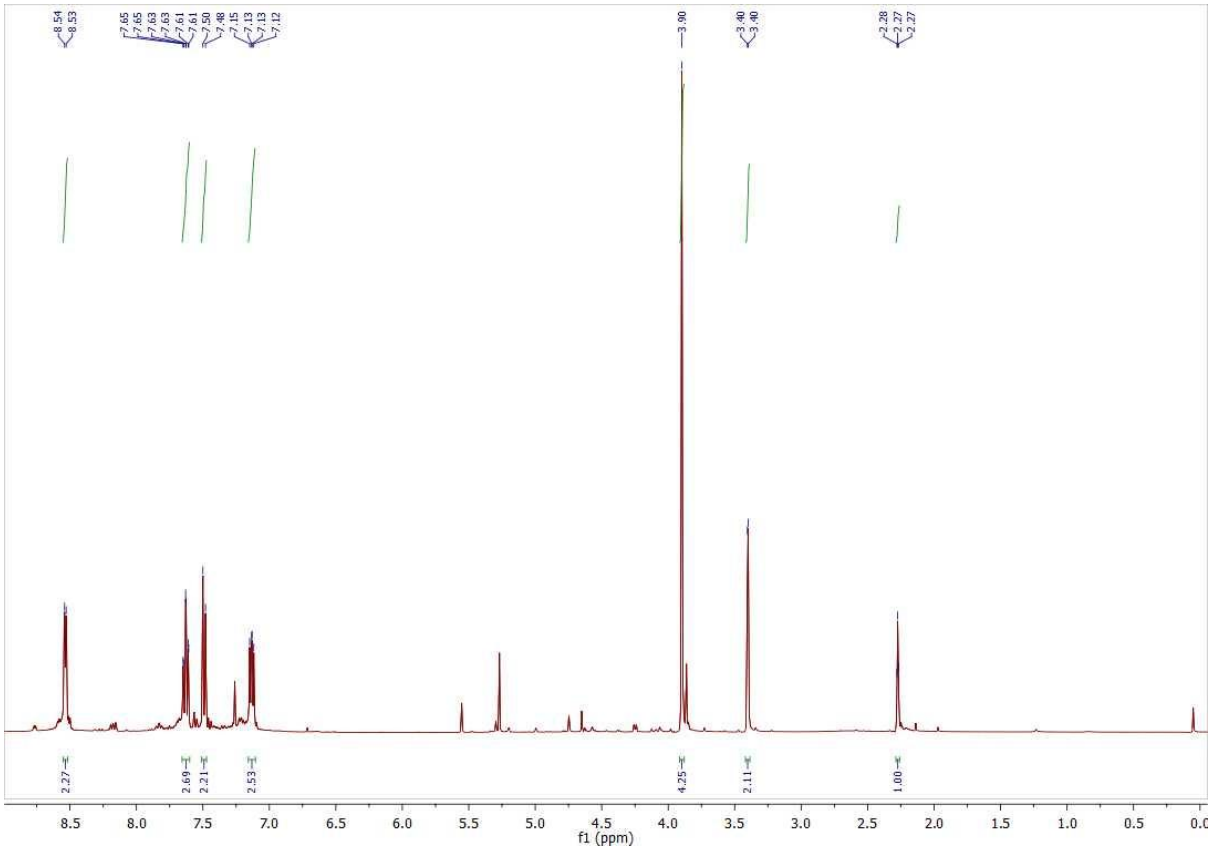
8.54
8.53
7.65
7.65
7.63
7.63
7.61
7.61
7.50
7.48
7.15
7.13
7.13
7.12
3.90
3.40
3.40
2.28
2.27
2.27
2.27
2.69
2.21
2.53
4.25
2.11
1.00
f1 (ppm)

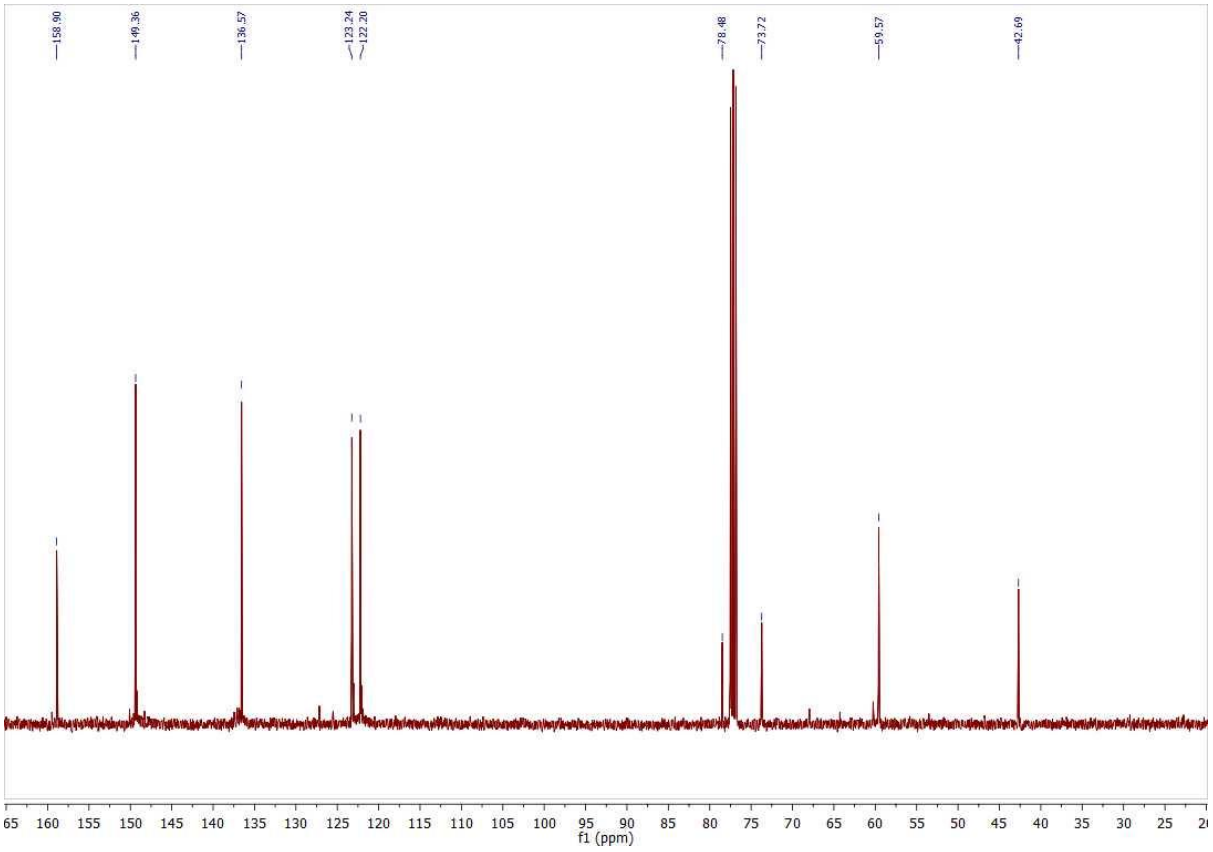
158.90
149.36
136.57
123.24
122.20
78.48
73.72
59.57
42.69
f1 (ppm)

***N*,*N*-bis(pyridin-2-ylmethyl)prop-2-yn-1-amine (49).** Propargyl amine (0.42 g, 7.6 mmol) and potassium carbonate (2.5 g, 18.1 mmol) was added to a solution of 2-chloromethyl pyridine hydrochloride (2.5 g, 15.2 mmol) in CH_3CN (20 mL). This mixture was allowed to reflux for 72 h at 80 °C. The CH_3CN was removed under reduced pressure (60 °C), and the crude mixture allowed to cool to room temperature. DCM (20 mL) was added and the insoluble solids were removed by filtration. The DCM was removed under reduced pressure (30 °C) and the residual solid redissolved in DCM (25 mL) and extracted with water (2 x 20 mL). The organic phases were collected, dried with $MgSO_4$, filtered, and the DCM removed under reduced pressure to give **49** as a black viscous tar (0.68 g, 37%). (Following the procedure by Castro and co-workers[63])

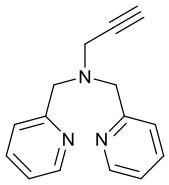

49

49 (0.68 g, 37%). υ_{max}/cm^{-1} 3300 (alkyne CH), 2910 (sp^3 CH), 1600 (C=N). δ_H (400 MHz; $CDCl_3$): 2.27 (1H, t, *J* 2.3, HC≡C), 3.40 (2H, d, *J* 2.3, HCCC*H*$_2$), 3.90 (4H, s, CH_2), 7.12-7.15 (2H, m, Ar-H), 7.48 (2H, d, *J* 7.8, Ar-H), 7.63 (2H, td, *J* 15.3, *J* 7.8, *J* 1.6, Ar-H), 8.54 (2H, d, *J* 4.7). δ_C (100 MHz; $CDCl_3$) 42.7, 59.6 (2 x C), 73.7, 78.5, 122.2 (2 x C), 123.2 (2 x C), 136.6 (2 x C), 149.4 (2 x C), 158.9 (2 x C). LRMS (ESI) m/z 238.5 $[M+H]^+$ (68%).

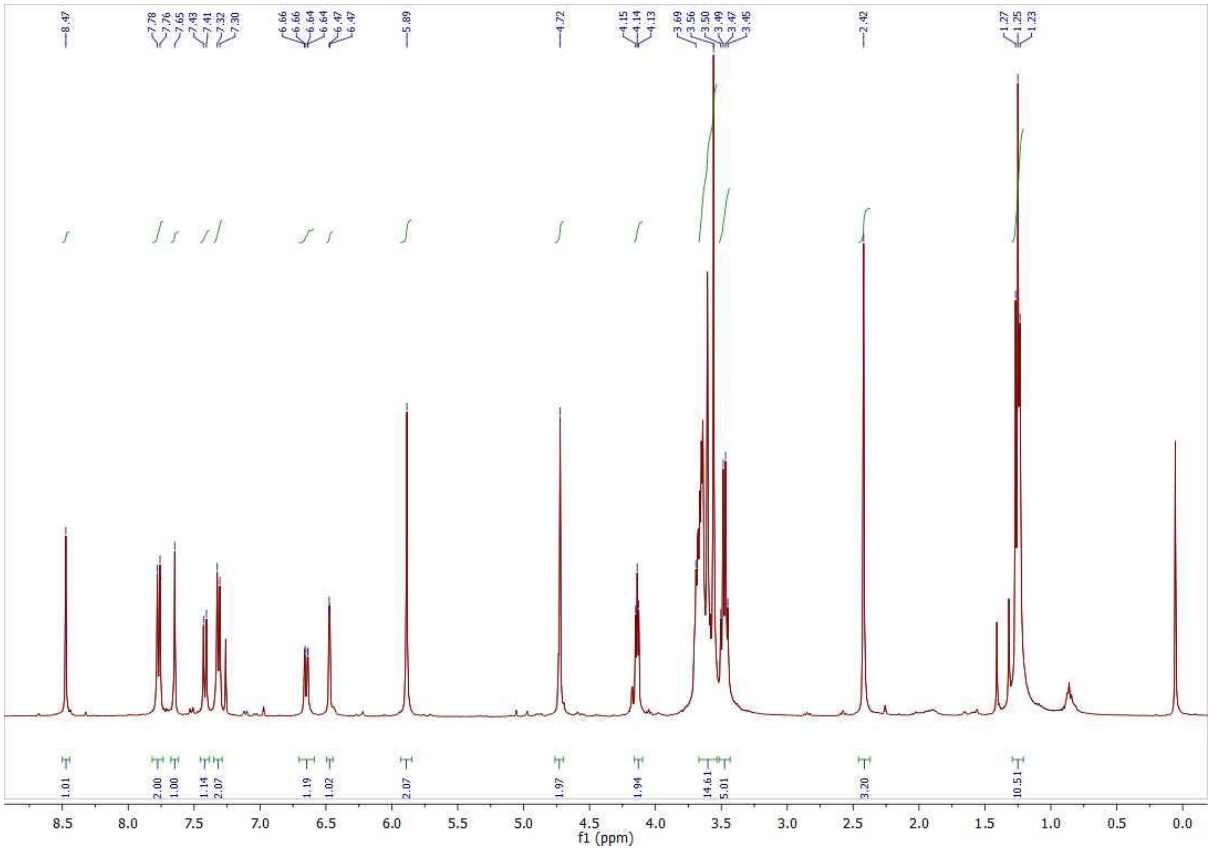
8.47
7.78
7.76
7.65
7.43
7.41
7.32
7.30
6.66
6.66
6.64
6.64
6.47
6.47
5.89
4.72
4.15
4.14
4.13
3.69
3.56
3.50
3.49
3.47
3.45
2.42
1.27
1.25
1.23
1.01
2.00
1.00
1.14
2.07
1.19
1.02
2.07
1.97
1.94
14.61
5.01
3.20
10.51
f1 (ppm)

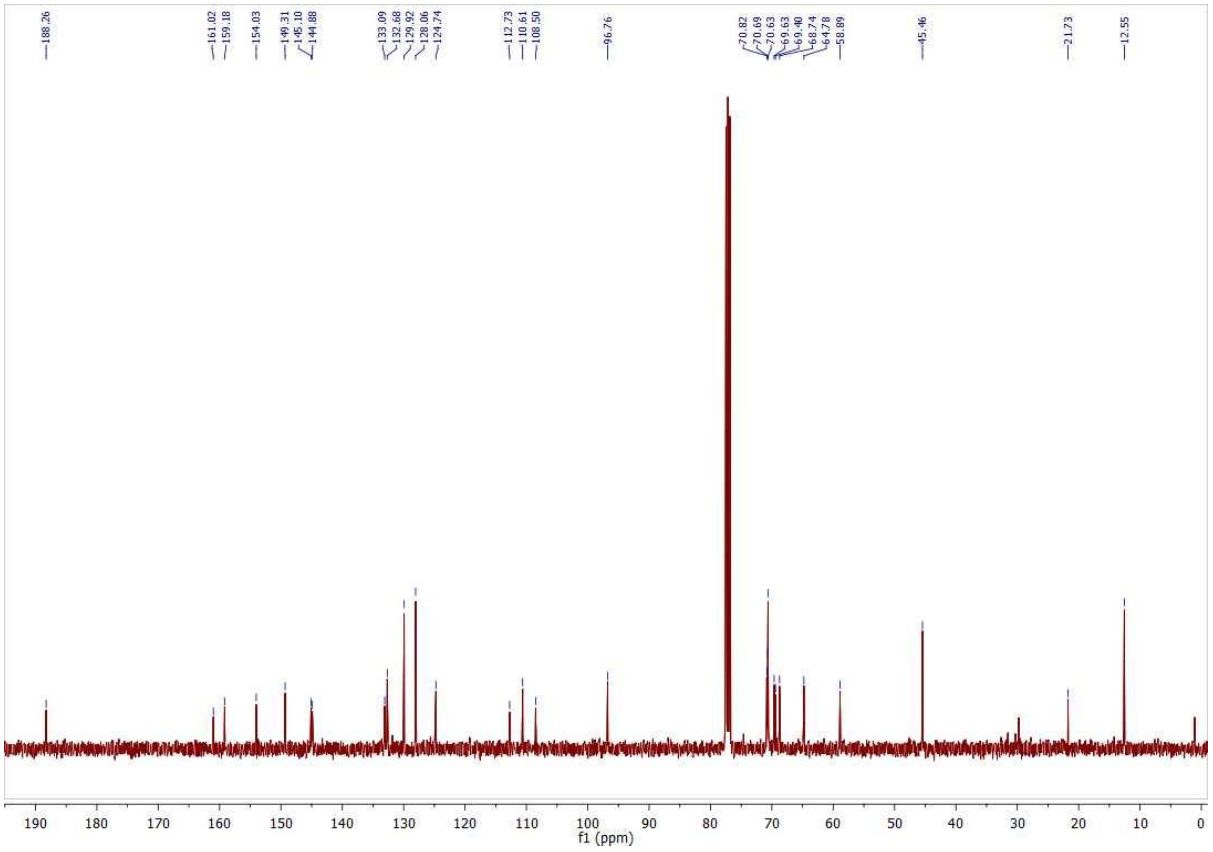
188.26
161.02
159.18
154.03
149.31
145.10
144.88
133.09
132.68
129.92
128.06
124.74
112.73
110.61
108.50
96.76
70.82
70.69
70.63
69.63
69.40
68.74
64.78
58.89
45.46
21.73
12.55
f1 (ppm)

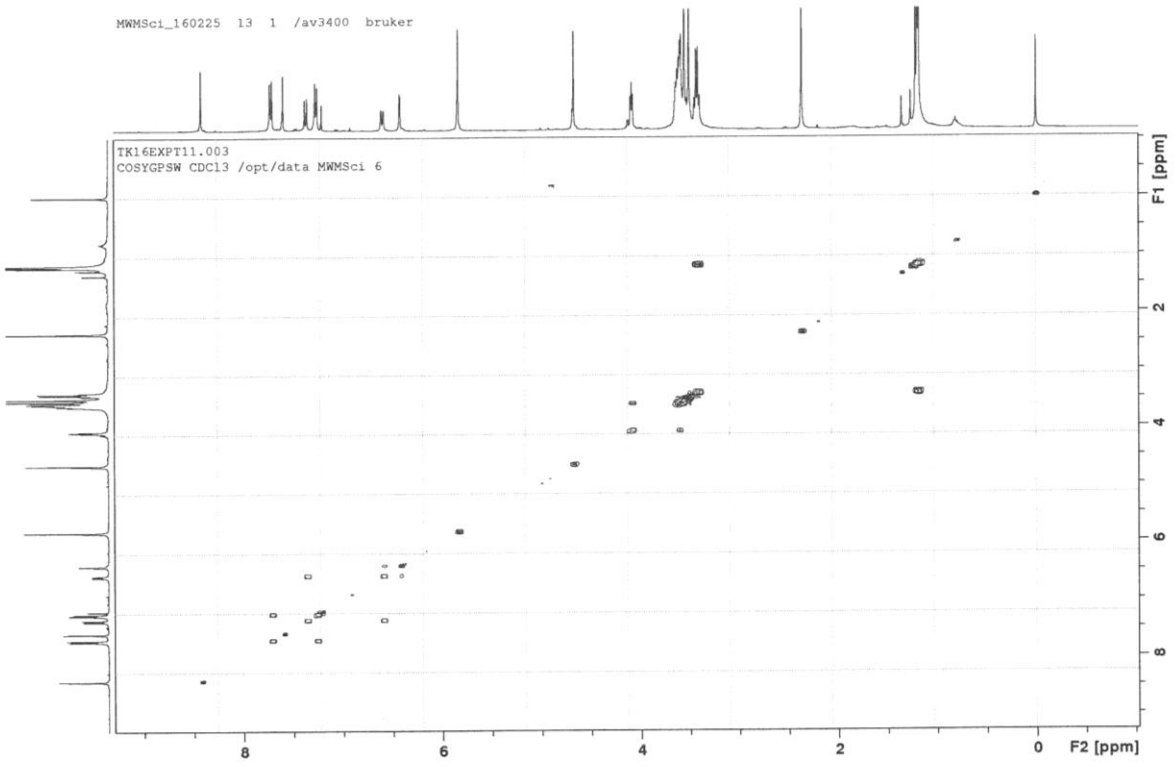
MWMSci_160225 13 1 /av3400 bruker
TK16EXPT11.003
COSYGPSW CDCl3 /opt/data MWMSci 6
F1 [ppm]
F2 [ppm]

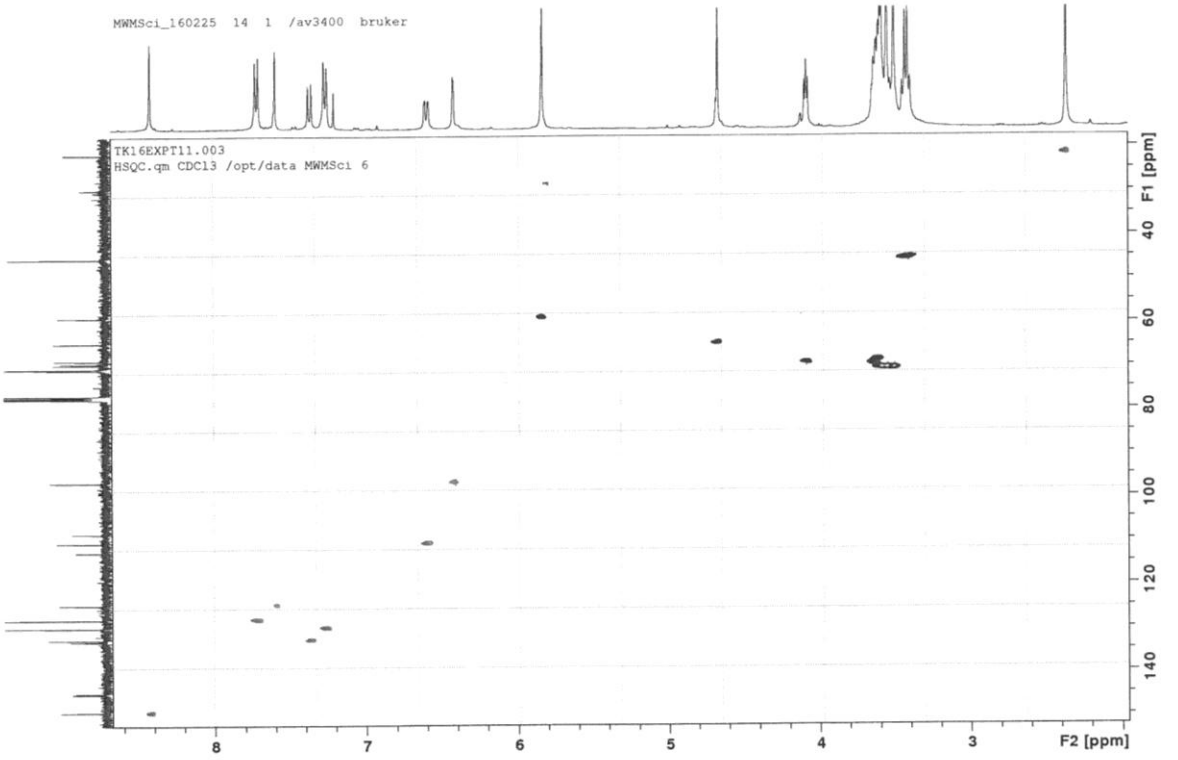
MWMSci_160225 14 1 /av3400 bruker
TK16EXPT11.003
HSQC.qm CDCl3 /opt/data MWMSci 6
F1 [ppm]
F2 [ppm]

1-(1-(2-(7-(Diethylamino)-2-oxo-2H-chromen-3-yl)-2-oxoethyl)-1H-1,2,3-triazol-4-yl)-2,5,8,11-tetraoxatridecan-13-yl 4-methylbenzenesulfonate (50). 39 (0.101 g, 0.336 mmol) and **47** (0.134 g, 0.347 mmol) were added to dry DCM (15 mL). This was flushed with N_2 and then DIPEA (0.058 mL, 0.333 mmol) and tetrakis(acetonitrile)copper(I) hexafluorophosphate (0.02 g, 0.054 mmol) were added to the reaction mixture. This was allowed to reflux under N_2 at room temperature for 72 h. The DCM was removed under reduced pressure (30 °C). The resulting residue was redissolved in minimal DCM and then extracted with a solution of EDTA in saturated sodium bicarbonate (3 x 25 mL, 1 M). Silica gel chromatography, eluting first with a DCM/MeOH (95:5) mixture and then an EtOAC/MeOH (92:8) mixture, gave **50** as a light brown oil (0.0465 g, 20%).

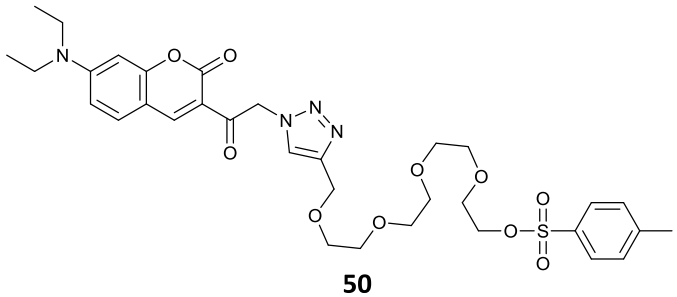

50

50 (0.0465 g, 20%). υ_{max}/cm^{-1} 3090 (C-H), 2870 (sp^3 CH), 1730 (ester C=O), 1690 (ketone C=O), 1350 (C-N), 1270 (ester C-O), 1100 (aliphatic ether CO), 920 (S-O), 810 (*p*-disubstituted Ar). δ_H(400 MHz; $CDCl_3$): 1.25 (6H, t, *J* 7.0, C*H*$_3$CH$_2$), 2.42 (3H, s, Ar-C*H*$_3$), 3.48 (4H, q, *J* 7.1, CH$_3$C*H*$_2$), 3.56-3.69 (14H, m, OCH$_2$), 4.14 (2H, t, *J* 4.7, CH$_2$OS), 4.72 (2H, s, OC*H*$_2$C=CH), 5.89 (2H, s, CH$_2$N$_3$), 6.47 (1H, d, *J* 2.0, Ar-H), 6.65 (1H, dd, *J* 2.0 and 9.0), 7.31 (2H, d, *J* 8.2, Ar-H), 7.42 (1H, d, *J* 9.0, Ar-H), 7.65 (1H, s, OCH$_2$C=C*H*), 7.77 (2H, d, *J* 8.2, Ar-H), 8.47 (1H, s, Ar-H). δ_C(100 MHz; $CDCl_3$) 12.6, 21.7, 45.5, 58.9, 64.8, 68.7, 69.4, 69.6, 70.6 (2C), 70.7, 70.8, 96.8, 108.5, 110.6, 112.7, 124.7, 128.1, 129.9, 132.7, 133.1, 144.9, 145.1, 149.3, 154.0, 159.2, 161.0, 188.3. LRMS (ESI) m/z 238.5 [M+H]$^+$ (42%).

5. References

[1] J. C. King, D. M. Shames and L. R. Woodhouse, *J. Nutr.*, 2000, **130**, 1360-1366.
[2] L. M. Plum, L. Rink, and H. Haase, *Int. J. Environ. Res. Public Health*, 2010, **7**, 1342-1365.
[3] N. Roohani, R. Hurrell, R. Kelishadi, and R. Schulin, *J. Res. Med. Sci.*, 2013, **2**, 144–157.
[4] C. Andreini, L. Banci, I. Bertini, and A. Rosato, *J. Proteome. Res.*, 2006, **5**, 196-201.
[5] V. Kumar, A. Kumar, S. K. Singh,S. K. Tripathi, D. Kumar, R. Singh and S. Dwivedi , *Int. J. Mol. Genet. And Gene*, 2016, **1**, 1-7.
[6] D. Schachter, *J. Lab. Clin. Med.* 1959, **54**, 763-768.
[7] J. F. Callan, A. P. de Silva and D. C. Magri, *Tetrahedron*, 2005, **61**, 8551-8588.
[8] K. Jobe, C. H. Brennan, M. Motevalli, S. M. Goldup and M. Watkinson, *Chem. Commun.*, 2011, **47**, 6036-6038.
[9] J. Pancholi, D. J. Hodson, K. Jobe, G. A. Rutter, S. M. Goldup and M. Watkinson, *Chem. Sci.*, 2014, **5**, 3528–3535.
[10] B. Valeur and M. N. Berberan-Santos, *Molecular Fluorescence Principles and Applications*, Wiley-VCH, Second Edi., 2012.
[11] Z. Liu, W. He and Z. Guo, *Chem. Soc. Rev.*, 2013, **42**, 1568–1600.
[12] A. P. de Silva, H. Q. N. Gunaratne, T. Gunnlaugsson, A. J. M. Huxley, C. P. McCoy, J. T. Rademacher and T. E. Rice, *Chem. Rev.*, 1997, **97**, 1515–1566.
[13] A. P. de Silva, T. S. Moody and G. D. Wright, *Analyst*, 2009, **134**, 2385–2393.
[14] D. Y. Zhang, M. Azrad, W. Demark-Wahnefried, C. J. Frederickson, S. J. Lippard and R. J. Radford, *ACS Chem. Biol.*, 2015, **10**, 385-389.
[15] J.-S. Wu, W.-M. Liu, X.-Q. Zhuang, F. Wang, P.-F. Wang, S.-L. Tao, X.-H. Zhang, S.-K. Wu and S.-T. Lee, *Org. Lett.*, 2007, **9**, 33-36.
[16] Y. Zhou, H. N. Kim and J. Yoon, *Bioorg. Med. Chem. Lett.*, 2010, **20**, 125-128.
[17] K. R. Gee, Z.-L. Zhou, D. Ton-That, S. L. Sensei and J. H. Weiss, *Cell Calcium*, 2002, **31**, 245-251.
[18] T. Gunnlaugsson, T. Clive Lee and R. Parkesh, *Org. Biomol. Chem.*, 2003, **1**, 3265-3267.
[19] E. Roussakis, S. Voutsadaki, E. Pinakoulaki, D. P. Sideris, K. Tokatlidis and H. E. Katerinopoulos, *Cell Calcium*, 2008, **44**, 270-275.
[20] M. E. Huston, K. W. Haider and A. W. Czarnik, *J. Am. Chem. Soc.*, 1988, **110**, 4460-4462.
[21] J. A. Sclafani, M. T. Maranto, T. M. Sisk and S. A. Van Arman, *Tetrahedron Lett.*, 1996, **37**, 2193-2196.
[22] E. Tamanini, A. Katewa, L. M. Sedger, M. H. Todd and M. Watkinson, *Inorg. Chem.*, 2009, **48**, 319–324.
[23] K. Sreenath, R. J. Clark and L. Zhu, *J. Org. Chem.*, 2012, **77**, 8268–8279.
[24] A. K. Mandal, T. He, S. K. Maji, H. Sun and Y. Zhao, *Chem. Commun.*, 2014, **50**, 14378–14381.
[25] C. J. Frederickson, E. J. Kasarskis, D. Ringo and R. E. Frederickson, *J. Neurosci. Meth.*, 1987, **20**, 91-103
[26] Y. Zhang, X. Guo, W. Si, L. Jia and X. Qian, *Org. Lett.*, 2008, **10**, 473-476.
[27] Z. Xu, J. Yoon, and D. R. Spring, *Chem. Soc. Rev.*, 2010, **39**, 1996–2006.
[28] H.-H. Wang, Q. Gan, X.-J. Wang, L. Xue, S.-H. Liu and H. Jiang, *Org. Lett.*, 2007, **9**, 4995-4998.
[29] E. M. Nolan J. Jaworski, K.-I. Okamoto, Y. Hayashi, M. Sheng and S. J. Lippard, *J. Am. Chem. Soc.*, 2005, **127**, 16812-16823.
[30] Z. Xu, K.-H. Baek, H. N. Kim, J. Cui, X. Qian, D. R. Spring, I. Shin and J. Yoon, *J. Am. Chem. Soc.*, 2010, **132**, 601-610.
[31] Z. Xu, X. Qian, J. Cui and R. Zhang,*Tetrahedron*, 2006, **62**, 10117-10122.
[32] C. Lu, Z. Xu, J. Cui, R. Zhang and X. Qian, *J. Org. Chem.*, 2007, **72**, 3554-3557.
[33] S. Huang, R. J. Clark and L. Zhu, *Org. Lett.*, 2007, **9**, 4999-5002.
[34] K. Umezawa D. Citterio and K. Suzuki, *Anal. Sci.*, 2014, **30**, 327-349.
[35] W. Shi and H. Ma, *Chem. Commun.*, 2012, **48**, 8732-8744.

[36] Y. Yamaguchi, Y. Matsubara, T. Ochi, T. Wakamiya and Z.-I. Yoshida, *J. Am. Chem. Soc.*, 2008, **130**, 13867-13869.
[37] G. K. Walkup, S. C. Burdette, S. J. Lippard and R. Y. Tsien, *J. Am. Chem. Soc.*, 2000, **122**, 5644–5645.
[38] R. J. Radford, W. Chyan and S. J. Lippard, *Chem. Sci.*, 2013, **4**, 3080–3084.
[39] M. Ceresole, *D. R. Patent 44002*, 1887.
[40] L. Yuan, W. Lin, Y. Yang and H. Chen, *J. Am. Chem. Soc.*, 2012, **134**, 1200-1211.
[41] K. Kolmakov, C. A. Wurm, R. Hennig, E. Rapp, S. Jakobs, V. N. Belov and S. W. Hell, *Chem. Eur. J.*, 2012, **18**, 12986-12998.
[42] D. Shi, X. Zhou, T. Zheng, Y. Zou, S. Guo, J. Lv and F. Yan, *J. Iran Chem. Soc.*, 2015, **12**, 293-308.
[43] M. Tasior, D. Kim, S. Singha, M. Krzeszewski, K. H. Ahn and D. T. Gryko, *J. Mater. Chem. C*, 2015, **3**, 1421-1446.
[44] L. Y. Zhao, Q. L. Mi, G. K. Wang, J. H. Chen, J. F. Zhang, Q. H. Zhao and Y. Zhou, *Tet. Lett.*, 2013, **54**, 3353-3358.
[45] S. S. Bag, R. Kundu and S. Talukdar, *Tetrahedron Lett.*, 2012, **53**, 5875-5879.
[46] S. T. McCarron and J. J. Chambers, *Neuropharmacology*, 2015, **98**, 41-47.
[47] C. Tahtaoui, I. Parrot, P. Klotz, F. Guillier, J.-L. Galzi, M. Hibert and B. Ilien, *J. Med. Chem.*, 2004, **47**, 4300-4315.
[48] A. Kumar, M. K. Pandey, R. Anandakathir, R. Mosurkal, V. S. Parmar, A. C. Watterson and J. Kumar, *Sensors Actuat. B-Chem.*, 2010, **147**, 105-110.
[49] P. G. de Gennes, *Adv. Colloid Interface Sci.*, 1987, **27**, 189–209.
[50] J. Ramchander, N. Rameshwar, T. Reddy, G. Raju and A. Reddy, *J. Chem. Sci.*, 2014, **126**, 1063-1074.
[51] H. C. Kolb, M. G. Finn, K. B. Sharpless, *Angrew. Chem. Int. Ed. Engl*, 2001, **40**, 2004–2021.
[52] V. V. Rostovtsev, L. G. Green, V. V. Fokin, K. B. Sharpless, *Angew. Chem. Int. Ed.*, 2002, **41**, 2596-2599.
[53] L. Jin, D. R. Tolentino, M. Melaimi and Guy Bertrand, *Sci. Adv.*, 2015, **1**, 1-5.
[54] D. Secci, S. Carradori, A. Bolasco, P. Chimenti, M. Yáñez, F. Ortuso and S. Alcaro, *Eur. J. Med. Chem.*, 2011, **46**, 4846–4852.
[55] W. Lin, X. Cao, L. Yuan and Y. Ding, *Chem. – A Eur. J.*, 2010, **16**, 6454-6457.
[56] R. W. Evans, J. R. Zbieg, S. Zhu, W. Li, and D. W. C. MacMillan, *J. Am. Chem. Soc.*, 2013, **135**, 16074−16077.
[57] W. C. Still, M. Kahn and A. Mitra, *J. Org. Chem.*, 1978, **43**, 2923-2925.
[58] E. Lieber, C. N. R. Rao, T. S. Chao and C. W. W. Hoffman, *Anal. Chem.*, 1957, **29**, 916–918.
[59] M. S. Gibson, R. W. Bradshaw, *Angew. Chem. Int. Ed. Engl.*, 1968, **7**, 919-930.
[60] G. Pintér, I. Bereczki, E. Roth, A. Sipos, R. Varghese, E. E. Udo, E. Ostorhazi, F. Rozgonyi, O. A. Phillips and P. Herczegh, *Med. Chem.*, 2011, **7**, 45-55.
[61] G. M. Entract, F. Bryden, J. Domarkas, H. Savoie, L. Allott, S. J. Archibald, C. Cawthorne and R. W. Boyle, *Mol. Pharmaceutics*, 2015, **12**, 4414-4423.
[62] J. Rosenthal and S. J. Lippard, *J. Am. Chem. Soc.*, 2010, **132**, 5536-5537.
[63] J. Chaignon, S.-E. Stiriba, F. Lloret, C. Yuste, G. Pilet, L. Bonneviot, B. Albela and I. Castro, *Dalton Trans.*, 2014, **43**, 9704–9713.
[64] H. Staudinger, J. Meyer, *Helv. Chim. Acta.*, 1919, **2**, 635-646.
[65] W. Lin, X. Cao, L. Yuan, and Y. Ding, *A, Eur. J.*, 2010, **16**, 6454-6457.
[66] O. Takechi and M. Nishizono, *Chem. Pharm. Bull.*, 2000, **48**, 1702-1710.
[67] Q. Zhang, H. Ren and G. L. Baker, *Tet. Lett.*, 2014, **55**, 3384-3386.